Investigation of cilia-associated kinesin families

Thesis submitted to the University of Nottingham for the degree of Master of Philosophy.

2017

Charles E. Littledale

4214264

School of Life Sciences

Abstract

Kinesins are a protein superfamily that function via microtubules by converting energy released from ATP hydrolysis into mechanical work. Kinesins have been classified into 14 families; the distribution of which can highlight potential roles of the family members. Kinesin-16s are found solely in organisms that build cilia/flagella, whilst Kinesin-13s are only absent in organisms that do not build cilia. The Kinesin-13 family is comprised of three subfamilies. Both 13A and 13B have motors involved in ciliary function, but the roles of 13C are still unknown. The purpose of this research is to identify novel roles of kinesin families and/or subfamilies, with a particular focus on those that may function in the cilia/flagella. Human KIF12 was investigated as a representative of Kinesin-16 whilst the roles of Kinesin-13 subfamilies A and C motors were investigated using the kinesin subfamily members found in *Trypanosoma brucei*.

An inducible system of ciliogenesis in IMCD3 cells was sought to allow investigation into the difference in KIF12 localisation and expression before and after ciliogenesis occurred. Induction of ciliogenesis in IMCD3 cells was unsuccessful with no significant change in the percentage of ciliated cells post-serum starvation and/or contact inhibition.

To characterise KIF12-microtubule interactions *in vitro*, the human RefSeq reference standard KIF12 (rsKif12) sequence was used. After multiple failed attempts to express and purify rsKif12, sequence analysis showed rsKif12 lacks nucleotide-binding motifs conserved across the kinesin superfamily. To determine the *KIF12* major splice variant, RNA-sequencing data and sequence alignments of KIF12 homologues were used. kif12ΔPPGGG, harbouring a five amino acid deletion that reduced polycystic kidney disease severity in mice, and KIF12 motor domain only samples were also determined.

Having determined the correct major splice variant of KIF12, several expression constructs were created to find a soluble version of KIF12 as well as kif12MD and kif12ΔPPGGG. Expressed KIF12, kif12MD and kif12ΔPPGGG were tagged individually with 6x His or 6x His and GFP at either the N- or C-terminus. Only kif12MD tagged with a C-terminal GFP and 6x His was soluble.

***T. brucei* Kinesin-13s Kin13-1, -3 (both 13A) and -6 (13C) interactions with microtubules were observed *in vitro*. Kin13-6 does not significantly change microtubule dynamics *in vitro*. This suggests that Kinesin-13Cs do not function in microtubule regulation. Kin13-3 depolymerises microtubules, consistent with the functions of other Kinesin-13A members. Kin13-1 controls microtubule length in a novel manner by cleaving at the microtubule lattice. Kin13-1 cleaving activity has revealed a possible means of regulating the mitotic spindle, and thus chromosome segregation, which was previously unidentified.**

Acknowledgements

I would like to first thank the BBSRC and The University of Nottingham for their financial support, making the research within this thesis possible. I would also like to thank the University of Nottingham Doctoral Training Programme team for their support and for organising CPD opportunities throughout my time at the institution. I have had the privilege of working with some wonderful peers whose support in times of distress and demotivation has been invaluable. I would like to thank Claire Friel and Bill Wickstead for their supervision during the project. Their training, ideas and imparting of knowledge has undoubtedly helped enhance my abilities to work independently and think critically. Finally, I would like to thank my family and friends for their perspective and unwavering support during the project.

Table of Figures

Figure 1. Microtubules: basic structure and dynamics 17

Figure 2. Motor protein domain architecture in a selection of mouse kinesins 18

Figure 3. Microtubule-regulating kinesins 20

Figure 4. Distribution of ancient kinesin paralogues in 45 diverse eukaryotes 25

Figure 5. The canonical structure of mammalian primary cilia 27

Figure 6. The structures of doublet and triplet microtubules 29

Figure 7. Centrosomes, cilia and the cell cycle in animal cells. ... 33

Figure 8. The building blocks of intraflagellar transport (IFT). 36

Figure 9. Intraflagellar transport within the primary cilium. 37

Figure 10. Distributions of kinesin families among eukaryotes ... 44

Figure 11. Phylogenetic analysis of Kinesin-13 family members. 48

Figure 12. Tagged rskif12 and rskif12MD protein constructs. 67

Figure 13. Sf9 transfection with baculovirus containing GFP-rskif12 and rskif12MD respectively. 68

Figure 14. rskif12 protein expression levels when expressed in Sf9 expression cultures 69

Figure 15. Cation exchange chromatography of rskif12. 71

Figure 16. Nickel-affinity chromatography of rskif12 cation exchange (CE) fractions 72

Figure 17. Cation exchange chromatography of GFP-rskif12 (88.2 kDa) Sf9 expression culture 41 hours post-induction 73

Figure 18. Screening of rskif12-GFP transfected HeLa cells 75

Figure 19. rskif12-GFP (85.2 kDa) solubility 76

Figure 20. Sequence architecture of mouse and human Kif12 ... 79

Figure 21. RefSeq predicted human KIF12 protein models 80

Figure 22. Amino acid alignment of human KIF12 and human and mouse kif12 reference sequences 82

Figure 23. KIF12 exon 3 and 4 boundaries. The KIF12 sequence is aligned against a segment of human chromosome nine (Chr9_GRCh38.p2) where the gene is located..... 83

Figure 24. Mouse kif12 protein alignment. Mouse reference sequence kif12 amino acid sequence aligned against other laboratory mouse kif12 sequences 84

Figure 25.Kif12 PPGGG INDEL analysis..... 855

Figure 26. Construction of KIF12 cloning vectors 866

Figure 27. Expression of KIF12 and kif12ΔPPGGG..... 888

Figure 28. Solubility of KIF12 and kif12ΔPPGGG in Sf9 cells... 888

Figure 29. Two step purification of KIF12-GFP (100.1 kDa)..... 899

Figure 30. Tagging on the C- or N-terminus impacts the solubility of kif12MD 911

Figure 31. Mouse KIF12 expression levels in different mouse tissues..... 933

Figure 32. The effect of KIF12 siRNA knockdown on ciliogenesis and cilia maintenance is inconclusive..... 977

Figure 33. KIF12 knockdown impacts cell survival 988

Figure 34. IMCD3 growth rate. Cell number/cm^2 is the number of the cells found within an area of 1 cm^2 999

Figure 35. Ciliation of IMCD3 cells 100

Figure 36. Induction of ciliogenesis in IMCD3 cells 1022

Figure 37. Induction of ciliogenesis in IMCD3 cells using serum starvation 104

Figure 38. Induction of ciliogenesis in IMCD cells using prolonged serum starvation..... 1066

Figure 39. Acetylated α-tubulin signal profiles from IMCD3 cells at 0.5 x 10^5 cells/cm^2..... 1088

Figure 40. Acetylated α-tubulin signal profiles from IMCD3 cells at 1 x 10^5 cells/cm^2..... 109

Figure 41. Acetylated alpha tubulin signal profiles from IMCD3 cells at 2 x 10^5 cells/cm^2..... 110

Figure 42. Acetylated alpha tubulin signal profiles from IMCD3 cells at 4 x 10^5 cells/cm^2..... 1111

Figure 43. Protein alignment of *T. brucei* Kinesin-13s motor domains. 1144

Figure 44. SDS-PAGE of Kin13-1 & 2 Sf9 expression cultures. 1166

Figure 45. SDS-PAGE of Kin13-3 & 4b Sf9 expression cultures 1177

Figure 46. SDS-PAGE of Kin13-5 & 6 Sf9 expression cultures 1188

Figure 47. Nickel-affinity chromatography of Kin13-1 expressing Sf9 cells..... 1199

Figure 48. Nickel-affinity chromatography of Kin13-3 expressing Sf9 cells..... 120

Figure 49. Nickel-affinity chromatography of Kin13-6 expressing Sf9 cells..... 1211

Figure 50. Depolymerisation rate of MTs in the presence of *T. brucei* kinesin-13s..... 1233

Figure 51. Kinesin 13-dependent MT depolymerisation 1233

Figure 52. MT dynamics in the presence of Kin13-1 1255

Figure 53. Comparison of MT dynamics in the presence of Kin13-1 and MCAK 1266

Figure 54. MT cleavage events in the presence of Kineisn 13s 1277

List of Tables

Table 1. z_{cilia} scores of IFT proteins, KIF12 and secondary screen candidates 94

Table 2. Depolymerisation rate of MTs in the presence of *Trypanosoma brucei* kinesin-13s 122

Table of Contents

Abstract 2

Acknowledgements 3

Table of Figures 4

List of Tables 7

List of abbreviations 14

1 Introduction 15

1.1 Cytoskeletal motors 15

1.2 Kinesins 16

1.2.1 Microtubules 16

1.2.2 Kinesin architecture 17

1.2.3 Microtubule regulators 20

1.2.4 Kinesin classification 23

1.3 Cilia 25

1.3.1 Ciliary roles in cells 26

1.3.2 Motile vs immotile cilia 26

1.3.3 Ciliary structure 28

1.3.4 Ciliopathies 31

1.3.5 Polycystic kidney disease 31

1.4 The cilia cycle 32

1.4.1 A cilia-centric view of the cell cycle 32

1.4.2 Ciliogenesis 33

1.5 Intraflagellar transport 35

1.5.1 IFT motors 36

1.5.2 IFT particles 38
1.5.3 IFT trains 39
1.6 Cilia-associated kinesins 41
1.6.1 Kinesin family 3 41
1.6.2 Kinesin family 4/10 42
1.6.3 Kinesin family 9 42
1.6.4 Kinesin family 13 43
1.7 Kinesin-16 family 45
1.7.1 KIF12 45
1.8 Kinesin-13 family diversity 47
1.8.1 Characterised Kinesin-13 members 49
1.8.2 The extended *T. brucei* Kinesin-13 repertoire 51
2 Aims 53
3 Materials and Methods 55
3.1 Expression and protein purification of rsKif12 and rsKif12MD 55
3.1.1 PCR amplification of rsKif12 and rsKif12MD and insertion into cloning vector 55
3.1.2 Expression of rsKif12 using the baculovirus expression system 55
3.1.3 Two-step protein purification by cation exchange and nickel affinity chromatography 56
3.2 Expression of rsKif12 in mammalian cell lines 57
3.2.1 Construction of cloning vectors 57

3.2.2 Transfection and expression of rsKif12 and rsKif12MD 58

3.2.3 rsKif12 and rsKif12MD solubility in mammalian expression systems 58

3.3 Expression and purification of KIF12 and Kif12ΔPPGGG ... 58

3.3.1 Identification of KIF12 58

3.3.2 Construction of KIF12 and Kif12ΔPPGGG cloning vectors 59

3.3.3 Transfection into insect cells and expression 59

3.3.4 Protein purification of KIF12 and Kif12ΔPPGGG 60

3.4 Expression and purification of Kif12MD 60

3.5 Induction of ciliogenesis in IMCD3 cells..... 60

3.5.1 IMCD3 growth culture..... 60

3.5.2 IMCD3 growth curve..... 61

3.5.3 Ciliation of IMCD3 cells 61

3.5.4 Inducible system for ciliogenesis in IMCD3 cells 62

3.6 Expression and purification of *T. brucei* Kinesin-13s 63

3.7 Characterisation of *T. brucei* Kinesin-13s interaction with microtubules 64

3.7.1 Depolymerisation assay 64

3.7.2 Recording of MT - Kinesin-13 interaction 64

3.7.3 Microtubule cleavage events..... 65

4 Results..... 66

4.1 Characterisation of human Kif12 66

4.1.1 Reference standard human Kif12 is insoluble in the baculovirus expression system. 66

4.1.2 Expressed recombinant GFP tagged rskif12 and rsKif12MD cannot be successfully purified due to insolubility . 68

4.1.3 Human rsKif12 remains insoluble when expressed in mammalian expression systems 74

4.1.4 Human RefSeq reference standard Kif12 lacks two conserved nucleotide binding motifs within the kinesin motor domain 76

4.1.5 Determination of the major human KIF12 isoform ... 79

4.1.6 The 5 amino acid sequence PPGGG is deleted in the mouse reference standard Kif12 sequence 82

4.1.7 Expression of KIF12 in Sf9 cells 85

4.1.8 Motor domain only Kif12 truncation is soluble 90

4.2 The role of KIF12 in ciliogenesis and primary cilia maintenance 92

4.2.1 Data from genome-wide ciliogenesis screens are consistent with a role for KIF12 but not conclusive 92

4.2.2 Evidence for KIF12 essentiality in cell viability is inconclusive 97

4.2.3 Analysis of IMCD3 cells growth and inhibition 99

4.2.4 Evidence for ciliogenesis in IMCD3 cells 99

4.2.5 Lack of robust induction of ciliogenesis by contact inhibition or serum starvation 100

4.2.6 Length of serum starvation has no effect on ciliation in IMCD3 cells 105

4.2.7 Docked basal bodies produce confounding signal for analysis of ciliogenesis 106

4.3 Characterisation of the *T. brucei* sp. kinesin 13 repertoire 113

4.3.1 *T. brucei* kinesin-13 gene sequences appear to be correctly defined 113

4.3.2 Tb-Kin13s are successfully expressed in Sf9 cells. . 115

4.3.3 *T. brucei* Kin13-1, -3 and -6 are soluble 116

4.3.4 Kin13-1, -3 and -6 can be purified using 1-step Nickel-affinity. 118

4.3.5 Kin13-3 causes slow depolymerisation of MTs 122

4.3.6 The depolymerisation assay fails to show Kin13-6 as a MT depolymeriser 124

4.3.7 Kin13-1 displays MT severing behaviour 125

5 Discussion 128

5.1 Expression and purification of recombinant protein 128

5.1.1 Human KIF12 129

5.1.2 *T. brucei* Kinesin-13 repertoire 134

5.2 Kinesin-mediated microtubule regulation 135

5.3 Essentiality of KIF12 in cilia function and cell viability 136

5.4 Inducing ciliogenesis in IMCD3 cells 137

5.5 *T. brucei* kinesin-13 motors differ in their interaction with microtubules 139

5.5.1 Katanin-like activity of Kin13-1 gives insight into possible chromosome segregation mechanism in *T. brucei* .. 139

5.5.2 *T. brucei* possesses extra-nuclear depolymerisers . 141

5.5.3 Kin13-6 does not regulate microtubule length 141
5.5.4 Limitations of the *T. brucei* kinesin-13 depolymerisation assays 141
5.6 Recommendations for future work 143
5.6.1 Characterisation of KIF12 143
5.6.2 Functional analysis of *T. brucei* kinesin-13s 143
6 Conclusions 146
7 References 147

List of abbreviations

6H	6 x Histidine
ADP	Adenosine diphosphate
ATP	Adenosine triphosphate
BB	Basal body
gDNA	Genomic DNA
GDP	Guanosine diphosphate
GFP	Green fluorescent protein
GTP	Guanosine triphosphate
HEK293	Human embryonic kidney 293 cells
IMCD3	Inner medullary collecting duct
ISR	Intron spanning reads
MCAK	Mitotic centromere-associated kinesin
MD	Motor domain
MT	Microtubule
P-loop	Phosphate-binding loop
PCM	Pericentriolar matrix
Sf9	*Spodoptera frugiperda* 9 cells
SOFA	Site of flagellar autonomy
TF	Transition fibres
TZ	Transition zone

1 Introduction

1.1 Cytoskeletal motors

Cytoskeletal motors are a group of proteins that convert chemical energy from ATP hydrolysis into mechanical work. Molecular motors interact with cytoskeletal structures to carry out their cellular functions. Cytoskeletal motors comprise three superfamilies of molecular motors: dyneins, kinesins and myosins; all of which are thought to have been present at the root of eukaryotes (Wickstead et al. 2010a). Despite this, it is only kinesins that are present in all eukaryotic organisms studied so far (Lawrence et al. 2001; Matsuzaki et al. 2004; Richards & Cavalier-Smith 2005).

All three motor superfamilies are ATPases harbouring a Walker A motif (P-loop), and are able to generate force by coupling ATP hydrolysis to conformational changes in their protein structure. The force generated enables these molecular motors to transport themselves and their bound cargo around the cell. Dyneins are part of the AAA+ superfamily (Kull et al. 1996), which, like kinesins, use MTs as their scaffold on which to travel, whilst myosins use actin filaments to move along.

Despite their similarities, dyneins, kinesins and myosins are not homologous to one another. The structure of the catalytic core (motor domain) in myosins and kinesins is much more similar than between themselves and dyneins, suggesting a common evolutionary origin, but they are not homologous (Amos & Cross 1997). Kinesins and myosin motor domains are much more comparable in molecular size and structure than dyneins (360aa and 400aa compared to 3000aa). Newly-found motors can be assigned to the appropriate superfamily through their motor domain.

Cytoskeletal motors fulfil wide-ranging functions throughout the cell, including muscle contractions (reviewed in Tyska & Warshaw 2002), transport of proteins and vesicles (Cole et al. 1998), and formation of spindle apparatus and the separation of chromosomes during mitosis and meiosis (Vaisberg et al. 1993; Tanenbaum et al. 2009).

1.2 Kinesins

1.2.1 Microtubules

To best introduce kinesins, and their cellular function, it would be prudent to first describe the scaffolding structures on which they work. Microtubules (MT), a major component of the eukaryotic cytoskeleton, are long and highly-dynamic tubular structures made up of protofilaments. Each protofilament consists of a head-to-tail arrangement of alpha-beta tubulin dimers. The consistent orientation of the alpha-beta tubulin dimers gives MTs polarity, which is very important to their biological function. The plus end possesses greater dynamism than the minus end (Figure 1).

Tubulin dimers have two bound nucleotides. Alpha tubulin is always bound to GTP. Beta tubulin is able to exchange GTP for GDP. During plus-end polymerisation, beta-tubulin present at the MT tip is bound to a single GTP molecule, which gives the dimer a straightened conformation. Dimers in this state bind stably to one another, creating a GTP-cap. At the MT tip, hydrolysis of GTP-bound beta tubulin to GDP causes a bent structure (Figure 1). These GDP-bound dimers at the tip are more likely to dissociate from the MT triggering "catastrophe" – rapid MT depolymerisation and shrinkage (Wang & Nogales 2005). This dynamic instability is crucial in the creation of cell-wide MT-networks.

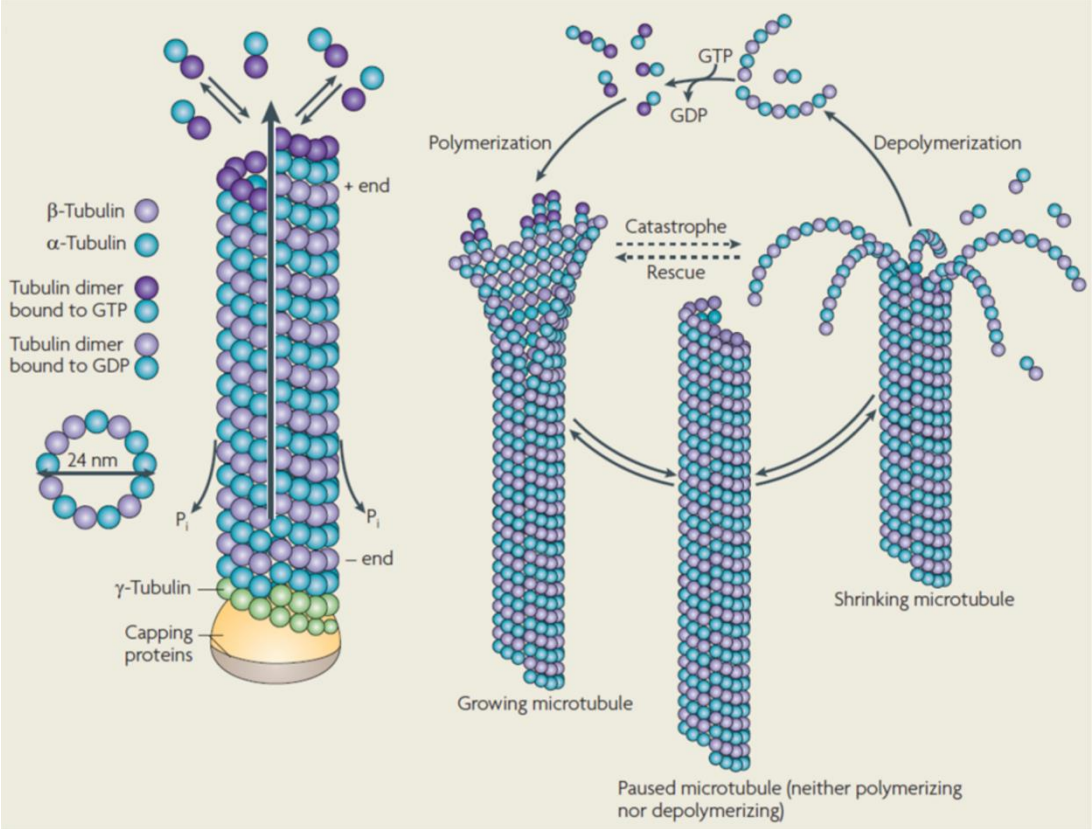


Figure 1. Microtubules: basic structure and dynamics (Conde & Cáceres 2009). MT structure during growth (polymerisation), shrinkage (catastrophe) and treadmilling states shows the change in protofilament conformation and GTP/GDP binding.

1.2.2 Kinesin architecture

Kinesins are made up of a highly conserved motor domain region, otherwise known as the "head", a more divergent "tail" region, and in some cases a "neck" region (Figure 2). The kinesin motor domain is the site of nucleotide binding and hydrolysis, with all kinesins studied (thus far) having four conserved motifs that are crucial in this function. These four motifs are the P-loop, Switch 1, Switch 2 and RXRP (otherwise known as N4). The phosphate binding loop (P-loop) binds the nucleotide (ATP) together with an associated Mg ion. Binding of the nucleotide causes the Switch 1 and 2 domains that flank the active site to close into a catalytically active configuration that allows for ATP hydrolysis. The RXRP motif forms the base of the nucleotide pocket (Kull et al. 1996).

The neck region has been defined in some kinesins where it is located between the motor and tail domains. The neck domain has been found in certain translocating kinesins to determine the motor polarity (Case et al. 1997; Endow & Waligora 1998).

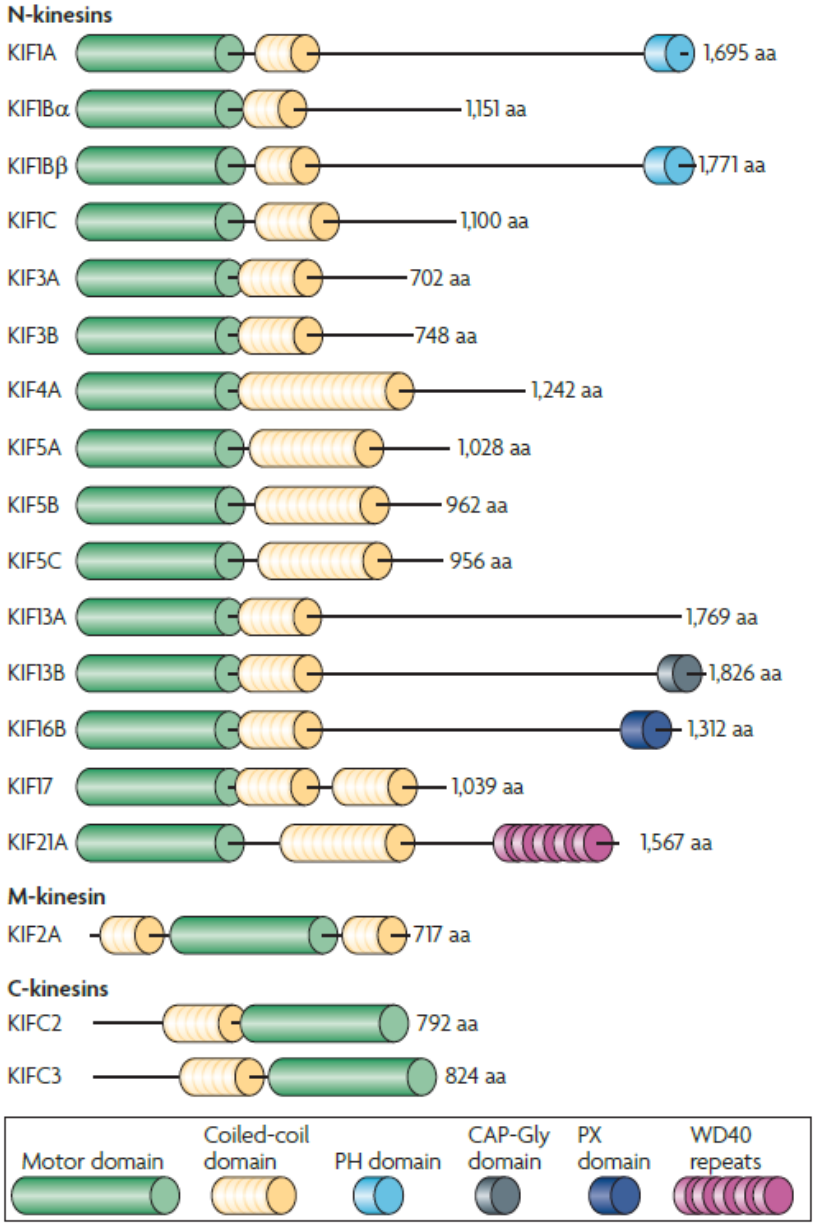


Figure 2. Motor protein domain architecture in a selection of mouse kinesins. Motors are grouped in terms of the position of the motor domain in relation to the rest of the protein. The grouping is determined by whether the motor domain is towards the C- or N-terminus, or if it is situated in the middle of the protein (C-kinesins, N-Kinesins and M-Kinesins respectively. The motor domain size is consistent regardless of the group (taken from Hirokawa et al. 2009).

The kinesin tail domain is far less conserved than the motor domain and is often predominantly comprised of long coiled-coil domains. The tail domain is responsible for allowing single motors to multimerise, and/or interact, with light chain proteins, cargoes or other macromolecules. The multimerisation of motor proteins through the tail allows kinesins to fulfil a wider range of functional capabilities within the cell. Kinesins with two or more motor domains are able to translocate along the MT filament for long distances without dissociating, thus allowing kinesins to work as part of the cells transport system. Examples of kinesin binding partners include vesicles (Kamal et al. 2000), chromosomes (Mazumdar et al. 2004) and organelles (Okada et al. 1995). The step-by-step mechanism of translocating kinesins allows tetrameric motor proteins, kinesins that possess four motor domains, to slide MTs past one another in an anti-parallel fashion. Kinesins, such as Cin8 (reviewed in Tytell & Sorger 2006), use this to control spindle formation during cell division.

When not bound to cargo, kinesins must closely regulate their activity in order to prevent unnecessary ATP hydrolysis and to free up MT tracks. Previous research has suggested that autoinhibition might be a general mechanism used to regulate motor activity (Coy et al. 1999; Friedman & Vale 1999). The proposed model suggests that in the absence of cargo binding, the tail region interacts with the motor domain in a manner that prevents nucleotide binding. This inhibition is only relieved in the presence of cargo for which the tail region has a greater binding affinity (Coy et al. 1999; Imanishi et al. 2006).

The direction of motor translocation is dictated by the position of the motor domain (MD) in relation to the rest of the protein (Figure 2). In general, N-terminal MDs are plus end-directed motors,

whereas C-terminal MDs are minus end-directed. Kinesins with centrally positioned MDs (M motors) cause destabilisation of the MT structure, rather than walking along the lattice (Verhey & Hammond 2009).

1.2.3 Microtubule regulators

Although the majority of kinesins function in the transport of cargo, nine of the 45 predicted kinesins encoded in the human genome are known to regulate MT dynamics (Figure 3; Sturgill & Ohi 2013). MT regulation predominantly works by promotion or prohibition of catastrophe, or acceleration of tubulin subunit addition (Figure 3), and aids cellular functions such as building and breaking up the mitotic spindle. Evidence of MT dynamics suppression as well as

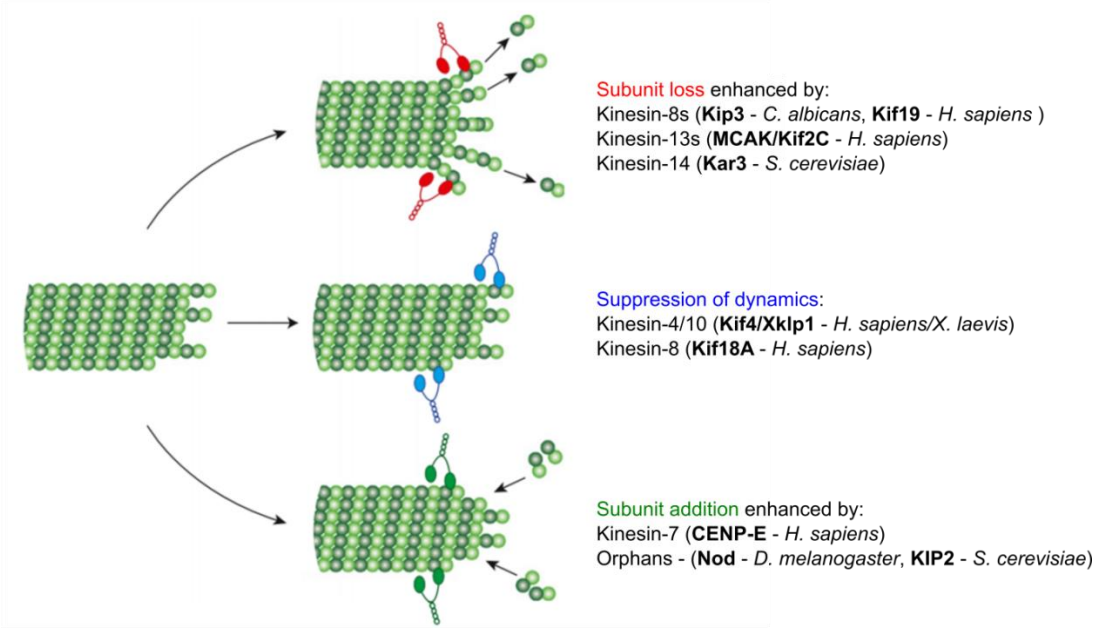


Figure 3. Microtubule-regulating kinesins. Regulatory kinesins can be conceptually partitioned into three classes: depolymerases (red) promote microtubule disassembly; pause factors (blue) suppress the inherent dynamicity of MTs; and elongases (green) promote MT assembly. Examples of depolymerases, pause factors and elongases are shown in black beneath the associated colour for each functional group (Kip3, Varga et al. 2006; Kif19, Niwa et al. 2012; MCAK/Kif2C, Hunter et al. 2003; Kar3, Sproul et al. 2005; Kif4, Hu et al. 2011; Xklp1, Castoldi & Vernos 2006; Kif18A, Stumpff et al. 2008; CENP-E, Sardar et al. 2010; KIP2, Hibbel et al. 2015). Taken and amended from Sturgill & Ohi (2013).

tubulin subunit loss enhanced by kinesins has been observed across eukaryotes (reviewed in Sturgill & Ohi 2013), but less so for the addition of tubulin subunits (CENP-E; Sardar et al. 2010). However, research has shown kinesin-enhanced MT polymerisation *in vitro* in the presence of Nod (*Drosophila melanogaster*; Cui et al. 2005) and KIP2 (*Saccharomyces cerevisiae*; Hibbel et al. 2015), providing evidence that MT polymerisers exist, at least *in vitro*.

1.2.3.1 Microtubule depolymerisers

Microtubule depolymerisers aid removal of tubulin subunits from the MT ends. This tends to be through promotion of a bent confirmation between tubulin dimer, which then leads to tubulin subunit loss (Figure 3). The most prominent examples of kinesin MT deploymerisers in the literature are KIF2A/B/C (*Homo sapiens*; Hunter et al. 2003; Manning et al. 2007) with Kip3 (*Candida albicans*), Kar3 (*Saccharomyces cerevisiae*) also highlighted as promoting shortening of the MT (Varga et al. 2009; Endow et al. 1994). Interestingly, this trio also represents examples of N- (Kip3), C- (Kar3) and M-motors (KIF2).

The best researched depolymerising kinesins are the human KIF2 subfamily – KIF2A/B/C; members of the kinesin-13 family. KIF2C, otherwise known as the mitotic centromere-associated kinesin (MCAK), is a homodimer that diffuses on the MT lattice rather than translocating (Helenius et al. 2006). This one-dimensional diffusion does not have a directional bias and therefore MCAK does not favour either of the MT ends for depolymerisation. MCAK recognises the MT end, that promotes nucleotide exchange driving MCAK into an ATP-bound state (Friel & Howard 2011), which is proposed to deform tubulin dimers, resulting in depolymerisation (Moores et al. 2002). Asenjo et al. (2013) solved the structure of a kinesin-13 in complex with a tubulin dimer and showed that three

secondary structural elements of the MT binding face (loop 2, loop 8 and the α4 helix), form a "crossbow-type tubulin bending mechanism". MCAK oversees the fidelity of MT-kinetochore attachment and chromosome movement. This ensures faithful segregation of chromosomes in mitosis, thus reducing the risk of aneuploidy, a characteristic of cancer cells (Maney et al. 1998; Walczak et al. 2002; Pihan & Doxsey, 2003).

Kip3 (*S. cerevisiae*), a dimeric plus-end directed motor, is highly processive. The motor continues to walk until it reaches the end of the MT and it binds strongly to the terminal tubulin dimer. Subsequent Kip3 motors reaching the MT terminus cause the endmost Kip3 motor to be bumped off, taking the tubulin subunit with it, thus causing a reduction in MT length. Kip3 depolymerises MTs in a length-dependent manner, depolymerising long MTs faster than short ones. The current model for the length-dependent manner in which it shortens the MT was proposed by Varga et al. (2006). Varga et al. (2006) suggest that the longer the microtubule, the more motors land on it, and therefore, because Kip3 is a highly processive motor, more motors reach the plus end of longer microtubules where they remove tubulin dimers.

Kar3, a minus-end directed motor, depolymerises taxol-stabilised MTs from the plus-end, when it is part of a heterodimer with the non-catalytic protein Cik1. Sproul et al. (2005) propose that Kar3-Cik1 is able to depolymerise MTs from the plus end because Cik1 targets Kar3 to the MT plus-end, and, once at the plus-end, the minus-end directed force of Kar3 depolymerises MTs with each tubulin-subunit release event coupled to one ATP turnover. However, in yeast species analysed to date, Kar3 is almost always present in cells that also express Kip3, a more prolific plus-end MT

depolymeriser. This brings into question whether the primary role of Kar3 is to depolymerise MTs in yeast.

1.2.4 Kinesin classification

Different naming schemes for kinesins have led to confusion and miscommunication. As the number of kinesins identified increased, the lack of a clear kinesin family classification made the process of naming and identifying previously defined kinesins unmanageable. The task of creating a naming system that dealt with all identified kinesins and kinesins with multiple names was initially investigated by Lawrence et al. (2004). The researchers involved in this project took the known kinesins and, on the basis of motor domain homology, sorted them into 14 distinct families. To gain the status of family, the group had to contain kinesin sequences from at least two kingdoms of eukaryotes.

Subsequent analysis of complete genomes taken across the eukaryotic domain by Wickstead et al. (2006, 2010a) showed amendments to the Lawrence et al. (2004) classification were required. Wickstead et al. (2010a) proposed a 15 family classification, following the same definition of a kinesin family as the classification by Lawrence et al. (2004). Greater sampling of sequences resolved the Kinesin-12 family into two new families; 15 and 16. A cross-kingdom kinesin clade was proposed as Kinesin-17 family, whilst their analysis brought together Kinesin-4 and -10 families into a single "Kinesin-4/10" family.

Orphan kinesin members are kinesins whose sequences have diverged so far that they are without detectible homologues in other kinesin families. This orphan group included both suggested MT polymerisers Nod and Kip2.

Amoebozoa
Holozoa
Fungi
Alveolata
Stramenopiles
Archaeplastida
Metamonada
Discicristates
Entamoeba histolytica
Dictyostelium discoideum
Monosiga brevicollis
Trichoplax adhaerens
Nematostella vectensis
Drosophila melanogaster
Apis mellifera
Caenorhabditis elegans
Capitella sp. I
Lottia gigantea
Strongylocentrotus purpuratus
Ciona intestinalis
Takifugu rubripes
Danio rerio
Gallus gallus
Homo sapiens
Schizosaccharomyces pombe
Saccharomyces cerevisiae
Neurospora crassa
Ustilago maydis
Rhizopus oryzae
Batrachochytrium dendrobatidis
Encephalitozoon cuniculi
Paramecium tetraurelia
Tetrahymena thermophila
Cryptosporidium parvum
Toxoplasma gondii
Theileria annulata
Plasmodium falciparum
Phytophthora sojae
Thalassiosira pseudonana
Phaeodactylum tricornutum
Aureococcus anophagefferens
Cyanidioschyzon merolae
Ostreococcus tauri
Chlamydomonas reinhardtii
Physcomitrella patens
Populus trichocarpa
Arabidopsis thaliana
Oryza sativa
Trichomonas vaginalis
Giardia lamblia
Naegleria gruberi
Leishmania major
Trypanosoma brucei
C
Kinesin-1
Kinesin-1A
Kinesin-1B
Kinesin-1C
Kinesin-1-X
Kinesin-2
Kinesin-2A
Kinesin-2B
Kinesin-2C
Kinesin-2D
Kinesin-2-X
Kinesin-3
Kinesin-3A
Kinesin-3B
Kinesin-3C
Kinesin-3D
Kinesin-3E
Kinesin-3-X
Kinesin-4/10
Kinesin-4/10A
Kinesin-4/10B
Kinesin-4/10C
Kinesin-4/10-X
Kinesin-5
Kinesin-6
Kinesin-6A
Kinesin-6B
Kinesin-6-X
Kinesin-7
Kinesin-8
Kinesin-8A
Kinesin-8B
Kinesin-8-X
Kinesin-9
Kinesin-9A
Kinesin-9B
Kinesin-13
Kinesin-13A
Kinesin-13B
Kinesin-13C
Kinesin-13-X
Kinesin-14
Kinesin-14A
Kinesin-14B
Kinesin-14C
Kinesin-14D
Kinesin-14-X
Kinesin-15
Kinesin-16
Kinesin-16A
Kinesin-16B
Kinesin-16-X
Kinesin-17
Kinesin-18
Kinesin-19
Kinesin-20

Figure 4. Distribution of ancient kinesin paralogues in 45 diverse eukaryotes. The presence or absence of paralogue(s) in a genome for a particular family is indicated by a filled or open circle respectively. Filled circles indicate the presence of full kinesin family members (dark blue) and subfamily paralogues (light blue; suffixed A, B, C, etc. beneath the family). Kinesins within a family, but outside of the well-supported subfamilies within that family, are suffixed "-X" (e.g. Kinesin-1-X). Taken from Wickstead et al. (2010).

1.2.4.1 Distribution of kinesin families in eukaryotes

The work by Wickstead & Gull (2006) highlights that the paralogue distribution of kinesins across eukaryotes strongly suggests that the last eukaryotic common ancestor (LECA) possessed nearly all extant kinesin families. However, there are many lineages that have lost kinesin families (Figure 4). No single kinesin family is 100% conserved, suggesting that, for the common kinesin-mediated cellular processes, there is functional overlap within the superfamily. For example, yeast do not possess the kinesin family, which includes the MT depolymerising Kif2 subfamily, but they possess Kip3 which carries out similar functions (Varga et al. 2006, 2009).

1.3 Cilia

The evolution of the cytoskeleton in eukaryotes has enabled them to carry out several cellular processes, including cilia-mediated motility (Wickstead & Gull 2011). Eukarotic cilia and flagella are membrane-bound, MT-based protrusions from the cell membrane. Despite undoubtedly playing a prominent role in cells harbouring the organelle, not all eukaryotic organisms possess cilia. Loss of cilia has occurred independently on multiple occasions; most notably in fungi and angiosperms (Hodges et al. 2012).

The terms cilia and flagella are not used interchangeably, despite being structurally identical. Distinctions are often made based on function and/or length (Haimo & Rosenbaum, 1981). Structures named as cilia in the literature tend to be short, present in

multiples within the cells, or harbouring an asymmetrical beat in motile cilia. Structures named as flagella tend to be longer than cilia, always motile, and usually one per cell. In this thesis, unless convention dictates otherwise, this organelle is referred to as the cilium.

1.3.1 Ciliary roles in cells

The role of cilia in eukaryotes is often dependent on whether it is immotile (primary cilia) or motile. Motile cilia help eukaryotic cells move, such as spermatozoa, or to move substrates, such as detritus along the lining of the lungs up towards the throat. Primary cilia, and most motile cilia, function as a sensory organelle for mechanical and chemical environmental cues that regulate cellular functions such as cell division. In metazoans, ciliary signalling is significant in developmental and homeostatic controls. The metazoan primary cilia possesses receptors for the Hedgehog, Wnt and platelet-derived growth factor signalling pathways (Plotnikova et al. 2009).

1.3.2 Motile vs immotile cilia

Motile and immotile cilia are both built on MT scaffolding found in both the basal body (BB) and axoneme (Figure 5; both described below). These structures are either MT triplets (BB) or MT doublets (axoneme). Both cilia types share the same triplet and doublet structures (Figure 6). Microtubule doublets are comprised of a complete A-tubule (13 protofilaments) and an incomplete B-tubule (10 protofilaments; Figure 6). These MT doublets, like standard MTs, possess polarity, with the plus end being the site of greater dynamism (Cassimeris et al. 1987). The MT doublets grow directly from the A and B templates provided by the BB MT triplets.

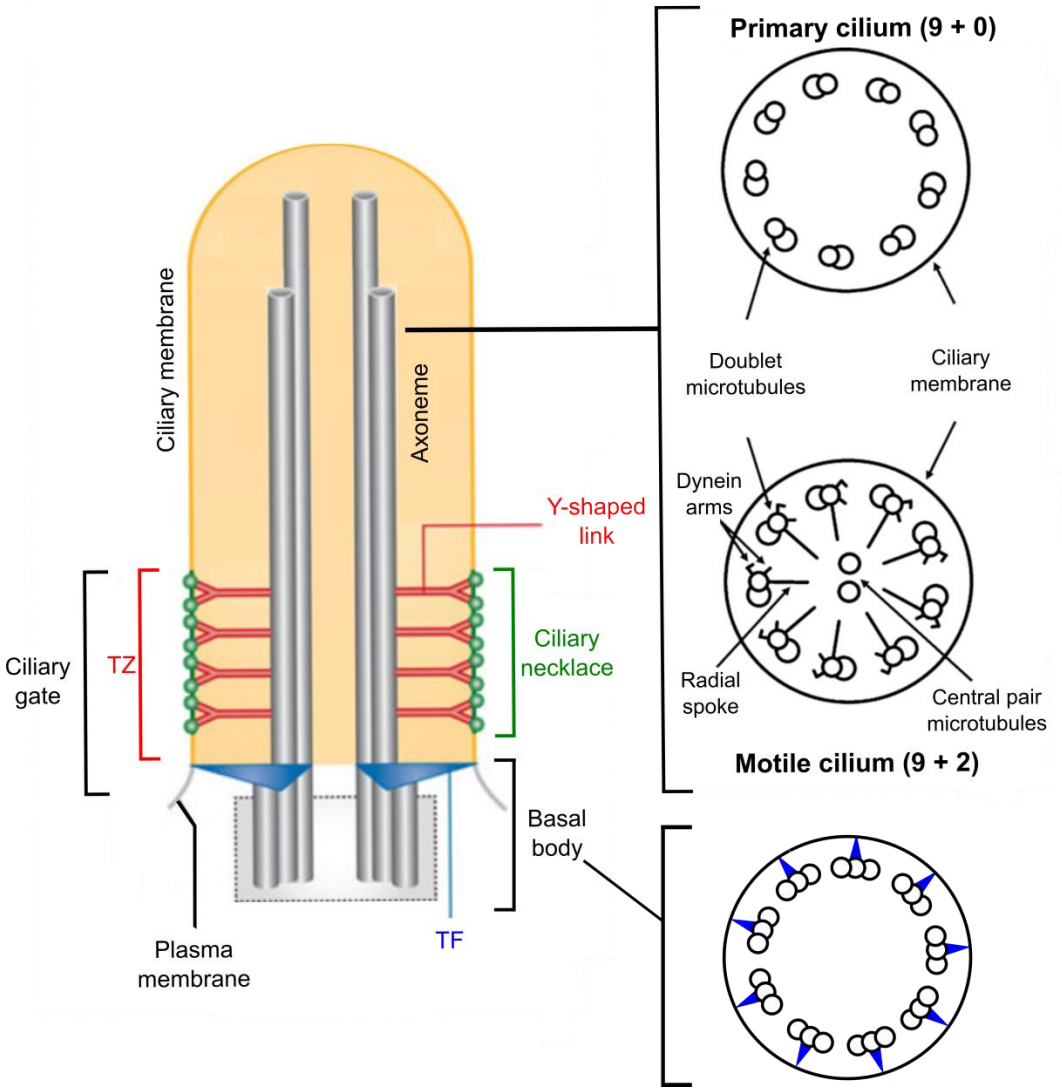


Figure 5. The canonical structure of mammalian primary cilia. The make-up of the mammalian primary cilia is shown through a longitudinal cross section. The microtubule-based axoneme emerges from the basal body (BB). The transition fibres (TF) allow the cilium to remain docked in the cell plasma membrane. Y-shaped proteins link the axoneme to the ciliary membrane. These Y-shaped links are decorated with proteins that form the ciliary necklace which can be observed on the outside of the organelle. Moving from the base to the tip, the region from the TFs to the end of the ciliary necklace is called the transition zone (TZ). The TZ, plus a small region of the BB, is the site of the ciliary gate, a diffusion barrier separating the cilium from the cytoplasm. The axoneme starts as a nine MT doublet structure nucleated from the BB triplet MT structure. The doublets all vary in size, with some becoming MT singlets towards the ciliary tip. If motile, the cilium will also contain a central microtubule pair (not shown in the cilia longitudinal section). Cross-sectional diagrams show views of the BB, and motile and primary cilia observed. The BB possesses nine triplet microtubules, each attached to a transition fibre. Motile cilia are characterized by the presence of motility-related structures such as pairs of dynein arms, radial spokes, and a central pair of microtubules. Primary cilia retain doublet microtubules but lack the motility-related features of motile cilia. Motile and primary cilia are both

bounded by a membrane that is continuous with the plasma membrane of the cell. Taken and amended from Deane & Ricardo (2012) and Reiter et al. (2012).

Motile cilia possess a central pair of MTs, along with the nine radial doublets (9 + 2), which allows for bending and thus propulsion through a substrate; whereas primary cilia lack this central pair (9 + 0)(Figure 5). The central MT pair are complete individual tubules rather than a doublet. As shown in Figure 5, motile cilia also possess dynein arms, motors permanently anchored to the A-tubules and directed towards the B-tubule of their next doublet MT in a clockwise radial direction (when looking base to tip), and radial arms. Both radial and Dynein arms are thought to be crucial in regulating axoneme motion (Gibbons & Grimstone 1960).

1.3.3 Ciliary structure

The ciliary structure described here is focused on that of the primary cilium.

1.3.3.1 The Basal body

When cells capable of building a cilium exit from the cell cycle, the centrosome – consisting of two centrioles (mother and daughter) embedded in a peri-centriolar matrix (PCM) – differentiates into a BB to initiate cilia formation (Kim & Tsiokas 2011). The BB docks to the cell membrane through their transition fibres (also known as distal appendages; Figure 5). The essential component of the BB is the mother centriole. The mother centriole, and thus the BB, harbours nine triplet MTs located toward the outskirts of the BB with ninefold symmetry (more details of the triplet MT structure shown in Figure 6). These nine triplet microtubules provide the template for the extension of other MT-based structures in the primary cilium. As a result, the position and orientation of the BB dictates the position and orientation of the cilium.

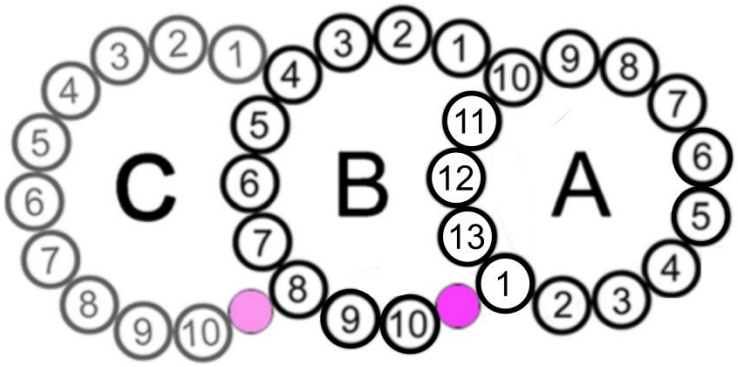


Figure 6. The structures of doublet and triplet microtubules. Basal body triplet microtubules are made up of A, B and C microtubules, with A being a complete tubule (13 protofilaments) and B and C being partially complete (10 protofilaments each). Microtubule doublets, that make up the axoneme, are made up of A and B tubules. Protofilaments are numbered according to convention (Linck & Stephens 2007). Tubules are partially joined by junctional proteins, A-B junctional protein shown in bright pink, B-C junctional protein shown in pale pink (Nicastro et al. 2006, 2011). Taken and amended from Linck et al. (2016).

1.3.3.2 Transition zone

The continuous region between the transition fibres of the BB and where the MT doublets are connected to the membrane via Y-shaped protein structures, is called the transition zone (Figure 5). The transition zone is proposed to function as a diffusion barrier for non-ciliary proteins (Kee et al. 2012; Nachury et al. 2010; Reiter et al. 2012; Rosenbaum & Witman 2002). The diffusion barrier or "ciliary gate" is helpful in compartmentalising and concentrating signalling proteins within the organelle (Garcia-Gonzalo & Reiter 2012; Reiter et al. 2012; Sang et al. 2011; Williams et al. 2011).

1.3.3.3 Ciliary gate

Organelles like the mitochondria or Golgi apparatus are membrane-bound and therefore possess a barrier between the organelle and the cytoplasm allowing for control over which proteins they allow to traverse that boundary. However, the cilium, is not fully membrane-bound, sharing a continuous membrane with the cell. Despite the lack of membrane boundary between cilia and the cytoplasm, there is a clear restriction of which substances are

permitted to cross into the organelle. In order to gain control over the contents entering and exiting, the cilium has a ciliary gate provided by a ciliary pore complex (CPC) that shares molecular and mechanistic properties with nuclear gating (Takao & Verhey 2016).

The gating system has to be sophisticated enough to not only filter through molecules, but also to adjust to proteins changing location in response to extracellular cues. This is crucial as mislocalisation of ciliary components leads to malfunction and, as a result, a wide range of diseases called ciliopathies. Evidence has been found for size-exclusion at the ciliary gate, with larger molecules required for ciliary function being facilitated through the gate by active transport, importins and Ran (G protein; Breslow et al. 2013; Dishinger et al. 2010; Fan et al. 2011; Kee et al. 2012). A ciliary localisation sequence (CLS), homologous to the nuclear localisation sequence (NLS), has been identified for proteins that function within the cilium and are recognised by transportin-1, a known ciliary barrier transporter (Dishinger et al. 2010). The importance of the ciliary gate is highlighted by the essentiality of many of its genes, whilst its morphology is highly conserved (Reiter et al. 2012; Wei et al. 2015).

1.3.3.4 Axoneme

The axoneme is the cytoskeletal scaffolding that provides the backbone to the organelle. It is made up of nine radial MT doublets that are extended from the A and B tubules of the BB triplet MT structure (Figure 6). The axoneme varies in length depending on the cilia or cell type, and the organism. Just like the cytoplasmic MT structures, the axoneme acts as the railway system enabling molecular motors to deliver or retrieve cargo along the "stalk" or the "tip". Due to the unsynchronised nature of MT dynamics the MT doublets will differ in length towards the apical end of the

axoneme. For the same reasons, at the ciliary tip it is likely that many of the "doublets" will have become singlet structures.

1.3.4 Ciliopathies

Diseases caused by defective ciliary function are known collectively as ciliopathies. The genetic basis of ciliopathies is simple, often caused by mutations in a single gene (reviewed in Badano et al. 2006). Proteins involved in ciliopathies are localised throughout the cilia structure including the BB, transition zone, axoneme and cytoplasm. Ciliated cells, and therefore ciliopathic diseases, are found in almost every organ in the human body, underlining their importance in system function. Over 100 genes have been implicated in ciliopathies (Song et al. 2016).

1.3.5 Polycystic kidney disease

Polycystic kidney disease (PKD) is an example of a ciliopathy disease. This genetic disorder causes the development of renal cysts which disurb kidney function. It is the cause of almost a tenth of end-stage renal disease cases seen each year (Tamparo & Carol, 2011). There are two types of PKD, autosomal dominant or autosomal recessive polycystic kidney disease (ADPKD and ARPKD, respectively). ADPKD is the more common of the two, with 1:500 live births suffering from the disease (Calvert & Grantham 2001). Genetic mutations in any of three genes cause a polycystic phenotype in the kidneys. These genes are PKD-1, -2 and -3, all of which encode primary cilia membrane polycystin membrane proteins (Kimberling et al. 1993; Peters et al. 1993; Reeders et al. 1985).

ARPKD is the less common of the two PKD types (1:20,000 live births; Zerres et al. 1998) but it impacts kidney function at a much earlier stage, with many sufferers having underdeveloped kidneys

at birth (Guay-Woodford et al. 1996). The genetic cause of ARPKD is linked to mutations in the PKDH1 gene (Zerres et al. 1994). A kinesin has been identified as a modifier gene for ARPKD in mouse models (Mrug et al. 2005).

1.4 The cilia cycle

Most cells that possess a primary cilium are terminally differentiated. Ciliated cells that are not terminally differentiated are required to dismantle and reassemble their cilia during the cell cycle in order to free up the centrosome, which has the dual cellular functions of microtubule organisation centre (MTOC) and the BB (Figure 7). As a result the cilia have a cycle that it follows through rounds of cell division and quiescence.

1.4.1 A cilia-centric view of the cell cycle

In most non-terminally differentiated cells that harbour a primary cilium, the dual use of the BB/centrosome means that there is periodic building and dismantling of the cilium synchronised with the cell cycle (reviewed in Kobayashi & Dynlacht 2011). In most animal cells G1 starts with disengagement of the centrioles (Figure 7), and if the cell exits the cell cycle (G0) the primary cilium can be built (Archer & Wheatley 1971). When the cell re-enters the cell cycle the cilia is disassembled to free the mother centriole and enable duplication of the centrosome. The centrosomes then function as the cells MTOC during mitosis.

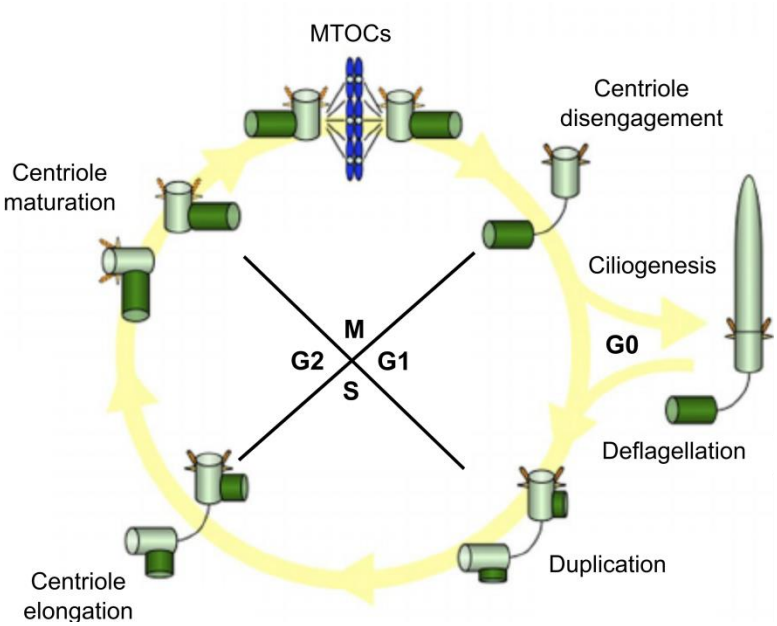


Figure 7. Centrosomes, cilia and the cell cycle in animal cells. In S phase the centrosome, comprised of a mother and daughter centriole, duplicates. During G2 the daughter centrioles elongate and mature in preparation for mitosis. During the M phase the centrosomes separate to opposite cell forms and organise the mitotic spindle through their role as microtubule-organising centres (MTOC). Post-cytokinesis (G1), the mother and daughter centrioles disengage. In quiescence cells the cell will exit the cell cycle entering G0. Here, ciliogenesis in initiated and the mother centriole/basal body docks to the plasma membrane. The primary cilium will persist in the cell until the cell exits the cell cycle. Once the cell is stimulated to re-enter the cell cycle, deflagellation occurs to allow the mother centriole/basal body to be duplicated. Taken and amended from Kobayashi & Dynlacht (2011).

1.4.2 Ciliogenesis

1.4.2.1 Different methods of building a primary cilium

Due to the lack of ciliary ribosomes, all ciliary proteins are made in the cytoplasm and transported to the cilia. As a result, two main methods have emerged for building cilia. One revolves around BB docking at the plasma membrane and delivery of all ciliary proteins to the ciliary compartment. From here, an additional and exclusive transport system within the cilia, intraflagellar transport (IFT) functions by taking those proteins to the desired location within the organelle (Sung & Leroux 2013; Bhogaraju et al. 2013). In a second much less common mechanism, cilia are built in an IFT-independent manner, whereby the cilia is built in the cytoplasm

and then put into place; known as cytoplasmic ciliogenesis. Cytoplasmic ciliogenesis has three distinctive advantages over the more common method of ciliogenesis: 1. the cilium can be assembled faster; 2. longer cilia can be produced; and 3. the building process takes place closer to the energy-generating mitochondria (Avidor-Reiss & Leroux 2015). Examples of cytoplasmic ciliogenesis have been found in *Plasmodium* sp. male gametogenesis, *Drosophila* sp. spermatozoa and mammalian spermatozoa (Sinden et al. 2010; Malicki & Avidor-Reiss 2014).

1.4.2.2 IFT-dependent/in situ ciliogenesis

Initiation of ciliogenesis begins with the attachment of Golgi-derived ciliary vesicles to the distal ends of the mother centriole (Sung & Leroux 2013). The mother centriole then differentiates into a BB and the distal appendages (a fibrous structure at the distal end of the mother centriole) mature into the transition fibres (TF). TFs enable the BB to dock into the cell membrane and mediate the movement of the molecules between the nascent organelle and the cytoplasm (Kobayashi et al. 2011; Bornens 2012).

Once the BB has successfully docked, extension of the ciliary axoneme ensues. Axonemal extension takes place solely at the MT plus end, with the Golgi-derived ciliary vesicles providing the necessary membrane components required to keep the extending axoneme membrane-bound (Sorokin 1962; Sung & Leroux 2013). The building blocks for extension are provided by IFT, detailed in greater depth below.

The cilium is a highly dynamic structure, with constant turnover of protein even when growth is complete (Marshall & Rosenbaum 2001). As a result, once built the cilium still requires plenty of maintenance to keep it functioning correctly. The delivery and

collection of materials, mainly tubulin, is carried out by components of the IFT system.

1.4.2.3 Deflagellation

Deflagellation is caused by severing of the axoneme at a specific site between the axoneme and the transition zone, called the site of flagellar autonomy (SOFA; Mahjoub et al. 2004). Lohret et al. (1998) discovered that the severing of the axoneme during deflagellation in *Chlomydomanos rheinhardti* was caused by katanin, which severs the outer MT doublets of the axoneme before the cell can commit to mitosis (Rasi et al. 2009). Cells lacking katanin are unable to release their BB and thus cannot undergo mitosis as they are MTOC deficient (Rasi et al. 2009).

1.5 Intraflagellar transport

In organisms that build their cilia *in situ*, the ciliary gate prevents free movement of molecules between the cytoplasm and the cilia. Since cilia do not possess ribosomes, a transport system is required to ferry in and out molecules across this diffusion barrier and against potential concentration gradients (Craft et al. 2015).

This transport system is called the intraflagellar transport system (IFT) and is driven by two opposing molecular motors, Kinesin-II and cytoplasmic dynein-2. The motors carry essential cargo for ciliary functioning such as BBSomes (Figure 8). BBSomes contain at least seven Bardet Biedl syndrome (BBS) proteins and BBIP10 (Figure 8; Lechtreck et al. 2009; Pazour et al. 2005).

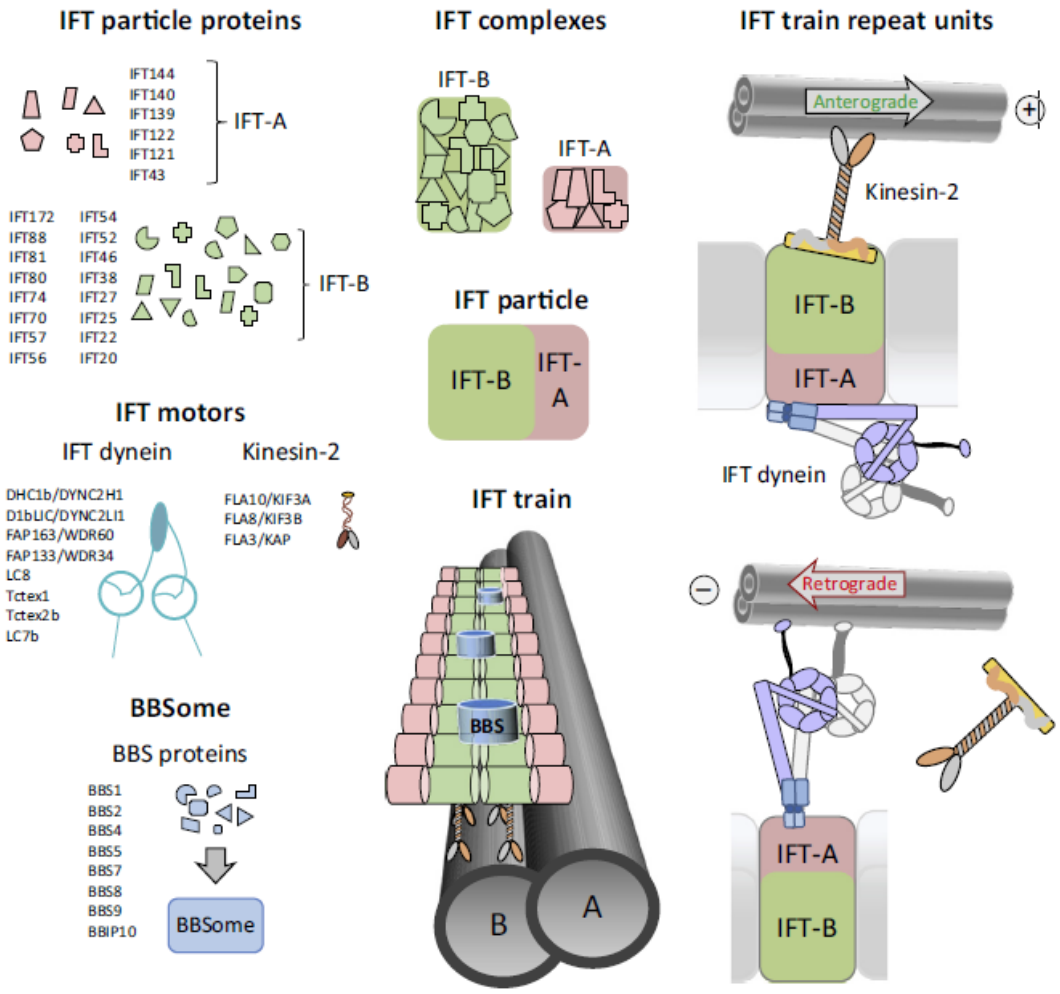


Figure 8. The building blocks of intraflagellar transport (IFT). IFT A & B complexes are comprised of IFT proteins. IFT A & B complexes join to form IFT particles, which, in turn, join up in large numbers to form IFT trains. Kinesin-2 motors are responsible for the anterograde transport of these trains, whilst retrograde transport of the trains is carried out by cytoplasmic dynein-2. These antagonistic motors carry each other as cargo, ensuring correct location for function. BBSomes, comprising at least seven Bardet Biedl syndrome (BBS) proteins, are transported to their functional locations by binding to the IFT trains and transported by the same method. Taken from Lechtreck (2015).

1.5.1 IFT motors

1.5.1.1 Anterograde motors

Anterograde transport (the movement from MT minus to plus end) in the cilia is carried out by Kinesin-2 (Figure 9). Animal kinesin-2 comes in two forms; heterotrimeric and homodimeric. Heterotrimeric Kinesin-II in humans is made up of Kif3a, Kif3b or c and an accessory protein Kinesin Associated Protein 3 (KAP3)

(Lippincott-Schwartz et al. 1995; Cole et al. 1998). Heterotrimeric Kinesin-II is essential for ciliogenesis in most studied organisms (Zhao et al. 2012), with the exception of *C. elegans* where homodimeric Kinesin-2 (OSM-3) is sufficient for ciliogenesis to successfully take place (Blacque et al. 2004). The essentiality of the kinesin-2 family in ciliary function is further supported by their absence in yeast and angiosperms, neither of which build cilia (Figure 4).

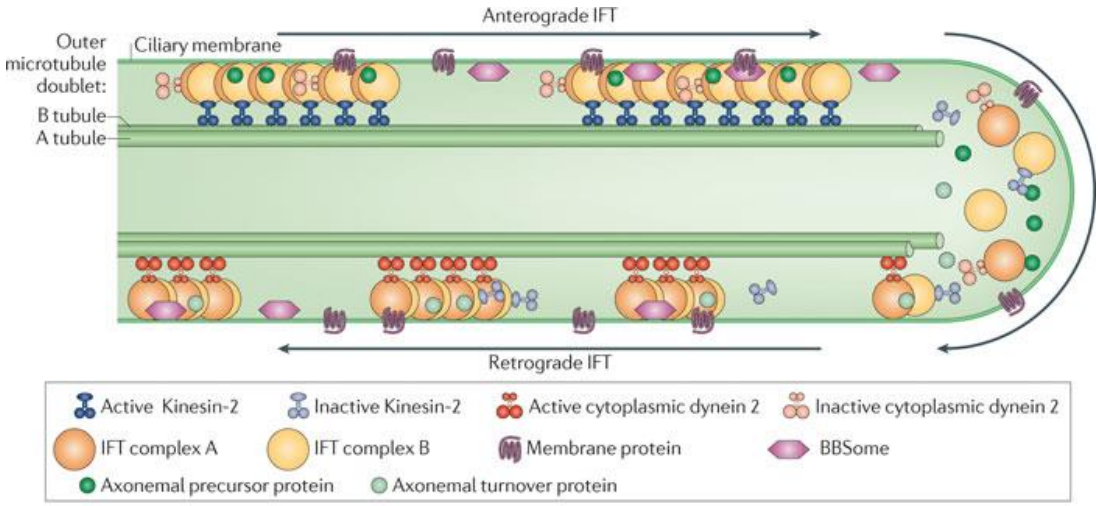


Figure 9. Intraflagellar transport within the primary cilium. Active heterotrimeric kinesin-2 transports cargo along the axoneme (MT doublet lattices) from the cilium base to the tip in anterograde IFT. The antagonistic retrograde IFT, performed by cytoplasmic dynein-2, involves the movement of substrates from the tip to the base. Cargo moved by these motors includes ciliary building blocks such as IFT complexes A & B, as well as membrane proteins involved in sensory functions. Modified from Ishikawa & Marshall (2011).

Interestingly, in *C. elegans* IFT depends on cooperation between OSM-3 and Kinesin-II to move cargo along the cilia. Prevo et al. (2015) identified a "handover zone" on the proximal axoneme whereby Kinesin-II passes cargo onto OSM-3. OSM-3 is more processive than Kinesin-II, and undergoes longer transport journeys. As mentioned previously, the functioning of *C. elegans* primary cilia is not dependent on Kinesin-II which raises the question why Kinesin-II has remained involved. Prevo et al.

(2015) propose that the handover zone acts like a relay changeover, enabling more rapid transportation of cargo.

1.5.1.2 Retrograde motors

Retrograde (MT plus end to minus end) trafficking is carried out by cytoplasmic dynein-2 which helps in bringing back cargo from the ciliary tip to the cell body (Figure 9; Wedaman et al. 1996). The cytoplasmic dynein-2 complex has four identified components: a heavy chain (DYNC2H1); a light intermediate chain (DYNC2LI1); a predicted intermediate chain (IC) repeat protein; and a light chain (LC) (Rompolas et al. 2007). Cytoplasmic dynein-2 has been found in almost all cilia-building eukaryotes studies to date. However, Wickstead & Gull (2007) identified two chromalveolate organisms with an IFT footprint, that do not possess cytoplasmic dynein-2.

Both anterograde and retrograde motors carry one another as cargo, ensuring that the motors are always present in the right location for correct functioning (Figures 8 and 9). The returning of motors back to their starting positions allows for frequent IFT cycles.

1.5.2 IFT particles

IFT particles function as packaging complexes for proteins essential for ciliary function. The packaging complexes that make up IFT particles are known as IFT complexes A and B. Between them they harbour 22 conserved IFT proteins, 16 in IFT-B, and 6 in IFT-A (Figure 8; Cole & Snell 2009; Taschner et al. 2012). Although IFT complexes A and B travel together as IFT particles (Figure 8), they do have distinct cellular roles. IFT-B binds directly with anterograde motors and is associated with harbouring ciliary precursors (Figure 8; Lechtreck, 2015). Non-functional IFT-B mutants caused defunct, or an inability to undergo, ciliogenesis

(Pedersen et al. 2008). The involvement of IFT-A in retrograde transport and recycling of ciliary components was shown in *Chlamydomonas* sp. harbouring temperature-sensitive IFT-A proteins. In cilia where the IFT-A proteins were heat-deactivated, ciliary defects specifcally appeared in retrograde transport. These defects included bulged membranes at the ciliary tip (Piperno et al. 1998). This is probably a result of a build-up of cargo that could not be transported out of the cilium.

IFT complexes are built from two pools situated at the ciliary tip and by the BB (Ahmed et al. 2008). Complexes built by the BB require anterograde IFT motors to take them across the ciliary gate, but complexes built at the ciliary tip require retrograde motors to transport them to the cell body. IFT-B complexes require IFT74 for bond stability at the BB IFT pool (Brown et al. 2015).

The loss of the cilium during cell differentiation enables IFT proteins to fulfil dual roles. Proteins such as IFT27 and IFT88 have been found to possess dual roles in the cilia, cytokinesis (IFT27; Qin et al. 2007) and cell cycle progression (IFT88; Robert et al. 2007).

1.5.3 IFT trains

IFT particles (IFT-A and IFT-B) travel in multi-particle complexes called an IFT train (Figure 8; Kozminski et al. 1993, 1995), travelling both to and from the ciliary tip (Bhogaraju et al. 2013; Craft et al. 2015). IFT trains exist in two categories, long and short. Long trains carry out the anterograde phase of IFT, whilst shorter trains are responsible for the retrograde phase (Figure 9; Pigino et al. 2009). The size of the IFT trains scales inversely with the length of the primary cilium (Engel et al. 2009).

IFT-A and B are weakly connected to one another, which allows for remodelling of the trains at either end of the cilia (Pedersen et al. 2008; Rosenbaum & Witman 2002). The remodelling process is assisted by kinases working at the tip (Buisson et al. 2013; Pedersen et al. 2006). Once unpacked, the proteins can localise to their functional sites (Wren et al. 2013). To ensure that these recently-released proteins are not repacked immediately by the newly assembled retrograde IFT trains, the retrograde trains may have a lower affinity for them. IFT trains are not restricted to release and rebinding at the ciliary tip, with these events also being observed along the MT doublet shafts (Craft et al. 2015; Wren et al. 2013).

As well as comprising essential IFT proteins, IFT trains are also packed with tubulin and other axonemal proteins during assembly. When the cilium is at full-length and in a steady state, the IFT trains still provide the axoneme tubulin, but they will have a reduced number of axonemal proteins (Craft et al. 2015; Wren et al. 2013). The mechanism for adjusting the quantity of cargo present in IFT trains was until recently unknown. Vannuccini et al. (2016) showed that long and short trains maintain their own length and structure throughout the entire regeneration process hinting that the function of each train is in some way tied to their ultrastructure. However, their second finding was that the relative abundance of long and short trains change during regeneration: long trains dominate early in cilia regeneration (ciliogeneis) and short trains dominate in full-length cilia. This suggests that although the length of the trains does not change throughout IFT, the regularity that anterograde and retrograde trains travel does change. In this way, the primary cilium is able to adjust the quantity of cargo depending on the phase the cilium is at.

In order to ensure that incompletely assembled IFT trains are not prematurely bound to anterograde IFT motors, IFT trains queue in order of stage of assembly at the ciliary base. These trains are then consecutively released into the cilium with tubulin loaded briefly before the train departs (Wingfield et al. 2017). This ensures that tubulin is present in all trains and therefore axoneme length can be maintained.

IFT trains move along the axoneme whilst remaining in contact with the ciliary membrane (Pigino et al. 2009). As both anterograde and retrograde trains will travel on the same MT doublets, it was unclear as to how the two train types were able to avoid collision. However, research by Stepanek & Pigino (2016) found that these trains were able to avoid each other by travelling on different tubules on the same doublet; the anterograde IFT trains move along the B-tubule, whilst the retrograde IFT trains move along the A-tubule. This shows that IFT motors are able to differentiate between the two tubule types found in the axoneme MT doublets.

1.6 Cilia-associated kinesins

Aside from the IFT motors, there are other kinesins known to function in cilia. Members of the Kinesin families 3, 4, 9 and 13 have distinct functions within the organelle in some organisms (Verhey et al. 2011).

1.6.1 Kinesin family 3

Kinesin-like protein 6 (KLP-6) is a translocating kinesin expressed in a small subset of ciliated sensory neurones, notably male-specific CEM in *C. elegans* (Peden & Barr, 2005). In *C. elegans* KLP-6 is an essential mediator of polycystin localisation and function in cilia (Peden & Barr, 2005; Barr & Sternberg, 1999).

Issues with polycystins, encoded for by PKD1 and PKD2 (Igarashi & Somlo, 2002), account for 95% of Autosome Dominant Polycystic Kidney Disease (ADPKD) in humans. KLP-6 also plays a role in modulation of IFT and Kinesin-II velocities, and acts as a positive regulator of cilia length extension (Morsci & Barr 2011).

1.6.2 Kinesin family 4/10

Mouse Kif7, a kinesin-4/10 family protein, is localised to the ciliary tip in mouse embryonic fibroblasts. Here it controls ciliary tip architecture, creating a single ciliary tip compartment (He et al. 2014). It is thought to achieve this through binding to the MT doublet plus-ends and controlling their dynamics. *In vitro* Kif7 binding to MT doublets reduced MT rate of polymerisation whilst increasing the rate of MT catastrophe (He et al. 2014). Kif7 is a crucial regulator of mammalian Hedgehog (Hh) signal transduction through the control of an upstream Hh regulator Gli-Sufu. Kif7 correctly regulates the activity of Gli-Sufu at the ciliary tip where the complex is enriched (Liem, 2009; Li et al. 2012). Despite being a molecular motor, Kif7 does not participate in transportation of Gli-Sufu, or Hh, to the ciliary tip. The mechanism with which Kif7 controls the activity of Gli-Sufu complexes is still unknown.

1.6.3 Kinesin family 9

KIF9A and KIF9B (members of the Kinesin-9A and 9B families, respectively) both localise in the *Trypanosoma brucei* flagellum (Demonchy et al. 2009). KIF9A, found exclusively in the axoneme, is crucial to functional motility of the flagellum. KIF9B localises to both the axoneme and the BB. KIF9B is essential in the assembly of the para-flagellar rod (a large extra-axonemal structure) and thus flagellar growth (Demonchy et al. 2009).

Chlamydomonas rheinhardtii KLP-1 (kinesin-9) is localised to the central axonemal doublet, regulating beat frequency of their motile cilia and assisting rotation and/or twisting of the central pair (Bernstein et al. 1994; Yokoyama et al. 2004).

1.6.4 Kinesin family 13

Many Kinesin-13s within the cilia have been characterised as regulators of axoneme length. This is in character with the regulation of MT dynamics by other kinesin-13s, such as MCAK.

1.6.4.1 KIF2A

Kif2A, part of the Kinesin-13 family and closely related to MCAK, is involved in the regulation of cilia length. KIF2A aids disassembly of the primary cilium by depolymerising MTs at the mother centriole (Miyamoto et al. 2015). KIF2A-deficient RPE1 cells were unable to disassemble their primary cilia when growth stimulated.

1.6.4.2 Crkinesin-13

Crkinesin-13 is associated with cilia shortening in *Chlamydomonas rheinhardtii* (Piao et al. 2009). Crkinesin-13 is deactivated by phosphorylation during ciliogenesis and then dephosphorylated when the cilia reaches its maximum length. Crkinesin-13 knockdown delayed shortening of the cilia. Crkinesin-13 is transported to the ciliary tip by IFT as cargo (Piao et al. 2009). No metazoan studies of Crkinesin-13 orthologues have been undertaken to date.

1.6.4.3 LmjKIN13-2

LmjKIN13-2 is a *Leishmania major* Kinesin-13 that localises to the cilium tip (Blaineau et al. 2007). Knocking down of LmjKIN13-2 or overexpression resulted in lengthening or shortening of the cilia, respectively.

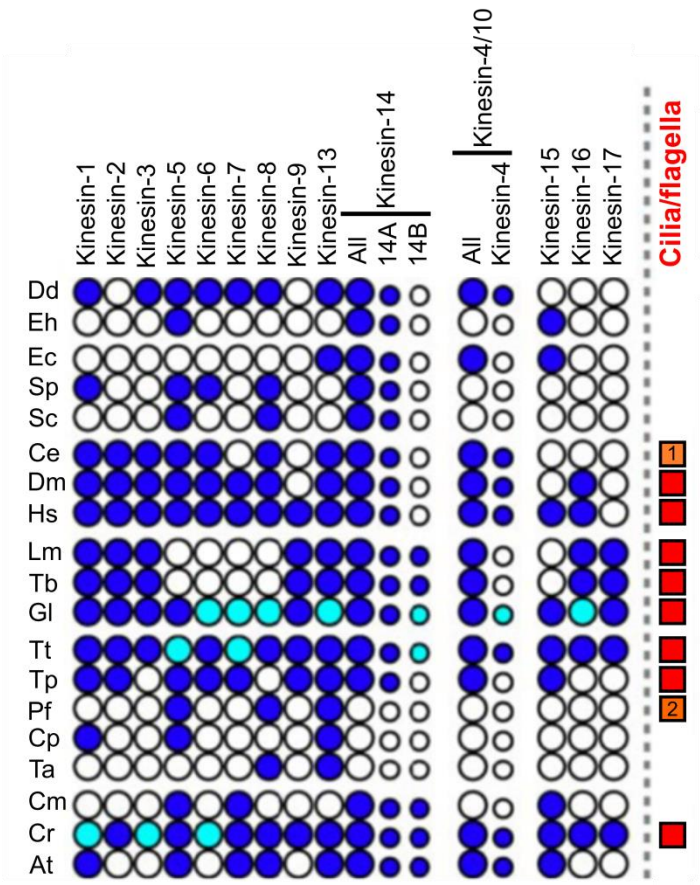


Figure 10. Distributions of kinesin families among eukaryotes. The taxonomic distribution of kinesin families can be used as an indicator of kinesin family function. The presence of a paralogue in an organism's genome is shown with a dark blue circle, the absence of a paralogue in an incomplete genome is shown in light blue, and the absence of a paralogue in a complete genome is shown as a white circle. Subfamilies are represented by smaller circles than families. Organisms that build cilia have a red/orange square in their row. Organisms with immotile cilia and those that build cilia in the absence of IFT apparatus are shown with a numbered orange box in their row (1 & 2, respectively). Prefixes are as follows: At, *A. thaliana*; Ce, *C. elegans*; Cm, *C. merolae*; Cp, *C. parvum*; Cr, *C. reinhardtii*; Dd, *D. discoideum*; Dm, *D. melanogaster*; Ec, *E. cuniculi*; Eh, *E. histolytica*; Gl, *G. lamblia*; Hs, *H. sapiens*; Lm, *L. major*; Pf, *P. falciparum*; Sc, *S. cerevisiae*; Sp, *S. pombe*; Ta, *T. annulata*; Tb, *T. brucei*; Tp, *T. pseudonana*; and Tt, *T. thermophila*. Figure is taken from Wickstead & Gull 2006.

1.6.4.4 KIF24

KIF24 is the second human kinesin-13 to be implicated in the regulation of the primary cilia. Kif24 localises to the mother centriole. From here, KIF24 interacts with centrosomal protein 110 (CP110) to remodel MTs and regulate ciliogenesis (Kobayashi et al. 2011). Loss of Kif24 from cells results in aberrant cilia assembly. As well as regulating ciliogenesis, KIF24 is also capable of

depolymerising MTs *in vitro* (Kobayashi et al. 2011). Activation of KIF24 is regulated by the kinase Nek2, ensuring it is deactivated during cell division (Kim et al. 2015).

1.7 Kinesin-16 family

The investigation into the patterns of kinesin evolution carried out by Wickstead et al. (2010a) highlighted the kinesin families associated with cilia-building organisms (Figure 10). Kinesin families 2 and 9 are only found in organisms that build cilia/flagella, strengthening the evidence that they primarily, if not exclusively, serve the functioning of that organelle (Figure 10; Wickstead et al. 2006, 2010a). This phylogenetic analysis also highlighted kinesin families 16 and 17 as potential contributors to cilia function due to their presence solely in cilia/flagella-building organisms.

1.7.1 KIF12

The suggestion that kinesin-16s play a role in generation and maintenance of cilia is supported by recent research focussed on the Kinesin-16 KIF12[1].

1.7.1.1 KIF12 is a polycystic kidney disease modifier gene

Mrug et al. (2005) identified KIF12 as a modifier gene for polycystic kidney disease (PKD) in a PKD mouse model. In this model, mice present with renal and biliary cysts akin to those seen in human PKD. The mouse model (B6) harbours a mutation in its cystin gene (Cys1cpk) that encodes for a truncated protein compared with the wild type (Hou et al. 2002; Yoder et al. 2002). When B6 was crossed with the CAST/Ei mouse line, individuals

[1] KIF12 is a mammalian kinesin 16 family member, not to be confused with "kif12", a kinesin-6 family member found in *Dictyostelium* sp.

screened for Cys1cpk homozygous presented varying expression and severity of disease caused by genetic background.

The severity of renal and biliary disease was only weakly correlated in the PKD mouse model crosses (Mrug et al. 2005). Genome scanning identified a major effect quantitative trait loci (QTL) complex for renal severity, and Kif12 was highlighted as the most probable modifier gene present. Kif12 alleles from B6 and CAST/Ei mouse strains were sequenced. CAST/Ei Kif12 contains an additional five amino acids compared with B6 Kif12. CAST/Ei possesses the additional PPGGG, predicted to be in loop-2 of the kinesin catalytic domain.

CAST/Ei x B6 mice presented with more severe PKD in individuals harbouring the CAST/Ei Kif12 allele compared with the B6 Kif12 allele (Mrug et al. 2005). Kif12 strain-specific haplotypes and Kif12 expression levels strongly correlated with renal disease severity in these intercross mice.

Further evidence for Kif12 as a PKD modifier gene has been provided by KIF12 localisation to the primary cilium in mouse kidney cells (IMCD3 cells; Mrug et al. 2015). This is the same location as Cys1, and most genes involved in renal cystic disease (Guay-Woodford et al. 2000). Kif12 and Cys1 expression in the IMCD3 mouse kidney cell line are closely correlated (Mrug et al. 2015).

1.7.1.2 HNF-1 transcription factor regulates Kif12 expression

Hepatocyte nuclear factor-1 (HNF-1) is a transcription factor that regulates expression of genes in the kidney, liver and the pancreas (Gong et al. 2009). Kif12 is a target gene of HNF-1 (Gong et al. 2009). HNF-1 mutations can lead to renal cysts, potentially as a result of uncontrolled Kif12 expression.

1.7.1.3 KIF12 is involved in antioxidant signalling

KIF12 has been shown to mediate an antioxidant cascade in beta cells as an intracellular target of excess fat intake (Yang et al. 2014). Yang et al. (2014) showed KIF12 knockout mice suffered from hypoinsulinemic glucose intolerance attributed to a higher level of beta cell oxidative stress. KIF12s involvement in the signalling cascade is as a scaffold for a transcription factor within the pathway.

In summary, KIF12 is a member of a kinesin family solely associated with cilia-building organisms. KIF12 has been identified as a PKD modifier gene and localises to the primary cilium. PKD disease severity varies and is dependent on the Kif12 allele expressed in the kidney. Allelic differences in Kif12 occur within the kinesin catalytic domain, potentially perturbing ATPase function. Its involvement in renal cystic diseases is further supported by its regulation by a kidney, liver and pancreas specific transcription factor (HNF-1).

In light of this research it is tempting to hypothesise that KIF12 functions within the primary cilium, and more specifically, by interacting with membrane-bound proteins such as cystin. KIF12 involvement in antioxidant signalling does not conflict with this hypothesis as many kinesins have dual cellular roles, nor does it preclude the possibility of antioxidant signalling taking place in the primary cilia.

1.8 Kinesin-13 family diversity

The kinesin-13 family is comprised of three subfamilies (Figure 11; Wickstead et al. 2010a). The Kinesin-13B subfamily, home to human KIF2A, B and C (MCAK), is the most extensively researched. The roles of KIF2, and homologues, have been clearly

defined (outlined below), but the Kinesin-13 family is extremely diverse with much of it unexplored.

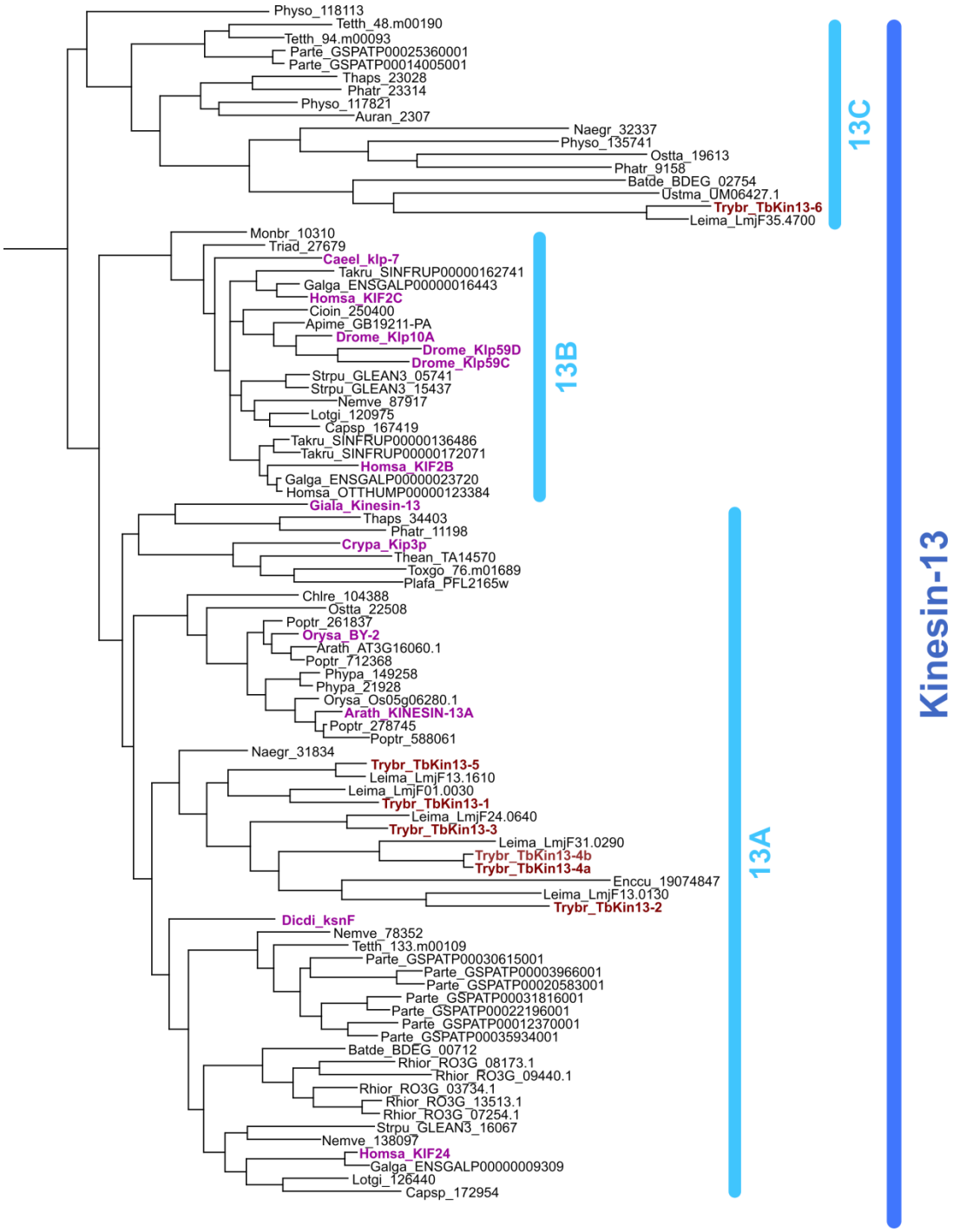


Figure 11. Phylogenetic analysis of Kinesin-13 family members. The phylogenetic tree shows Kinesin family 13 is divided into three subfamilies (13A, 13B and 13C). Protein sequence names that have been altered from their genome ID to a common name are highlighted (magenta). *Trypanosoma brucei* Kinesin-13s are emboldened and highlighted (red). Prefixes: Apime: *Apis mellifera*; Arath: *Arabidopsis thaliana*; Auran: *Aureococcus anophagefferens*;

Batde: *Batrachochytrium dendrobatidis*; Caeel: *Caenorhabdatis elegans*; Capsp: *Capitella* sp.; Chlre: *Chlamydomonas reinhardtii*; Cioin: *Ciona intestinalis*; Crypa: *Cryptosporidium parvum*; Dicdi: *Dictyostelium discoideum*; Drome: *Drosophila melanogaster*; Enccu: *Encephalitozoon cuniculi*; Galga: *Gallus gallus*; Giala: *Giardia lamblia*; Homsa: *Homo sapiens*; Leima: *Leishmania major*; Lotgi: *Lottia gigantea*; Monbr: *Monosiga brevicollis*; Naegr: *Naegleria gruberi*; Nemve: *Nematostella vectensis*; Orysa: *Oryza sativa*; Ostta: *Ostreococcus tauri*; Parte: *Paramecium tetraurelia*; Phatr: *Phaeodactylum tricornutum*; Phypa: *Physcomitrella patens*; Physo: *Phytophthora sojae*; Plafa: *Plasmodium falciparum*; Poptr: *Populus trichocarpa*; Rhior: *Rhizopus oryzae*; Strpu: *Strongylocentrotus purpuratus*; Takru: *Takifugu rubripes*; Tetth: *Tetrahymena thermophila*; Thaps: *Thalassiosira pseudonana*; Thean: *Theileria annulata*; Toxgo: *Toxoplasma gondii*; Triad: *Trichoplax adhaerens*; Trybr: *Trypanosoma brucei*; Ustma: *Ustilago maydis*. Taken and amended from Wickstead et al. (2010a).

The Kinesin-13A subfamily is believed to be the ancestral subfamily (Wickstead, Gull, et al. 2010a). Whilst, thus far, Kinesin-13B motors have been found to be similar in their cellular roles, mitotic spindle associated, Kinesin-13A harbours more variety. The variety of cellular roles carried out by Kinesin-13As include regulation of ciliogenesis (KIF24, described above; Kobayashi et al. 2011), deflagellation, and mitotic MT dynamics (both *Giardia lambia* "kinesin-13"; Dawson et al. 2007).

1.8.1 Characterised Kinesin-13 members

1.8.1.1 KIF2

Despite the high similarity in both sequence and ability to regulate MT dynamics, KIF2A, KIF2B and MCAK fulfil distinct cellular functions. MCAK localises to the tips of growing MTs, the spindle poles and kinetochores (Moore et al. 2005; Wordeman & Mitchison 1995). MCAK has minimal impact on bipolar spindle assembly or chromosome movement up to metaphase (Maney et al. 1998), but is crucial for the fidelity of chromosome segregation (Kline-Smith et al. 2004). MCAK carries out this role by destabilising inappropriate MT attachments at kinetochore (Wordeman et al. 2007).

Unlike MCAK, KIF2A is essential for both bipolar spindle assembly and chromosome movement (Ganem & Compton 2004). HeLa cells lacking KIF2A are unable to form bipolar spindles, instead forming monopolar spindles. Ganem & Compton et al. (2004) showed that KIF2A depolymerises spindle pole MTs at their minus ends, making a small contribution in chromosome migration towards the poles.

KIF2B largely localises to the centrosomes and midbodies, and to a lesser extent to the kinetochores and spindle MTs (Manning et al. 2007). U20S cells deficient in KIF2B are unable to form organised spindles, and although chromosome attachment is monitored correctly, the velocity of chromosomes migrating to the poles is greatly decreased. The importance of KIF2B localisation to the midbody is exhibited by cytokinesis failure in KIF2B deficient cells (Manning et al. 2007).

1.8.1.2 AtKinesin-13A & B

Arabidopsis thaliana motors Atkinesin-13A and Atkinesin1-13B are members of the Kinesin-13A subfamily. Atkinesin-13A is a MT depolymeriser and is involved in the movement and distribution of Golgi apparatus in plant cells (Folkers et al. 2002; Oda & Fukuda 2013a, 2013b). Atkinesin-13A and Atkinesin-13B regulate cell size with null mutants for either forming larger petals with larger cells (Fujikura et al. 2014). Double mutants display embryonic and developmental defects not seen in single mutants. This suggests that the two motors possess some redundant functions (Fujikura et al. 2014).

1.8.1.3 KLP-7

KLP-7 is in the "animal specific" Kinesin-13B subfamily. It is the sole Kinesin-13 member found in *C. elegans* and, like MCAK, is thought to regulate kinetochore-MT attachments during mitosis (Connolly et al. 2015). KLP-7 is responsible for maintaining spindle

tension in the *C. elegans* acentrosomal oocyte meiosis (Connolly et al. 2015). Also like MCAK, KLP-7 activity is regulated by an aurora kinase (Han et al. 2015).

1.8.2 The extended *T. brucei* Kinesin-13 repertoire

Trypanosoma brucei is a unicellular parasitic kinetoplastid. Due to its divergence near the root of the eukaryotic domain, it is frequently used as a model organism to gain insight into ancestral organisms. It possesses a flagellum that is essential for motility, cell division and morphogenesis, as well as a sensory role in cell-cell interactions (Rotureau et al. 2009). The flagellum contains a canonical 9 + 2 microtubular axoneme (Figure 5).

Trypanosomes lack homologues for kinesin families associated with mitosis, families 4, 5, 6, 7 and 8 (Berriman et al. 2005; Wickstead et al. 2006; Wickstead et al. 2010a). This has raised the possibility that other kinesin families present in *T. brucei* have become more diverse in their cellular function. *T. brucei* possesses an expanded catalogue of Kinesin-13s, representing both 13A and 13C subfamilies. *T. brucei* has seven Kinesin-13 motors in total (TbKin13-1, -2, -3, -4a, -4b, -5 and -6; Wickstead, Gull, et al. 2010a), TbKin13-4a and -4b are likely to be a recent gene duplication. TbKin13-1 to -5 are members of the Kinesin-13A subfamily, whilst Kin13-6 is the sole 13C representative (Figure 11).

Computational analysis of the *T. brucei* genome suggests that the six *T. brucei* 13As are a result of gene duplications from a single Kinesin-13 ancestor of Trypanosomes (Wickstead et al. 2010a). Predicted protein structures, along with on average only ~35% primary sequence level similarity between the TbKin13As, suggest that they fulfil differing cellular roles (Wickstead et al. 2010b). TbKin13-1 is localised within the nucleus throughout the cell cycle

(Wickstead et al. 2010). During mitosis TbKin13-1 is spread evenly across the mitotic spindle. Cells deficient in TbKin13-1 possess defects in both spindle dynamics and chromosome segregation (Wickstead et al. 2010b; Chan et al. 2010). TbKin13-2, an orthologue of the previously mentioned LmjKin13-2, is localised to the flagellar tip, but only has a limited effect on flagellar length in the procyclic stage of the *T. brucei* life cycle (Wickstead et al. 2010; Chan & Ersfeld, 2010). The remaining *T. brucei* Kinesin-13s are largely localised in the cell body and do not associate with the mitotic spindle (Wickstead et al. 2010b, Lambacher et al. 2015; Janke et al. 2002).

2 Aims

For this project, my research goal is to identify novel roles for kinesin families with a specific interest in those functioning within the primary cilium. The kinesin families focused on are Kinesin-16 and -13. A ciliary role for Kinesin-16s is indicated by their presence solely in organisms that build cilia/flagella (Figure 4). Ciliary roles for Kinesin-16s have been supported by research showing human KIF12 to be a modifier gene for PKD (Mrug et al. 2005), that it is present in the primary cilia of IMCD3 cells (Mrug et al. 2015) and that it has a more substantial impact on cilia function than known genes essential in ciliogenesis and/or maintenance (Wheway et al. 2015).

The Kinesin-13 family is comprised of three subfamilies (Wickstead et al. 2006). Two of these families (13A and 13B) have members that are involved in ciliary functioning and maintenance. Kinesin-13Bs, in particular Kif2A/B/C, have been more extensively researched than the other subfamilies. Only a few 13A members have been investigated, whilst the roles of 13C members are completely unknown.

T. brucei provides an excellent model for studying the cellular roles of Kinesin-13A and -13C. The organism possesses an extended selection of Kinesin-13s, with six 13A motors and one 13C motor. This large collection of Kinesin-13s begs the question 'why are they needed, and do the motors have distinct roles?' The absence of a 13B means that motors involved in spindle regulation in *T. brucei* will differ from metazoans, as perhaps will the method by which they regulate it. The study of these motor proteins may highlight novel roles for Kinesin-13 proteins.

In this research I aim to:

- Characterise the motor–MT interactions *in vitro* of human KIF12 and the *T. brucei* Kinesin-13s.

- Identify preferential motor binding sites (end or lattice) on the MT and whether the motors move along the MT lattice by translocation or diffusion.

- Investigate the impact ciliogenesis has on KIF12 expression dynamics and location.

- Examine KIF12 essentiality in both cilia function and cell viability.

- Study the impact, if any, of a five amino acid (PPGGG) deletion on KIF12 function.

3 Materials and Methods

3.1 Expression and protein purification of rsKif12 and rsKif12MD

3.1.1 PCR amplification of *rsKif12* and *rsKif12MD* and insertion into a cloning vector

The *rsKif12* open reading frame was cloned by PCR using oligonucleotides 5'- GGG GAG CUA TGC AGA GGA CCT TCG C -3' and 5'- GGG GAA CUT CAA TGG GGA GGG AGG -3', whilst the *Kif12MD* truncation was cloned using oligonucleotides 5'- GGG GAG CUA TGC AGA GGA CCT TCG C -3' and 5'- GGG GAA CUT TAC TGA GCT CGG CT GCA TA -3'. PCR was carried out in a final volume of 50µl containing 10ng pCMV6-XL5-rsKif12, 1 x DNA polymerase buffer, 2.5 units Pfu Cx turbo DNA polymerase, 0.4µM forward and reverse primer, 0.2µM dNTPs. The PCR assay was carried out with an initial denaturation at 95°C for 5 mins, 16 cycles of 95°C for 10 secs, 56°C for 10 secs and 72°C for 2 mins, then held at 72°C for 3 mins. Both amplified *rsKif12* and *rsKif12MD* DNA sequences were each cloned into pFB5- and pFB8-USER plasmids using the USER cloning method described in Nour-Eldin et al. (2006). The motor domain region was defined by sequence alignment to previously annotated Kif2C (MCAK). Correct orientation was confirmed by sequencing.

3.1.2 Expression of rsKif12 using the baculovirus expression system

0.5mg of cloning vector (pFB5-rsKif12 and -rsKif12MD and pFB8-rsKif12 and -rsKif12MD) transformed into DH10Bac *Escherichia coli* cells and recombinant bacmids were isolated. Bacmids were transfected into Sf9 insect cells using Escort® IV transfection reagent (SIGMA L-3287). P1 virus produced from the Sf9 transfection cultures was harvested and used to inoculate Sf9

expression culture. The methods involved in the baculovirus expression system are outlined in greater detail in Jarvis (2009).

Expression of GFP-tagged rsKif12 and rsKif12MD in Sf9 cells was confirmed using fluorescence microscopy. Samples were observed on a Zeiss Axiovert 100S inverted microscope fitted with a 10x objective, and images were captured using Axiovision 4.8 software and an Axiocam CCD camera with equal exposure settings and no prior illumination. Images were processed with identical pixel thresholds (minima and maxima); performed in ImageJ (Schneider et al. 2012).

Expression cultures were incubated at 27°C for 70 hours before cells were harvested and resuspended in MCAK lysis buffer (50mM HEPES pH7.5, 150mM NaCl, 5% (v/v) glycerol, 0.1% (v/v), TWEEN 20, 1mM $MgCl_2$, 1mM EGTA) in a 1:2 (w/v) ratio and frozen in liquid nitrogen.

Expression levels of both GFP and non-GFP tagged rsKif12 and rsKif12MD in Sf9 expression cultures was confirmed by SDS-PAGE and immunoblotting performed by standard methods, using dimonoclonal mouse α-GFP (0.4µg/ml; Roche) and HRP-conjugated Goat α-mouse secondary antibody (5µg/ml; Sigma) for the GFP-tagged samples and α-6x His tag® antibody (a rabbit polyclonal HRP conjugate; 20µg/ml; Abcam) for all 6xhis tagged samples.

3.1.3 Two-step protein purification by cation exchange and nickel affinity chromatography

Frozen cells from expression cultures resuspended 1:2 (w/v) in lysis buffer (50mM HEPES pH7.5, 150mM NaCl, 5% (v/v) glycerol, 0.1% (v/v) TWEEN 20, 1.5mM $MgCl_2$, 3mM EGTA, 1mM DTT and 0.5mM MgATP, 50mM CaCl, 1% nonidet P40 and 10U/ml Benzonase [Sigma]) and the following protease inhibitors:

Leupeptin (50µg/ml; Fisher), Pepstatin A (0.7µg/ml; Sigma), PMSF (18µg/ml; Life Technologies) and E64 (30µg/ml; Sigma). Lysates sonicated for 3 x 20 secs at 15 amplitude microns and twice passed through the French press (8,000 psi) prior to 60 mins centrifugation at x48,000g. The resulting cleared lysate was passed through a Cation exchange column (GE Healthcare Life sciences – 1 ml HiTrap SP HP).

The cation exchange column was washed many times with Cation exchange buffer (20mM HEPES.KOH pH7.5 and 1.5mM $MgCl_2$). Each wash included NaCl that was increased in concentration by 50mM with each wash, ranging between 200mM and 600mM, and a final elution step of 1.5M NaCl.

Selected fractions were ran through a Nickel-affinity column (GE Healthcare Life sciences – 1 ml His Trap HP), and washed and eluted in Nickel-affinity buffer (50mM Tris.HCl pH7.5, 300mM NaCl, 10% (v/v) glycerol, 1mM $MgCl_2$) with 9mM and 300mM Imidazole respectively.

Protein samples were resolved by SDS-PAGE on a 12% polyacrylamide gel and stained with instant blue (Expedeon) for 45 mins.

Additional purification attempts (outlined in the Results section) used amended cell lysis (of expression culture cell stocks) methodology. In independent experiments the lysis buffer was amended to contain the following: 50mM CaCl, 0.005% (v/v) nonidet P40, and 250U Benzonase.

3.2 Expression of *rsKif12* in mammalian cell lines

3.2.1 Construction of cloning vectors

rsKif12 and *rsKif12MD* were cloned into pCMV-GFP using the USER cloning method (Nour-Eldin et al. 2006).

3.2.2 Transfection and expression of *rsKif12* and *rsKif12MD*

HeLa cells were transfected with pCMV-rsKif12-GFP and pCMV-rsKif12MD-GFP using Fugene® 6 (Promega) at a ratio of 3:1 transfection reagent (µl):DNA (µg) and incubated at 37°C for 24 hours. HEK293 cells were transfected using the same method as that used for HeLa cells. Cells were incubated for 48 hours before being harvested. Both cell types were grown in Dulbecco's Modified Eagle's medium (DMEM; SIGMA-ALDRICH).

Live HeLa cells were imaged and captured using Axiovision 4.8 software associated with a Zeiss Axiovert 100S inverted microscope fitted with a 10x objective and an Axiocam CCD camera. Images were captured with equal exposure settings and no prior illumination. Images were processed with identical pixel thresholds (minima and maxima); performed in ImageJ (Schneider et al. 2012).

3.2.3 rsKif12 and rsKif12MD solubility in mammalian expression systems

Both HeLa and Hek293 cells lysed with RIPA buffer (Tris.HCl 50mM, NaCl 150mM, EDTA 1mM, 1% (v/v) Triton-100, 0.1% SDS and 5mg/ml Sodium deoxycholate) in the presence of Leupeptin (50µg/ml), Pepstatin A (0.7µg/ml), PMSF (18µg/ml) and E64 (30µg/ml) for 20 mins at 4°C. Lysate centrifuged at x200g for 5 mins, the resulting soluble and insoluble fractions resolved by SDS-PAGE and immunoprobed with a dimonoclonal mouse α-GFP (0.4µg/ml; Roche) and HRP-conjugated Goat α-mouse secondary antibody (5µg/ml; Sigma) performed by standard methods.

3.3 Expression and purification of KIF12 and Kif12ΔPPGGG

3.3.1 Identification of KIF12

Multiple Kif12 sequences were aligned using MAFFT version 7 (Katoh et al. 2002) and presented using Jalview 2.8.1.

Identification of human KIF12 using intron spanning reads outlined in the Results section.

3.3.2 Construction of KIF12 and Kif12ΔPPGGG cloning vectors

The start codon of the *KIF12* and *Kif12ΔPPGGG* coding sequences and the following ~450 nucleotides downstream (with *Kif12ΔPPGGG* having the 15 nucleotides encoding the PPGGG region removed) were synthesised as gBlocks. The gBlock sequences were codon optimised for expression in *Spodoptera frugiperda*. The gBlocks were inserted immediately upstream of the *rsKif12* start codon (in frame) in the pCMV-XL5-rsKif12 to create pCMV-XL5-KIF12 and pCMV-XL5-Kif12ΔPPGGG (see Figure 26).

KIF12 and *Kif12ΔPPGGG* open reading frames were cloned using oligonucleotides 5'- GGG GAG CUA TGG AAG AAC GCG GGT CA -3' and 5'- GGG GAA CUT CAA TGG GGA GGG AGG A -3' for N-terminal tagging, or 5'- GGG GAA CUA TGG GGA GGG AGG ACT -3' for C-terminal tagging. The PCRs were carried out in a final volume of 50µl containing 0.5 ng pCMV6-XL5-KIF12 or pCMV-XL5-Kif12ΔPPGGG, 1 x DNA polymerase buffer, 2.5 units Pfu Cx turbo DNA polymerase, 0.4µM forward and reverse primer, 0.2µM dNTPs. The PCR assay was carried out with an initial denaturation at 95°C for 5 mins, 20 cycles of 95°C for 10 secs, 55°C for 10 secs and 72°C for 2.5 mins, then held at 72°C for 5 mins. Both amplified *KIF12* and *Kif12ΔPPGGG* DNA sequences were each cloned into pFB5- and pFB8-USER plasmids using the USER cloning method described in Nour-Eldin et al. (2006).

3.3.3 Transfection into insect cells and expression

pFB5- and 8- KIF12 and -Kif12ΔPPGGG constructs were transfected, expressed and imaged in the same manner as described for rsKif12 and rsKif12MD.

3.3.4 Protein purification of KIF12 and Kif12ΔPPGGG

Separation of expressed KIF12 and Kif12ΔPPGGG protein samples into insoluble (pellet) and soluble (cleared lysate) fractions carried out in an identical manner to rsKIF12 and rsKIF12MD. KIF12-GFP was 2-step protein purified by cation exchange and Nickel-affinity chromatography, for methodology see "Expression and protein purification of rsKif12 and rsKif12MD" section.

3.4 Expression and purification of Kif12MD

Kif12MD was amplified from pCMV-XL5-KIF12 by PCR using oligonucleotides: 5'- GGG GAG CUA TGC AGA GGA CCT TCG C -3' and 5'- GGG GAA CUC TGA GCT CGG CTT GCA TA -3'. The PCRs were carried out in a final volume of 50µl containing 0.5 ng pCMV6-XL5-KIF12, 1 x DNA polymerase buffer, 2.5 units Pfu Cx turbo DNA polymerase, 0.4µM forward and reverse primer, 0.2µM dNTPs. The PCR assay was carried out with an initial denaturation at 95°C for 5 mins, 20 cycles of 95°C for 10 secs, 55°C for 10 secs and 72°C for 2 mins, then held at 72°C for 5 mins. Amplified Kif12MD was cloned into pFB5, 8 and 10 USER plasmids using the USER cloning method described in Nour-Eldin et al. (2006).

Kif12MD was then cloned, transfected, expressed and purified as outlined for rsKif12 and rsKif12MD.

3.5 Induction of ciliogenesis in IMCD3 cells

3.5.1 IMCD3 growth culture

IMCD3 cells were cultured at 37°C, 5% CO_2 in Dulbecco's Modified Eagle's medium (DMEM):Ham's F12 nutrient mixture (F12) (GIBCO).

3.5.2 IMCD3 growth curve

The growth curve of IMCD3 was recorded by counting the total number of cells in a $1cm^2$ area for five randomised locations and finding the mean for each time point. Measurements were taken consistently over a 250 hour period.

3.5.3 Ciliation of IMCD3 cells

3.5.3.1 Fixation

IMCD3 cells were grown in culture to contact inhibition (t = 0h). Once contact-inhibited cell were either fixed immediately or starved of Foetal Bovine Serum (FBS) for 24 hours. Cells were fixed in -20°C methanol.

3.5.3.2 Immunostaining of ciliated cells

IMCD3 samples were treated with blocking buffer (0.1% fish gelatine [SIGMA], 0.02% TWEEN and 0.2% Bovine Serum Albumin [BSA] in PBS) and then immunostained with mouse α-acetylated β-tubulin primary antibody (4µg/ml; Sigma – mouse monoclonal – T6793) and TRITC conjugated Goat α-mouse IgG primary antibody (50µg/ml; Sigma), counterstained with DAPI and mounted in DABCO.

3.5.3.3 Fluorescence microscopy

Images were captured on a BX51 microscope equipped with a 100× UPlanApo objective (NA 1.35; Olympus) and CoolSnap-HQ (Photometrics) camera. All images of fluorescent proteins were captured at room temperature with equal exposure settings and no prior illumination. Images for level comparison were also processed in parallel with the same alterations to minimum and maximum display levels. Analysis was performed in ImageJ (Schneider et al. 2012).

3.5.4 Inducible system for ciliogenesis in IMCD3 cells

Seeding densities and serum starvation of IMCD3 cells for induction of ciliogenesis in IMCD3 cells experiments is outlined in the Results section.

3.5.4.1 Immunostaining

IMCD3 cells were fixed and immunostained, as detailed above.

3.5.4.2 Microscopy

Images were captured on a Leica DMIRE2 microscope equipped with a Hamamatsu Orca ER-C4742-80 camera. All images of fluorescent proteins were captured at room temperature with equal exposure settings and no prior illumination. Images for level comparison were also processed in parallel with the same alterations to minimum and maximum display levels. Analysis was performed in ImageJ (Schneider et al. 2012).

Images of the fixed IMCD3 cell samples were captured at a range of focal depths moving up towards the apical end of the sample by 0.5µm each image.

3.5.4.3 Cilia counts

Cilia counts from these experiments were from cell populations in multiple randomly chosen fields of view. Cilia counts were completed using the cell counter function on ImageJ.

3.5.4.4 Characterisation of "dot" and "long" signal profiles from IMCD3 fluorescence microscopy

Images of the fixed IMCD3 cell samples captured at a range of focal depths were compiled into a "Z-stack" and turned from a display of XY axes, to XZ to enable visualisation of signal along the z axis. This was performed using ImageJ.

3.6 Expression and purification of *T. brucei* Kinesin-13s

T. brucei Kinesin-13s were amplified by PCR from *T. brucei* genomic DNA (gDNA) using oligonucleotides. *Kin13-1*: 5'-GGG GAG CUA TGG CGA AGT GGG AAT TAA AG-3' and 5'-GGG GAA CUA ATC CCG TTT TGC TCG AG-3'; *Kin13-2*: 5'-GGG GAG CUA TGA CCT CAC TCT GTC C-3' and 5'-GGG GAA CUC ACG CTT TCA AGT TCA TGA-3'; *Kin13-3*: 5'- GGG GAG CUA TGA ATA ATA GCC GCA TTT GC -3' and 5'- GGG GAA CUA TTG CGT CTC TTC ATG GAA-3' ; *Kin13-4b*: 5'-GGG GAG CUA TGC AGA AAA GTA TAC AAG ATG AAG-3 and 5'-GGG AAC UGT TTT GTT GCT GTT GTA TTT GAC-3'; *Kin13-5*: 5'-GGG GAG CUA TGG AGC GAC AGC TTC G-3' and 5'-GGG GAA CUT TGC CGA GAC TCC AGG-3'; *Kin13-6*: 5'-GGG GAG CUA TGC CCA ACA TAC CGT TAG-3' and 5'- GGG GAA CUT CTC CTC TGC GTA GCA-3'. The PCRs were carried out in a final volume of 50µl containing 50ng gDNA (*T. brucei*), 1 x DNA polymerase buffer, 2.5 units Pfu Cx turbo DNA polymerase, 0.4µM forward and reverse primer, 0.2µM dNTPs. The PCR assay was carried out with an initial denaturation at 95°C for 5 mins, 20 cycles of 95°C for 10 secs, 52°C for 10 secs and 72°C for 2.5 mins, then held at 72°C for 5 mins. Amplified Kin13-1, -2, -3, -4b, -5 and -6 were each cloned into pFB5, 7, 8 and 10 USER plasmids using the USER cloning method described in Nour-Eldin et al. (2006).

The *T. brucei* Kinesin-13s were then cloned, transfected, expressed as outlined for *rsKif12* and *rsKif12MD*. Different concentrations of imidazole were used for the purification of *T. brucei* Kinesin-13s than outlined for rsKif12 and rsKif12MD during the Nickel affinity purification step. The Nickel affinity column was washed with 70mM imidazole, eluted in 200mM imidazole and collected in 0.5ml fractions.

3.7 Characterisation of *T. brucei* Kinesin-13s interaction with microtubules

3.7.1 Depolymerisation assay

Porcine MTs were grown in a solution consisting of the following: 2µM porcine tubulin (25% rhodamine labelled), 1xBRB80, 1mM MgCl2 and 1mM GMPCPP in a final volume of 50µl. The MTs were incubated on ice for 5 minutes and then at 37°C for 2 hours. The solution was then diluted 1 in 9 with BRB80, centrifuged and the pellet resuspended in 200µl BRB80.

Microscope chambers were constructed with 18mm x 18mm and 22mm x 22mm coverslips separated by double-sided tape (Scotch 3M) to create channels 0.1mm thick, 3mm wide and 18mm long. Glass coverslips (no. 1.5; Corning) were cleaned in Piranha solution (H_2O_2/H_2SO_4, 3:5) before silanization in 0.05% dichlorodimethylsilane in trichloroethylene. To immobilize microtubules, channels were incubated with 0.2% Tub 2.1 antibody in BRB80 for 5 min, followed by 5 min with 1% Pluronic F-127 in BRB80, and finally GMPCPP microtubules in BRB80 for 15 min. Channels were rinsed with BRB20 (20mM PIPES-/KOH pH6.9, 1mM $MgCl_2$,1mM EGTA) before addition of the imaging solution (BRB20 supplemented with 75mM KCl, 0.1mg/ml BSA, 1mM ATP, 1% 2 mercaptoethanol, 40mM glucose, 40mM g/ml glucose oxidase, 16 μgml^{-1} catalase, and the *T. brucei* Kin13 protein sample; Helenius et al. 2006).

3.7.2 Recording of MT - Kinesin-13 interaction

Depolymerisation assays were recorded through microscope Leica DMIRE 2 on camera Hamamatsu Orca ER-C4742-80 using Volocity 6.3. Images were taken every 5 secs for 20 mins. The rate of depolymerisation is calculated from the average shrinkage over

this time period in at least 10 MTs per sample. Image analysis was carried out using ImageJ and calculation of depolymerisation rate using IGOR Pro 6.0.3.1. Statistical significance of rates of depolymerisation were calculated using pair-wise comparisons of the Kin13 sample vs. no protein control in IGOR Pro 6.0.3.1.

3.7.3 Microtubule cleavage events

MT cleavage events were calculated by observing the number of breakages in a randomly selected field of MTs when exposed to a given Kinesin-13 sample during the depolymerisation assay. The lengths of MTs were calculated in ImageJ. The graphic was produced in Graph Pad Prism 7.0.

4 Results

4.1 Characterisation of human Kif12

To characterise the human RefSeq reference standard kif12 (rskif12) *in vitro* (interaction with MTs and rate of ATP turnover), production of recombinant protein would be required. In order to achieve this, *kif12* would need to be identified from the NCBI database, inserted into an expression construct, expressed in an appropriate expression system, and purified so that the isolated protein can be characterised free from contaminants. The results from these steps are detailed in the sections below.

4.1.1 Reference standard human Kif12 is insoluble in the baculovirus expression system.

Human *rskif12* and a motor domain-only truncation (*rskif12MD*) were inserted into expression vectors containing 6 x histidine (6H) or 6H-eGFP N-terminal tags (Figure 12). These constructs were transfected together with an MCAK-6H-GFP containing expression vector, into Sf9 cells through lipofection (protocol outlined in Materials and Methods). In addition a construct containing MCAK-6H-GFP was used as a positive control as it is routinely and successfully expressed by our research group at using this method of transfection.

Using the expression of GFP as an indicator of transfection success, the transfection cultures showed ~50% of cells were successfully transfected with 6H-GFP-rskif12 compared with ~90% for MCAK-6H-GFP (Figure 13). Only 5-10% of cells showed evidence of GFP fluorescence in 6H-GFP-rskif12MD, lower than the other two samples. However, the percentage of successfully transfected cells is not an accurate measure for total protein yield as the levels of

recombinant protein synthesis within a cell are not measured, but it does act as a translational control.

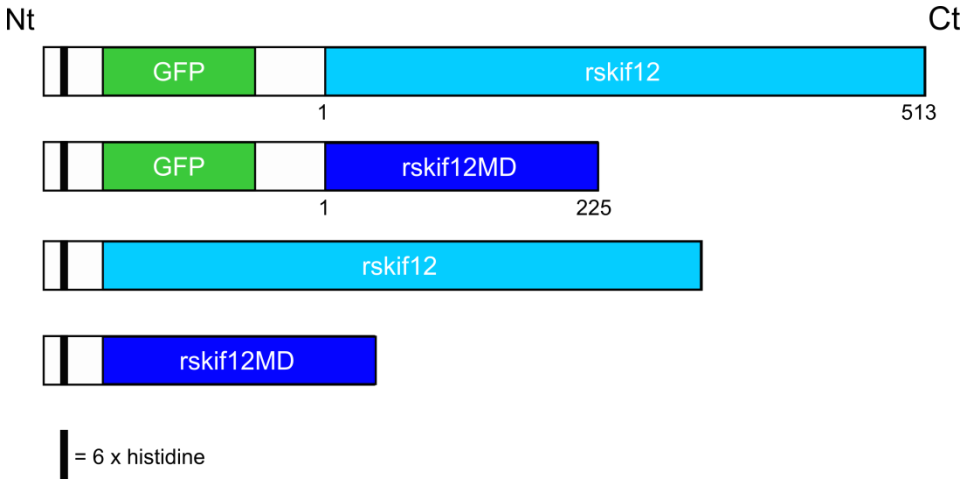


Figure 12. Tagged rskif12 and rskif12MD protein constructs. Both kif12 proteins are tagged at the N-terminal with six histidine residues allowing for purification by Nickel-affinity chromatography, as well as an additional GFP tag allowing for detection via microscopy. The numbers beneath the Kif12 proteins denote the amino acid residue. The motor domain (MD) of rskif12 was established by comparisons with the Kif5B (kinesin 1 family) motor domain sequence.

To examine total rskif12 protein expression in Sf9 cells, the relative protein yields were measured by immunoblotting. Transfected cell lysates were separated by SDS-PAGE, transferred to nitrocellulose membrane and probed with antibodies against the 6His tag and (where present) against the GFP tag (Figure 14). These immunoblots showed that neither 6H-rskif12 nor 6H-rskif12MD were expressed to a detectible level when probed with the α-His antibody. However, 6H-GFP-rskif12 was successfully expressed, although at roughly half to a third of the yield of MCAK, which was again used as a positive control for the reasons previously stated. The expression of 6H-GFP-rskif12MD is less clear as the signals produced in the sample at the expected molecular weight match additional bands seen in the 6H-GFP-rskif12 profile when probed with anti-GFP. The result from the immunoblotting experiment showed that the GFP tagged proteins were the most promising to

take forward for purification due to the failure to detect expression of 6H only tagged recombinant protein.

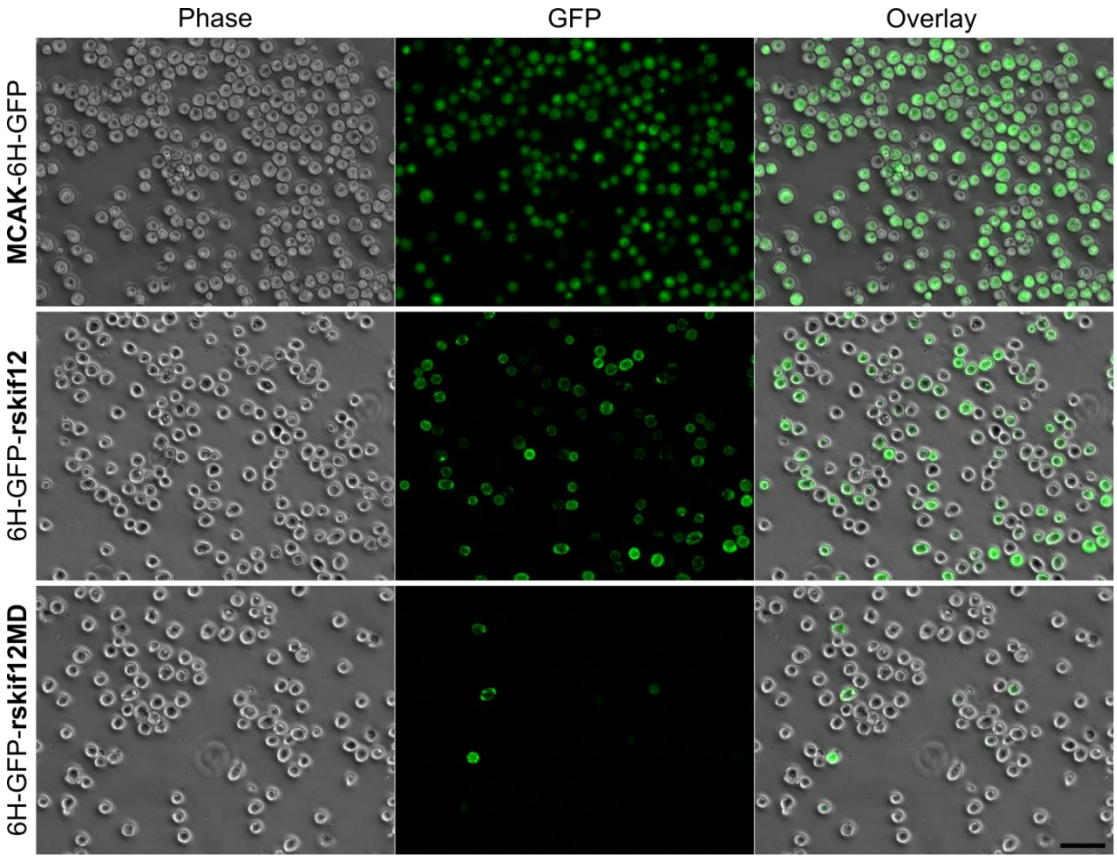


Figure 13. Sf9 transfection with baculovirus containing GFP-rskif12 and rskif12MD, respectively. Both phase contrast and GFP fluorescence micrographs are shown in addition to overlays of both these images. MCAK-6H-GFP was used as a positive control. Scale bar represents 50μm.

4.1.2 Expressed recombinant GFP tagged rskif12 and rsKif12MD cannot be successfully purified due to insolubility

To carry out the depolymerisation assay (outlined in Materials and Methods), purified protein is required. To obtain rskif12 and rsKif12MD, the Sf9 cells were lysed using detergent (Tween) and the lysate was separated into soluble and insoluble fractions by centrifugation (protocol outlined in Materials and Methods). The designed two-step protocol for protein purification comprises cation exchange followed by Nickel-affinity chromatography. Cation exchange was used as the motor domain region of kinesins is

generally positively charged, whilst Nickel-affinity was used as the expression constructs have an added 6x histidine tag. A 2-step

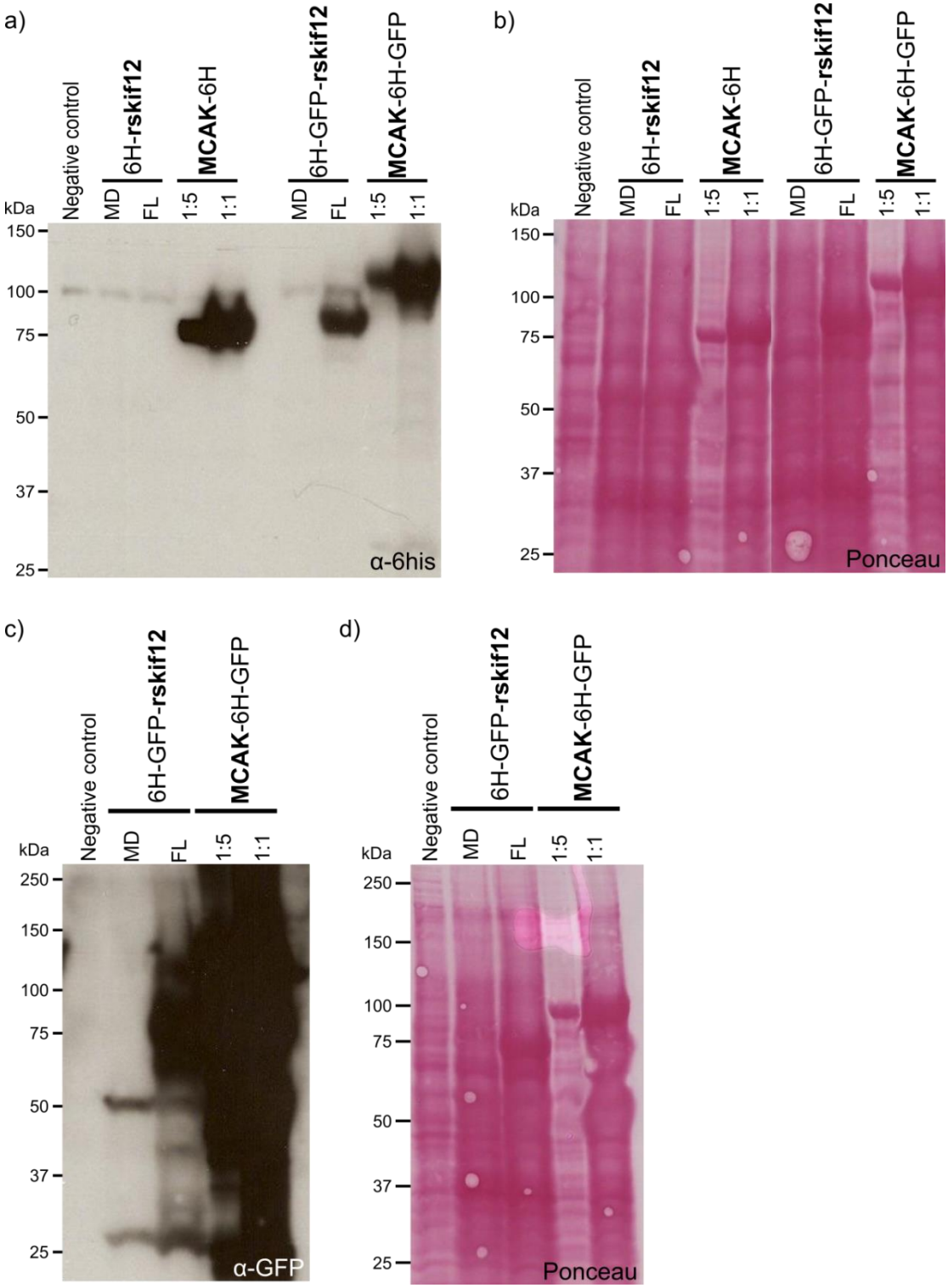


Figure 14. rskif12 protein expression levels when expressed in Sf9 expression cultures, demonstrated by Western blotting. a) Western blotting of 6H and 6H plus GFP tagged rskif12 variants - full length (FL) and motor domain (MD) - probed with α-6x histidine antibody. Tagged MCAK protein variants were used as

a positive control, whilst the negative control was Sf9 cells exposed to the same transfection process, but in the absence of vector. The expected molecular weights for 6H-rskif12 MD and FL were 29.0 kDa and 60.8 kDa respectively, whilst 6H-GFP-rskif12 MD and FL predicted weights were 56.5 kDa and 88.2 kDa, respectively. To help gauge the quantity of rsKif12 protein expressed relative to MCAK levels using the insect expression system, MCAK variants were present as both undiluted (1:1) and a 1:5 dilution. b) Using the same nitrocellulose membrane as in panel a, the protein profile of each Sf9 expression culture was Ponceau stained to ensure consistent protein quantities in the undiluted samples. c) Western blotting of 6H-GFP-rskif12 FL and MD using an α-GFP antibody. d) Ponceau staining of membrane shown in panel C.

protein purification approach was taken in order to attain recombinant protein of greater purity.

The separation of insoluble and soluble proteins (under non-denaturing conditions) showed that, for rskif12, a large quantity of insoluble protein was present at the predicted molecular weight for rskif12 (88.2 kDa) with little protein of the same molecular weight present in the soluble fraction (Figure 15a). The soluble material from the rskif12 and rsKif12MD experiments was added to the cation exchange column and the columns were washed with buffer of increasing salt concentration (Figure 15 b-d). This method failed to yield detectable levels of rskif12 or rsKif12MD in their respective purifications. As Figure 14 shows strong evidence of production of recombinant rsKif12 and rsKif12MD in the insect expression system, the interpretation of these results are that the proteins are not binding to the cation exchange column because they are either negatively charged, or they are not soluble.

To determine whether the lack of the desired protein post-cation exchange was due to a lack of soluble rskif12 and rsKif12MD in the cleared lysate added to the column, rather than an inability for these proteins to bind to the cation exchange column, the flow-through and selected fractions from cation exchange purification to a Nickel-affinity chromatography column were applied. If soluble,

both proteins would be expected to be enriched by the affinity column even if present at low levels.

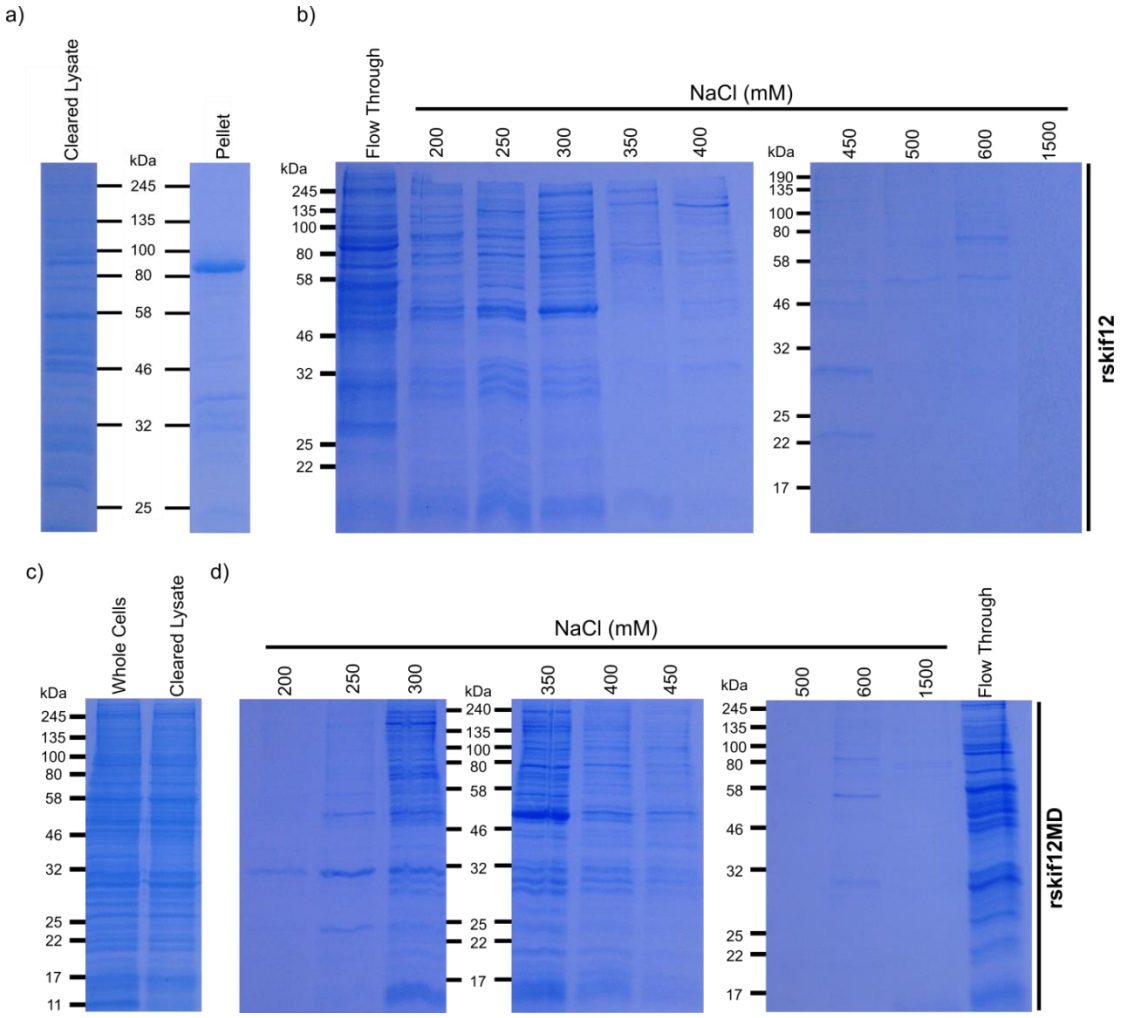


Figure 15. Cation exchange chromatography of rskif12. a) Separation of the 6H-GFP-rskif12 (88.2 kDa) Sf9 expression culture into cleared lysate (soluble material) and pellet (insoluble material). b) Cation exchange chromatography of 6H-GFP-rskif12 cleared lysate using increasing NaCl concentration. The "flow through" harbours material that did not bind to the cation exchange column when the cleared lysate was applied to the column. c) SDS-PAGE of 6H-GFP-rskif12MD (60.8 kDa) Sf9 expression culture whole cells and cleared lysate once the whole cells were separated into soluble and insoluble material – pellet protein profile not shown. d) Cation exchange chromatography of 6H-GFP-rskif12MD cleared lysate using increasing concentrations of NaCl.

For both rskif12 and rsKif12MD samples the flow through and the 350mM NaCl wash fraction were taken forward for this experiment. The flow through was chosen as it would harbour both proteins of interest if they were soluble, but did not bind to the cation exchange column, whilst the 350mM wash buffer was selected as it

harboured a detectible level of protein matching the predicted molecular weights of the proteins of interest.

As shown in Figure 16, attempts to obtain rskif12 and rsKif12MD protein (by Nickel-affinity chromatography) from cation exchange flow through and 350mM wash fractions were unsuccessful. The absence of purified protein in the eluent for both proteins strongly suggests that the inability to obtain pure protein from either step is not due to a difference in charge, and thus an inability to bind to the cation exchange column, but rather a lack of soluble recombinant protein at a detectible level under the expression and purification conditions used. The protein found in the Nickel-affinity eluents is likely caused by non-specific binding of insect protein.

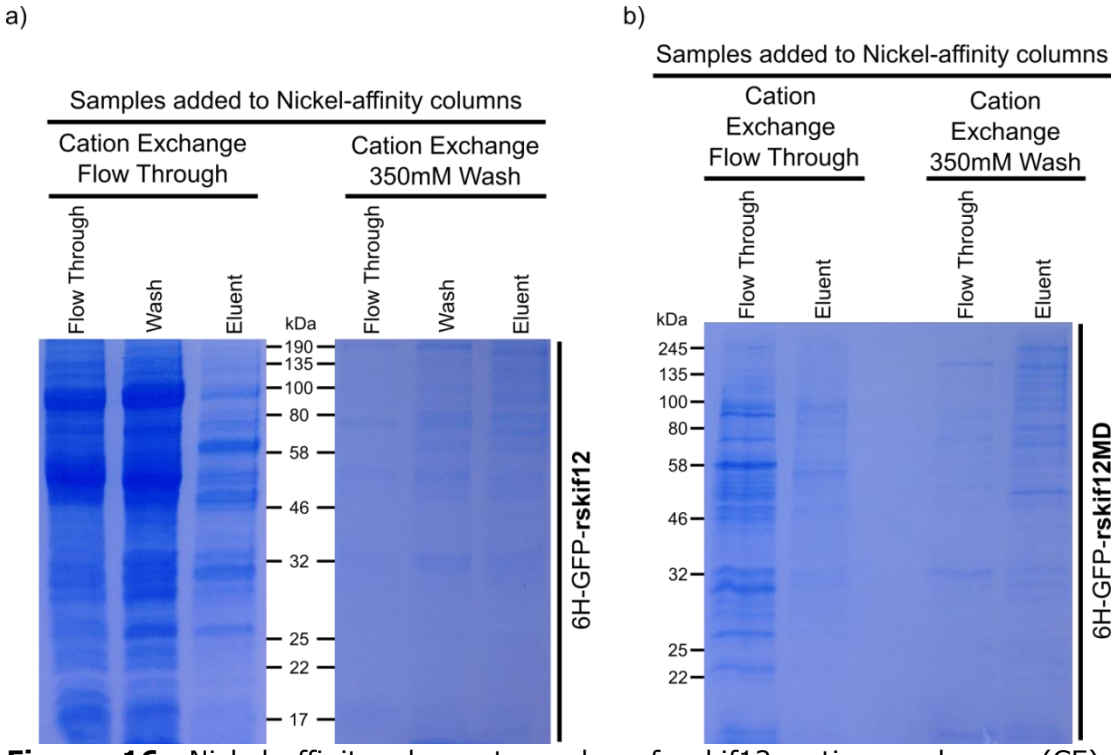


Figure 16. Nickel-affinity chromatography of rskif12 cation exchange (CE) fractions (Figure 15). The solutions collected from the CE flow through (FT) and 350mM NaCl wash steps were applied to Nickel-affinity columns for a second round of protein chromatography for 6H-GFP-rskif12 (88.2 kDa) and 6H-GFP-rskif12MD (60.8 kDa) shown in panels a) and b), respectively. Both the FT and 350mM samples were applied to Nickel-affinity columns. Any unbound solution was collected in the flow through. The wash and eluent samples represent the solutions collected when the columns were washed with imidazole containing buffer, with the eluent samples exposed to a greater concentration of imidazole

than the wash sample (300mM and 9mM respectively). b) Wash steps were carried out for 6H-GFP-rskif12MD columns but were not analysed by SDS-PAGE.

Amendments to the expression and purification methods used in the previous experiments (Figures 15 and 16) were made in an attempt to increase the quantity of soluble rskif12 protein (Figure 17). The changes to the protocol were as follows: 1) reducing the time between Sf9 baculovirus infection and harvesting the cells (70 hours down to 41 hours incubation) to reduce the possibility of protein aggregation; 2) an alternative detergent (nonidet P-40) was added to increase the probability of cell membrane breakdown in Sf9 cells in an attempt to obtain any protein trapped in vesicles; 3) addition of calcium chloride to the lysis buffer as a means of ensuring MT depolymerisation (possibility of MT-bound kinesins being pulled into the insoluble fraction); 4) Benzonase (a nuclease) was added as DNA can bind to the cation exchange column, thus preventing binding of the desired protein. As shown in Figure 17, despite the amendments to the protocol, there was no detectible change in rsKif12 solubility.

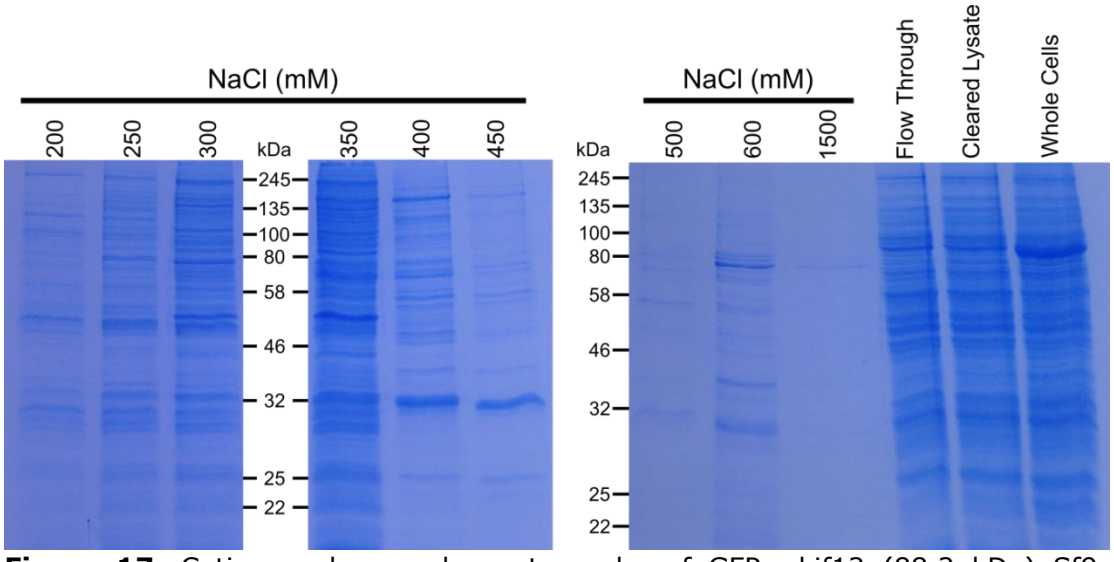


Figure 17. Cation exchange chromatography of GFP-rskif12 (88.2 kDa) Sf9 expression culture 41 hours post-induction. Whole cells were treated with non-idet P-40, calcium chloride and benzonase before being lysed by French press. Proteins bound to the cation exchange column were separated into fractions using washes of increasing NaCl concentrations.

4.1.3 Human rsKif12 remains insoluble when expressed in mammalian expression systems

Due to the inability to obtain soluble rsKif12 and rsKif12MD from the baculovirus expression system alternative expression systems would be required. The alternative expression systems readily available for use in the laboratory were bacterial (*E. coli*) and mammalian (HeLa and HEK293). A mammalian expression system was used because 1) the protein of interest is taken from a mammalian species and 2) the long coiled-coil domains found in kinesin tails have previously proved difficult to express in bacterial systems. Human *rskif12* was inserted into a pCMV mammalian expression vector with a C-terminal GFP tag (pCMV-rskif12-GFP). The transfection efficiency of the vector and expression of the gene of interest were tested in both HeLa and HEK293 cells. As with Sf9 cell transfections, GFP fluorescence was used as an indicator of successful transfection of the expression vector in both cell types. rskif12 was successfully expressed and showed a localisation distinct from an GFP only control (Figure 18). This showed that pCMV-rskif12-GFP could be successfully transfected and expressed in mammalian cells.

To scale up protein production, expression in HEK293 cells was selected rather than HeLa cells as they are easier to grow in larger volumes. HEK293 cells were transfected with pCMV-rskif12-GFP and cultured for 48 hours (conditions outlined in Materials and Methods). These cells were lysed and probed for GFP (Figure 19). Despite the GFP-only control being almost entirely soluble, and expressing a human *rskif12* in a mammalian cell line, an estimated 90% of the rskif12 expressed was insoluble. This result was surprising and, taken together with the outcomes of the attempts to express rskif12 in an insect expression system, suggests that

the RefSeq reference standard Kif12 model may not represent the *bona fide* soluble protein. Since many kinesins studied to date are readily soluble, this would most likely mean the gene model itself is incorrect.

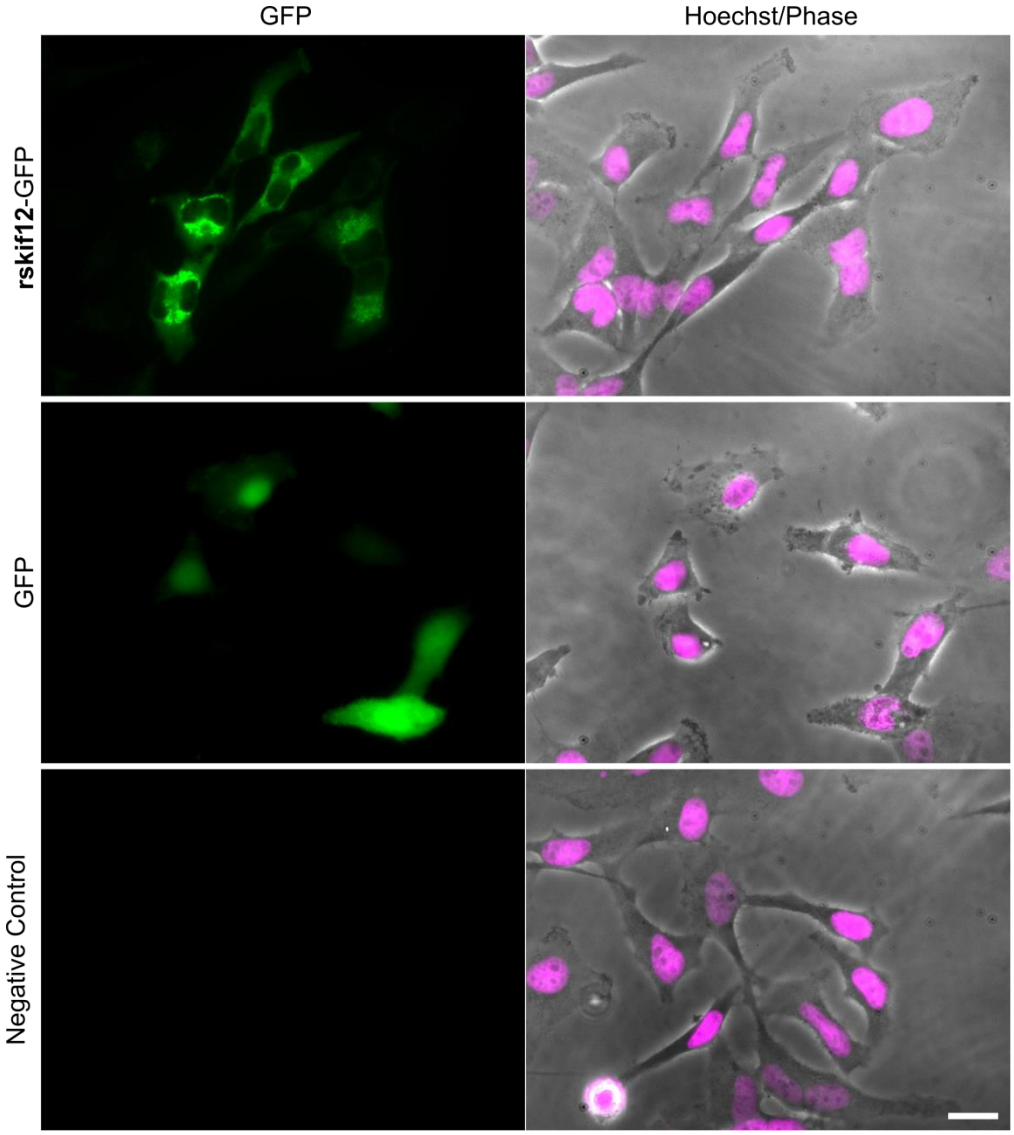


Figure 18. Screening of *rskif12*-GFP transfected HeLa cells. HeLa cells were transfected with pCMV-rskif12-GFP, pCMV-GFP (positive control) or with no vector present (negative control). The "GFP" column denotes images captured by fluorescence microscopy using native fluorescence of rskif12-GFP and GFP proteins, respectively. Images in the Hoechst/phase column show overlays of Hoechst (magenta) and phase contract images (greyscale). Cells imaged 48 hours post-transfection. Scale bar: 10μm.

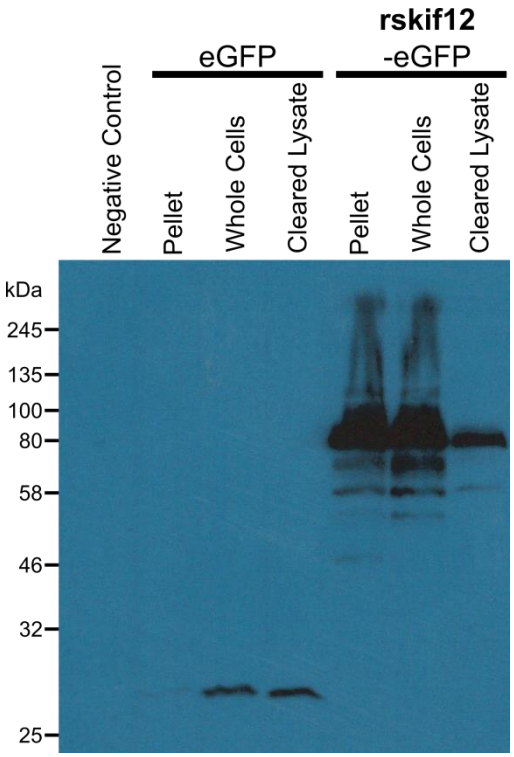


Figure 19. rskif12-GFP (85.2 kDa) solubility. rskif12-GFP expressing HeLa cells (whole cells), and whole cells separated into cleared lysate (soluble) and pellet (insoluble) - under conditions outlined in Materials and Methods – were probed with an α-GFP antibody. HeLa cell cultures expressing GFP (28.6 kDa) and untransfected cells served as the positive and negative controls, respectively.

4.1.4 Human RefSeq reference standard Kif12 lacks two conserved nucleotide binding motifs within the kinesin motor domain

The rsKif12 (GenBank accession number: NP_612433.1) is the reference standard sequence in the RefSeqGene project. This sequence is derived from cDNA created by reverse transcription of mRNA from a human cell. As the sequence is copied from an mRNA transcript, this shows that the sequence is expressed as all, or part, of a human gene. rsKif12 was chosen for the characterisation of human Kif12 as the reference standard sequences tend to match the major splice variants (MSV) more often than the predicted models. The inability to produce soluble rsKif12 from both insect and mammalian expression systems suggested that the gene model may be incorrect.

To investigate this, firstly Kif12 reference sequences for human and mouse Kif12 (GenBank accession number: NP_001304281) amino acids sequences, along with the RefSeq human Kif12 predicted protein models, were aligned in order to highlight noteworthy deviations from the common kinesin motor domain architecture (Figure 20). The predicted models were included as they are also informed by sequencing data derived from human mRNA (namely the intron spanning repeats described in more depth below), whilst the mouse rsKif12 offers a comparison to other mammalian species. The alignment displayed in Figure 20 shows that human rsKif12 is lacking in two conserved motifs found in all kinesin motor domains studied to data: RVRP and the P-loop. The P-loop in kinesins is responsible for ATP turnover, and although rsKif2 may possess another domain that fulfils the same function, the absence of these two domains further suggests that rsKif12 is not the correct model.

In addition to highlighting the absence of the RVRP and P-loop motifs in the rsKif12 sequence, Figure 20 also shows the N-terminal truncation in the rsKif12 amino acid sequence relative to the six predicted models and mouse rsKif12. This N-terminal truncation means that rsKif12 lacks the first 110 residues of the defined kinesin motor domain, suggesting that the insolubility issues previously encountered were caused by the inability of the motor domain region to fold correctly. At the DNA level, truncations of genes at the N-terminal end is a known issue with rt-PCR suggesting that the *rsKif12* sequence is from an incompletely reverse-transcribed mRNA transcript, with the upstream start codon having been missed.

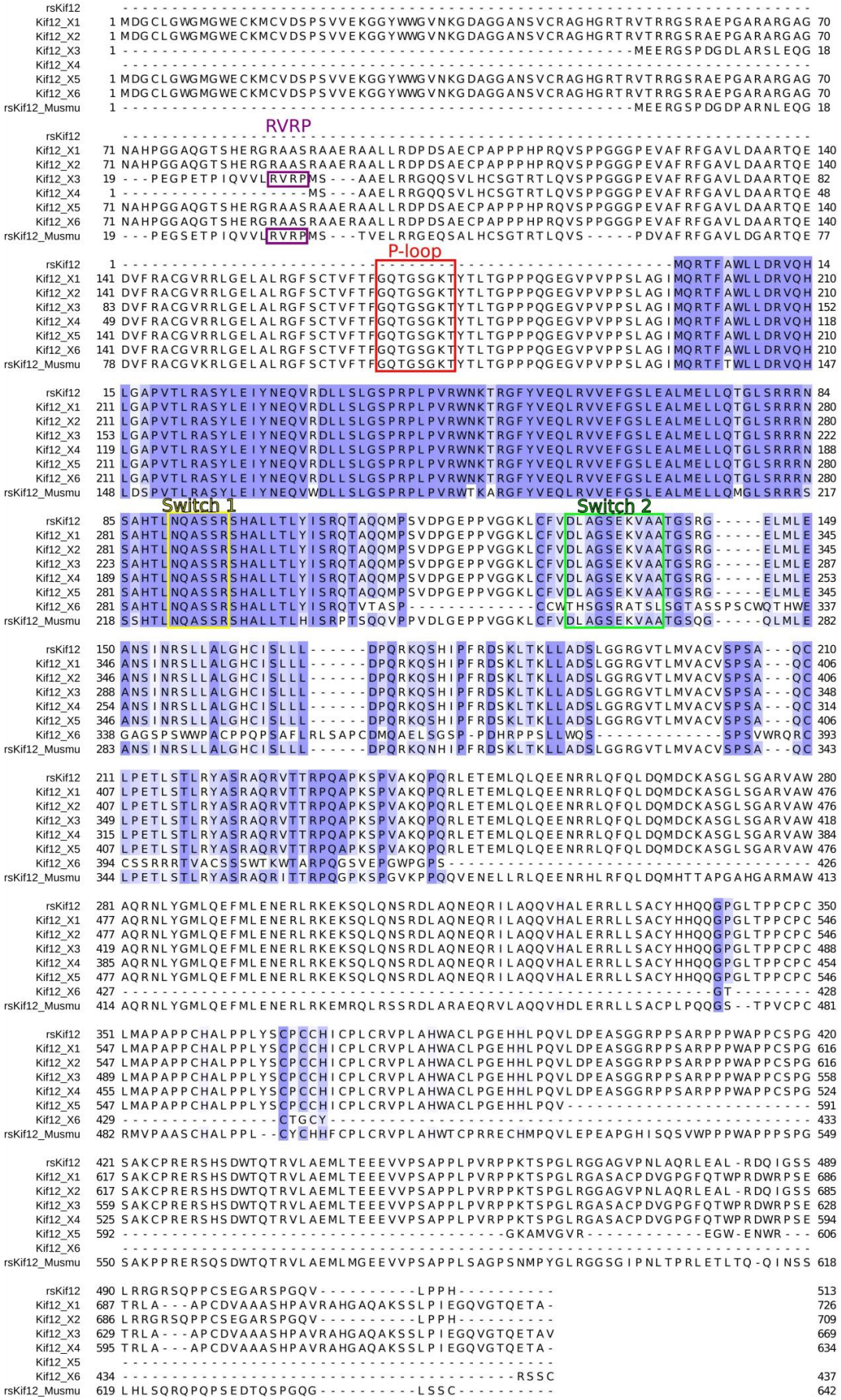

RVRP
P-loop
Switch 1
Switch 2

Figure 20. Sequence architecture of mouse and human Kif12. Amino acid sequence alignments of reference standard human and mouse Kif12 reference standard sequences (rsKif12 and rsKif12_Musmu, respectively) and RefSeq predicted human Kif12 protein models (Kif12_X1 – 6; GenBank accession numbers: XP_011516492, XP_011516493, XP_005251740, XP_006717010, XP_011516494, XP_011516495, respectively). Four conserved kinesin domains RVRP, P-loop, Switch-1 and Switch-2 are boxed. Sequence identity calculated using Blosum62 score (Jalview). Residue positions denoted by numbers flanking the sequences on each row.

4.1.5 Determination of the major human KIF12 isoform

In order to identify the major human KIF12 isoform the human *Kif12* major splice variant (the most abundant mRNA transcript) would first need to be determined. This was achieved by identifying the most abundant intron spanning reads (ISR) from RNA-seq alignments of sequenced mRNA transcripts. ISRs help identify the presence of an intron by reading across two exons in a pre-spliced mRNA transcript and aligning them to spliced transcripts. When aligned to these spliced transcripts, the intron is identified as an additional unaligned sequence of nucleotides flanked by regions of strong sequence identity. These can be verified by identifying known splice sites for an organism.

Using the ISRs is particularly useful when looking at RNA sequencing as the read lengths are often short. This leads to the creation of mRNA (and protein) models that are a prediction of the most likely transcripts rather than a representation of reads that have spanned the full gene sequence. As a result, the MSV was selected to be constructed using the most abundant ISRs as this would give the most probable (or most abundant) mRNA transcript, and thus isoform for KIF12. This approach highlighted that rskif12 is not the major isoform as the mRNA it is translated from is not, based on the abundance of each ISR, the most common transcript (Figure 21).

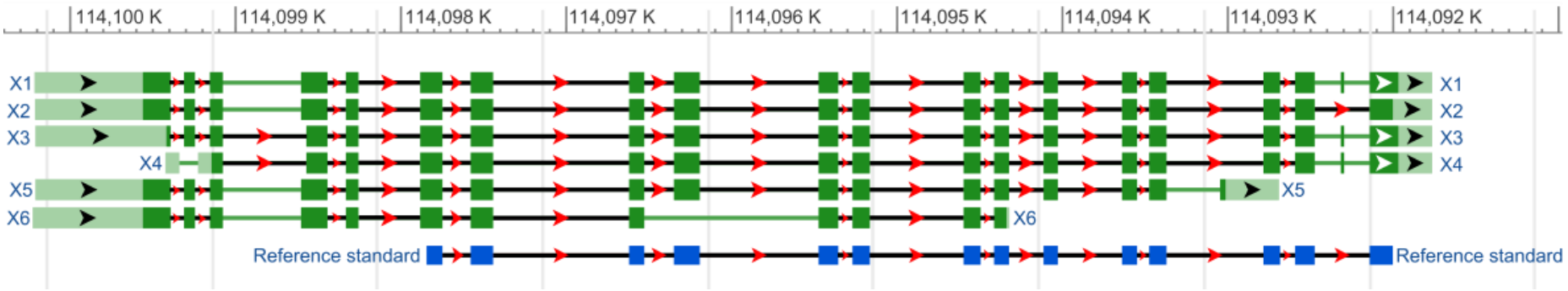


Figure 21. RefSeq predicted human KIF12 protein models (NCBI *H. sapiens* Annotation Release 108, July 2016, Assembly accession: GCF_000001405.33). X1 – X6 show six predicted protein models for KIF12 based on RNA sequencing data. Regions coloured in light green with black arrowheads represent sequence outside of the coding sequence for that predicted model; dark green regions (without arrowheads) denote predicted exonic sequence; regions between the predicted exonic sequences are intronic sequences, introns shaded black with red arrowheads shows the introns that match the most abundant ISR, introns shaded green do not. The reference sequence (Refseq) is coloured blue, this sequence matches the reference sequence inserted into cloning and expression vectors shown in previous Figures (rskif12). Taken and amended from NCBI sequence viewer.

None of the six Refseq predicted *Kif12* models, nor *rsKif12*, incorporate the full exonic sequence that would result from translation of the MSV. Figure 21 shows that the consensus KIF12 sequence, based on using the most abundant intron spanning reads, would be comprised of the first 17 exons from X3 and exons 18 and 19 from X2. This X3:X2 hybrid shares 100% sequence identity with human rskif12, but for an additional 138 amino acid residues upstream of the first rskif12 methionine.

Bioinformatic analysis of the RefSeq sequencing data, namely the use of ISRs, has provided strong evidence that the major Kif12 isoform is not rsKif12, but instead is a hybrid of two predicted protein models – X3 and X2. The X3:X2 sequence matches the *in silico* KIF12 sequence proposed by Katoh and Katoh (2005) despite using two separate methods. Katoh and Katoh (2005) characterised KIF12, in part, by comparing the sequence with the mouse Kif12 sequence. Using a similar strategy the Kif12 X3:X2 hybrid was aligned with the current RefSeq reference standard mouse Kif12 sequence in this study (Figure 22), having first checked that the mouse Kif12 reference standard matched the translation of the major splice variant and harboured the four nucleotide binding motifs in the motor domain (Figures 20 and 21).

The alignment between mouse rskif12 and the human Kif12 X3:X2 hybrid (KIF12) shows 81.0% sequence identity, and only differ in length by nine amino acids – Kif12 X3:X2 hybrid – 651 amino acids long and mouse rskif12 – 642 amino acids long (Figure 22). This provides further support that the X3:X2 is in fact the major human Kif12 isoform.

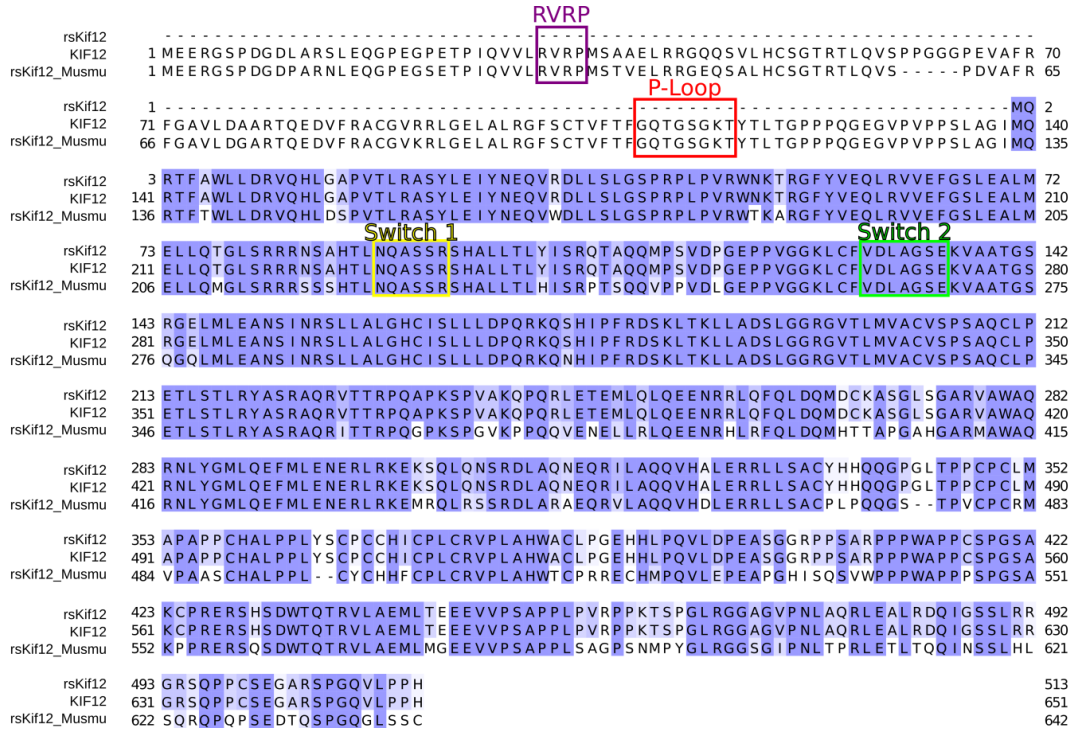


Figure 22. Amino acid alignment of human KIF12 and human and mouse kif12 reference sequences (rskif12 and rskif12_Musmu, respectively). Labelling matches that detailed in Figure 20.

4.1.6 The 5 amino acid sequence PPGGG is deleted in the mouse reference standard Kif12 sequence

The alignment between human KIF12 and mouse rsKif12 shows a region of clear divergence between the two sequences – a five amino acid residue (PPGGG) (Figure 22). This five amino acid sequence is also of interest as its presence/absence in mouse Kif12 plays a role in the severity of polycystic kidney disease in model lines (Mrug et al. 2004); most likely due to impacting kif12 function within the organ.

The PPGGG region is predicted to be located in the Kif12 loop 2 (Mrug et al. 2005). As Kif12 possesses an N-terminally positioned MD sequence it is reasonable to predict that, like other motors with similar MD sequence position, it is a translocating kinesin. In other translocating kinesins, such as KIF5A and KIF1A, loop 2 is positioned at the MT-kinesin interface (Atherton et al. 2014) and is involved in the binding of kinesins to the MT lattice (Scarabelli et

al. 2015). In Kif18A, the loop 2 is necessary for stable association of MTs that make up K-fibres during mitosis (Kim et al. 2014). If loop 2 possesses a similar function in Kif12, the insertion or deletion of 5 amino acids in the Kif12 loop-2 could be sufficient to prevent Kif12-MT binding and possibly preventing Kif12 from carrying out is cellular role. The fact that this 5 amino acid difference in Kif12 causes a change in polycystic kidney disease severity in mice indicates that it does have a substantial impact on Kif12 function.



Figure 23. KIF12 exon 3 and 4 boundaries. The KIF12 sequence is aligned against a segment of human chromosome nine (Chr9_GRCh38.p2) where the gene is located. The five amino acid residue sequence, PPGGG, is shown in the boxed region. Red lettering is the translation of the DNA sequence directly below it.

To determine whether the PPGGG region is a deletion or an insertion, the position of the PPGGG sequence was first checked against known human splice boundaries to ensure that the differences in the human and mouse sequences were not due to a splicing error. The five residues of this INDEL are three codons away from the splice boundary (Figure 23), suggesting that its presence in the human sequence is unlikely to be due to a splicing error. Secondly, an alignment of an inbred (CRA) and an outbred

(ICR) mouse line shows PPGGG to be present in the outbred line, but absent in the inbred line (Figure 24). Finally, the reference standard Kif12 sequences for other mammals were found to contain this PPGGG sequence (Figure 25). These results collectively suggest that PPGGG is present in the human KIF12, with the absence in the mouse rsKif12 being due to a deletion in an inbred line.

These bioinformatic approaches provide strong evidence that the human rskif12 used for expression is unlikely to be a genuine product in human or mouse cells, and is not encoded by a major splice variant. Instead, a combination of the NCBI RNA-seq X3 and X2 predicted models (Figure 22) is supported by the data as the wt human KIF12, and as a result will be produced and taken forward for expression.



Figure 24. Mouse kif12 protein alignment. Mouse reference sequence kif12 amino acid sequence aligned against other laboratory mouse kif12 sequences (ICR – Imprinting Control Region; CRA – Cramping). The PPGGG region is boxed in orange. Four conserved kinesin domains annotated as described in Figure 20.



Figure 25.Kif12 PPGGG INDEL analysis. Amino acid sequence alignments of the kif12 reference sequence for the following species: *Homo sapiens* (human); *Mus musculus* (Mouse); *Canis lupis* (grey wolf); *Bos taurus* (domestic cow); *Pteropus alecto* (black flying fox); *Ornithorhynchus anatinus* (platypus); *Gallus gallus* (Chicken). PPGGG deletion sequence is boxed in orange.

4.1.7 Expression of KIF12 in Sf9 cells

Having defined the wt *KIF12* sequence, an expression construct was then made for this sequence. *rskif12* shares complete sequence identity with *KIF12*, but *KIF12* possesses a further 414bp upstream from the *rskif12* start codon (Figure 22). In order to express KIF12 in Sf9 cells, the expression vector had the missing upstream sequence inserted to create both wt *KIF12* and *kif12ΔPPGGG* (identical to wt KIF12 with the PPGGG sequence deleted) variants (Figure 26). As previously described, the PPGGG sequence is of interest as it may play a crucial role in KIF12 function and so the kif12ΔPPGGG is required as a control. The upstream sequence was synthesised as double stranded DNA (gBlocks) having been codon optimised for translation in *Spodoptera frugiperda* (Sf9 cells). Variants were tagged at either the N- or C-terminal end in case this impacted expression levels and/or solubility.

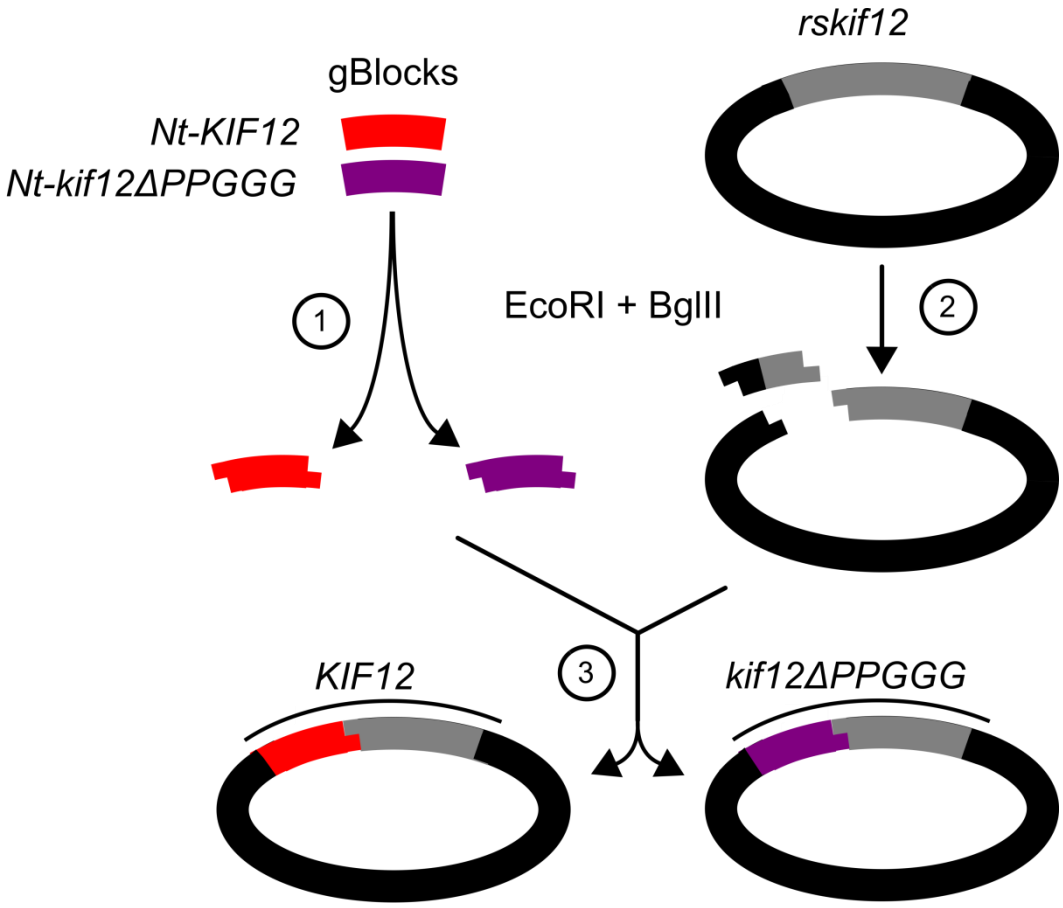


Figure 26. Construction of KIF12 cloning vectors. 1. *Nt-kif12* (red) and *Nt-kif12ΔPPGGG* (purple) synthesised gBlocks contain the N-terminal sequence – including the start codon – missing from the rskif12 sequence. The gBlocks are cut with *Eco*RI and *Bgl*II restriction enymes. 2. The parental vector - the same as that used for the initial steps of rskif12 expression in the baculovirus expression system – is also cut with *Eco*RI and *Bgl*II removing a sequence of DNA that contains part of the rskif12 sequence and the non-coding region upstream. 3. Each digested gBlock is ligated individually into the digested vector. The ligation completes the *KIF12* or *kif12ΔPPGGG* DNA sequence.

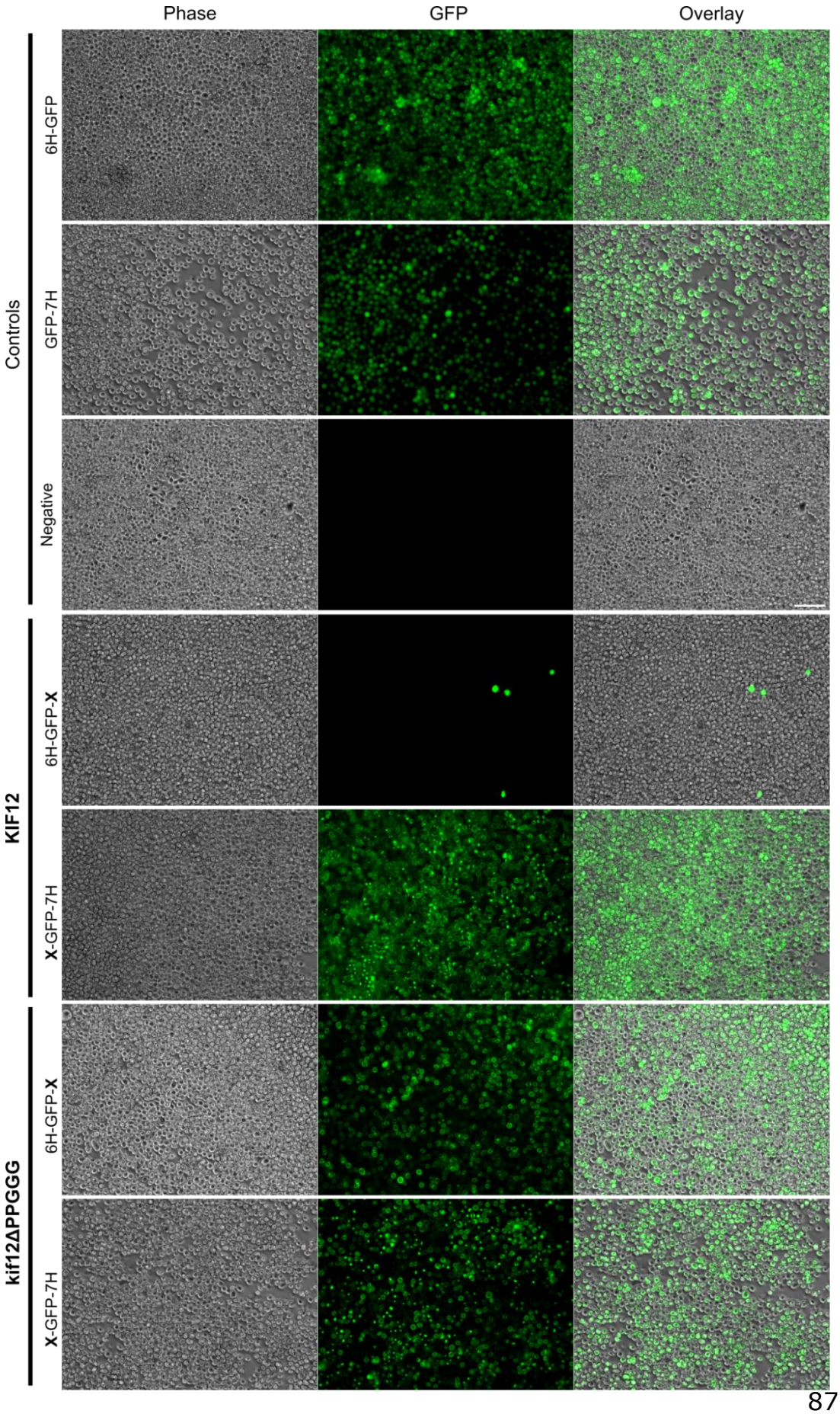

Phase
GFP
Overlay
Controls
6H-GFP
GFP-7H
Negative
KIF12
6H-GFP-X
X-GFP-7H
kif12ΔPPGGG
6H-GFP-X
X-GFP-7H

Figure 27. Expression of KIF12 and kif12ΔPPGGG. Sf9 expression cultures of baculovirus containing N or C terminally GFP tagged *KIF12* and *kif12ΔPPGGG*. "X" denotes that position of the kif12 variant sequence. Parental vectors (without either kif12 sequence variant) were used as a positive control. The negative control is described in Figure 14. Scale bar: 100μm.

These expression vectors were transfected into Sf9 cells and all proteins expressed successfully, as judged by GFP fluorescence (Figure 27). The transfection of 6H-GFP-KIF12 into insect cells was repeated due to the low expression levels during the first experiment. SDS-PAGE of the expression lysates confirms that all Kif12 variants successfully expressed, with bands visible at the predicted molecular masses matching (Figure 28).

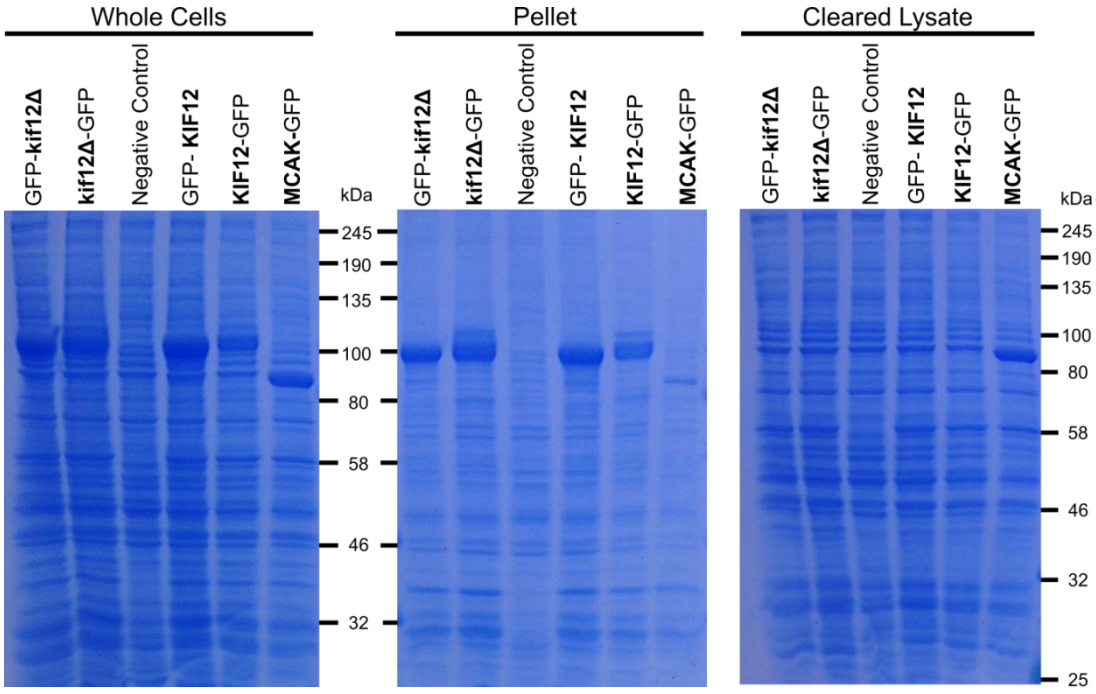


Figure 28. Solubility of KIF12 and kif12ΔPPGGG in Sf9 cells. Protein in the whole cell sample was divided into insoluble (pellet) and soluble (cleared lysate) – under the experimental conditions used – and then separated using SDS-PAGE. MCAK-GFP and no-DNA transfection samples acted as the positive and negative controls, respectively. Expected molecular weights are as follows: KIF12 – 102.9 kDa and 100.1 kDa (N- and C-terminal GFP tagging, respectively), and kif12ΔPPGGG (kif12Δ) – 102.5 kDa and 99.9 kDa (N- and C-terminal GFP tagging, respectively).

To check the solubility of KIF12 and kif12ΔPPGGG cell lysates from their respective expression cultures, they were separated into soluble and insoluble fractions. This showed an absence of

detectable full length kif12 in the soluble fraction under the lysis conditions used (outlined in Materials and Methods section), regardless of which terminus the protein was tagged (Figure 28).

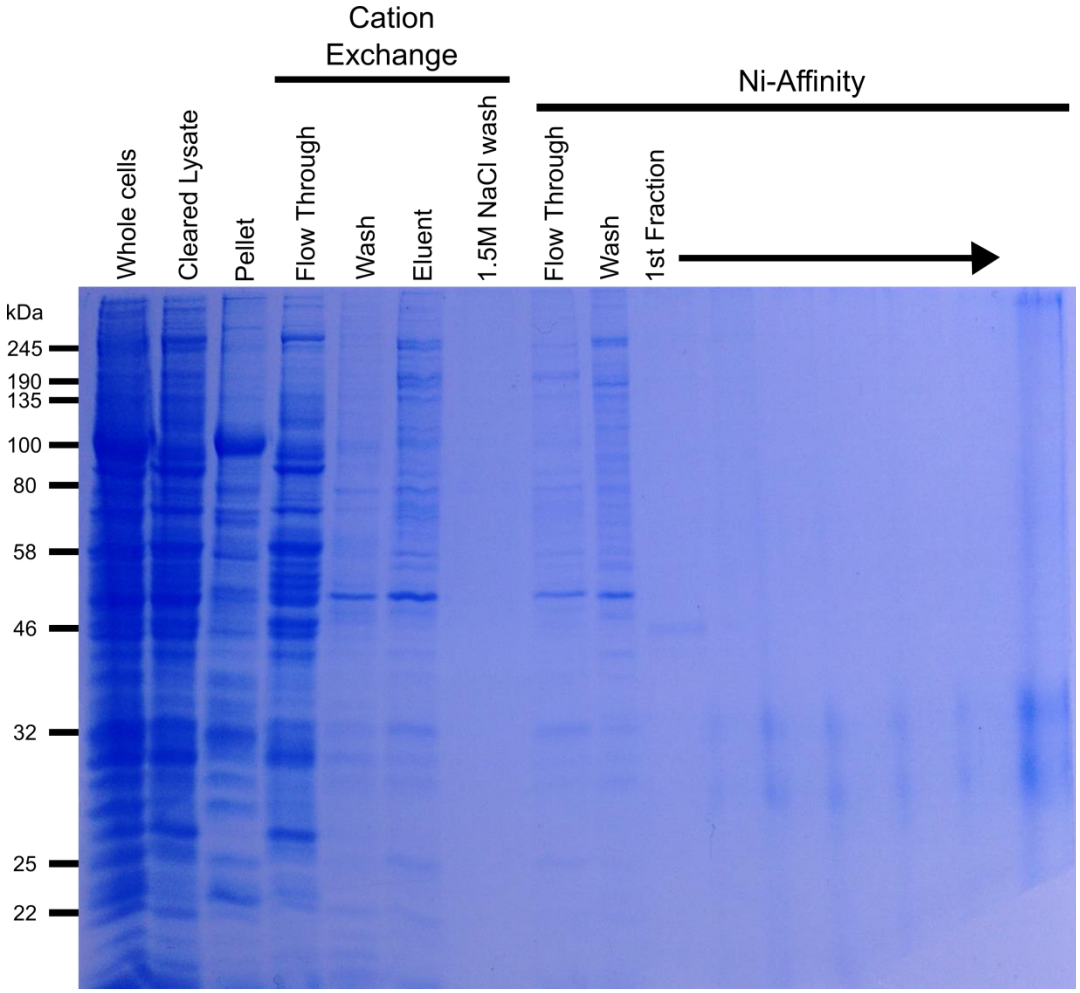


Figure 29. Two step purification of KIF12-GFP (100.1 kDa). KIF12-GFP expressed in Sf9 cells separated into cleared lysate and pellet, with the cleared lysate then applied to the CE column. The solution collected from the eluent step was then applied to the Nickel-affinity column in the second round of purification. The arrow denotes the protein profiles of further collected fractions (loaded in order).

In an attempt to solubilise KIF12-GFP the lysate was sonicated to break apart any sub-cellular compartments that may have been harbouring KIF12-GFP, thus dragging it into the insoluble fraction. Despite sonicating the lysate, KIF12-GFP remained below detectible levels in the soluble fraction (Figure 29). The soluble fraction was exposed to both cation exchange and Nickel-affinity

chromatography to ensure that low levels of soluble KIF12-GFP were not being missed. This showed no detectible levels of KIF12-GFP present in the soluble fraction (Figure 29).

The failure of sonication to solubilise the expressed KIF12-GFP suggests that the issue with solubility, under the used lysis conditions, is unlikely to be due to containment within an intracellular membrane-bound compartment. Among the many alternative hypothesese as to the lack of success in attaining KIF12-GFP is that there is an issue with Kif12-GFP folding within the expression system. This is not implausible as kinesins contain long alpha helical coiled-coil regions in their structures, something known to cause protein solubility issues.

4.1.8 Motor domain only Kif12 truncation is soluble

Although there are no structures available for members of the Kinesin-16 family, it is probable that they contain a tail domain made up of large regions of coiled-coils. To investigate whether it is these structures that are responsible for the solubility issues experienced previously, a motor domain-only truncation of KIF12 was produced. N- or C-terminally tagged, or no-tag kif12MD variants were created in case of differential stability and solubility. These truncated kif12MD samples were expressed in Sf9 cells, which were then lysed to check for expression levels and solubility. This showed that the expression levels of both N- and C- terminally GFP-tagged kif12MD were comparable; however there was no detectible expression of the no-tag kif12MD (Figure 30). This indicates that possessing a GFP tag aids expression within Sf9 cells under the conditions used.

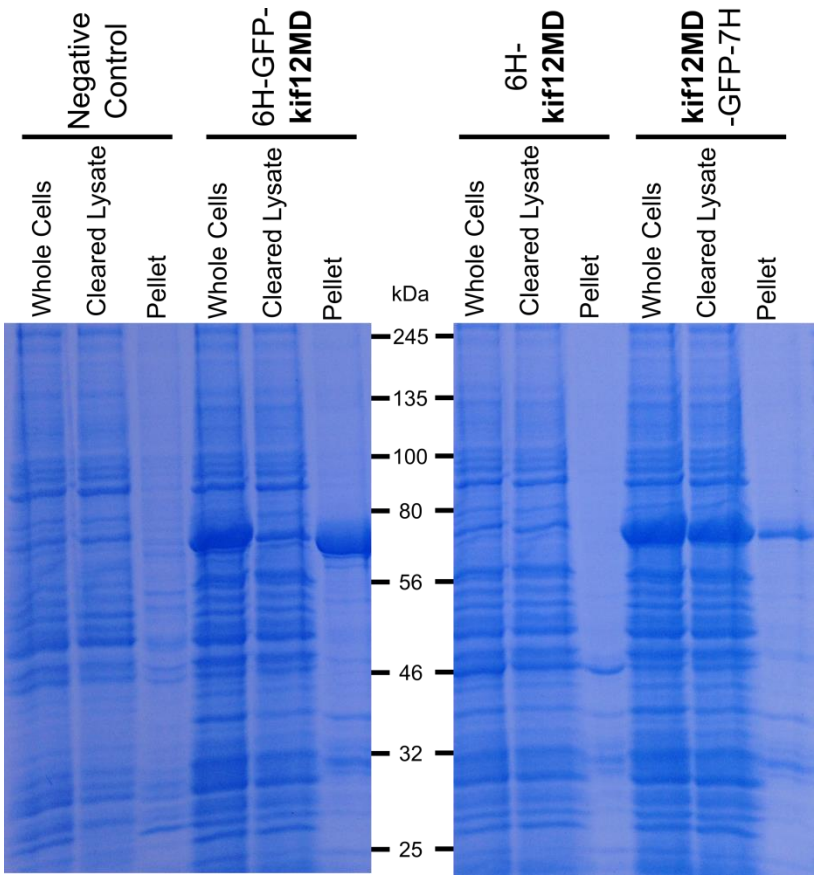


Figure 30. Tagging on the C- or N-terminus impacts the solubility of kif12MD. kif12MD was expressed in three variations within an insect expression system: GFP tagged on the N- (68.3 kDa) and C-terminus (71.6 kDa), respectively and without (50.0 kDa). Proteins within the whole cells from these cultures, along with the materials found in both the cleared lysate and pellet when the whole cells were divided, were separated by SDS-PAGE.

The position of the GFP tag did impact the solubility of kif12MD under the lysis conditions used. When tagged at the N-terminus, the majority of kif12MD insoluble and found in the pellet, whilst C-terminal GFP tagging resulted in the majority of protein being in the soluble fraction (Figure 30). The presence of soluble protein strongly suggests that the tail domain of KIF12 was the predominant cause of insolubility.

The production of soluble kif12MD allows for the purification and characterisation of the protein *in vitro*. It is hoped that now a soluble truncation has been identified, that the ΔPPGGG mutant too can be produced so that its potential impact on motor function can

be investigated. However, due to the nature of the truncation, there are limitations as to what information can be extracted. Firstly, the absence of the neck and tail domains prevents the formation of multimers; if that is how KIF12 exists in human cells. Secondly, the tail region is the site of cargo binding, thus its removal prevents investigation into the role of KIF12 in cargo transport and potentially, mechanisms for autoinhibition. Identifying KIF12 as a translocating kinesin is still possible, regardless of being monomeric when truncated, as alternative assays can be employed such as gliding assays.

4.2 The role of KIF12 in ciliogenesis and primary cilia maintenance

4.2.1 Data from genome-wide ciliogenesis screens are consistent with a role for KIF12 but not conclusive

Previous research by Mrug et al. (2004) has identified KIF12 as a polycystic kidney disease (PKD) modifier gene. To provide further support for this hypothesis, analysis of a recently published siRNA-based functional genomics screen (Wheway et al. 2015) might reveal KIF12 essentiality in the building and/or maintenance of the primary cilium, and thus how a dysfunctional KIF12 might lead to ciliopathies. This screen is particularly useful in the determination of KIF12 essentiality as it is carried out in mouse Inner Medullary Collecting Duct 3 (IMCD3) cells derived from the mouse kidney tissue, a region of extremely high KIF12 expression (Figure 31).

The genome-wide screen was carried out initially in IMCD3 cells (mouse-derived) using a siRNA library to knockdown each individual gene. The impact of each gene's knockdown on ciliation and cell survival was recorded, and each experiment was carried out in duplicate. The screen included 18,960 genes, with pools of four

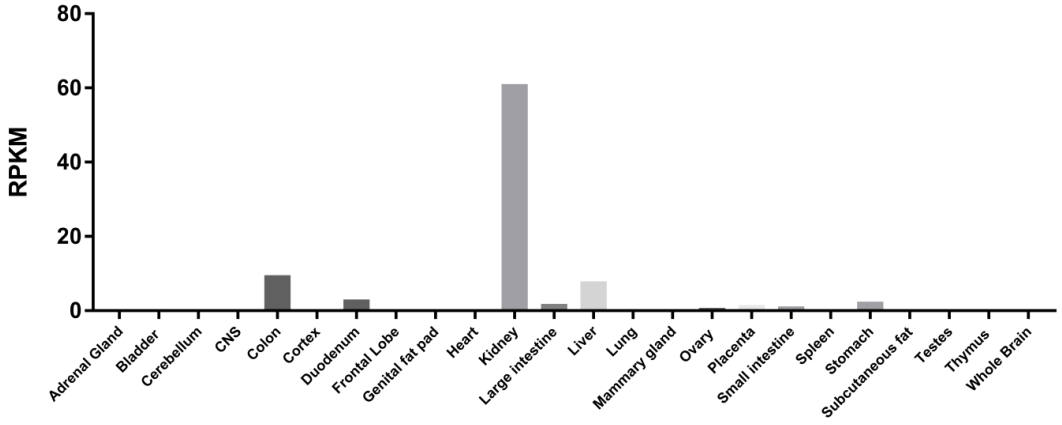


Figure 31. Mouse KIF12 expression levels in different mouse tissues. RPKM – Reads per kilobase of transcript per million mapped reads. Data informing this Figure is taken from Yue et al. 2014.

siRNAs targeted specifically to each gene. The knockdown experiments were grouped into batches, with each batch having the same set of positive controls to compare against. These positive controls were genes known to be essential for either cell viability or primary cilia production/maintenance in each respective experiment. The authors of the study opted to set the cut off for significant hits according to the median robust score of the positive controls within each respective batch, rather than z= -2. As a result, a test result greater in value than the median robust z score for the positive controls ($z_{cilia} < z_{cilia\ cutoff}$) for both replicates was deemed to have a greater effect on ciliogenesis than the median of the positive controls, and the result is taken as a significant hit.

In order for genes to be selected for the secondary screen in the Wheway et al. (2015) study, genes would have to successfully pass a series of filters in the primary screen (siRNA knockdown in IMCD3 cells). These filters included having significant hits in both the ciliogenesis/ciliopathy experiment and the cell viability experiment - $z_{cilia} < z_{cilia\ cutoff}$ and $z_{cell} < z_{cell\ cutoff}$, respectively. Some proteins (40 in total), having failed these filters, were still taken through to the penultimate filter before the secondary screen as

they were closely related to a protein family (G-coupled protein receptors) found to be enriched in the genes that had successfully passed the initial filters. This left 194 functional gene candidates, all of which were re-tested for essentiality in ciliogenesis and cilia maintenance in IMCD3 cells, this time with individual siRNAs. Only 68 of these 194 functional gene candidates were successfully filtered through to the secondary screen; KIF12 was not included in these 68 genes.

Table 1. z_{cilia} scores of IFT proteins, KIF12 and secondary screen candidates taken from Wheway et al. 2015. Z_{cilia} scores in bold red denote scores higher than the median positive control score for that run in that respective batch. For a gene to be identified as a significant "hit", z_{cilia} scores higher than the median positive control score were required for both runs.

Mouse gene	Run 1 Z_{cilia} score(s)	Run 2 Z_{cilia} score(s)	Mean Z_{cilia} score(s)
IFT20	-2.84508	0.821695	-1.01
IFT27	**-7.61669**	**-9.92473**	-8.77
IFT46	**-22.6702**	-0.84059	-11.75
IFT80	-3.53839	-0.98729	-2.26
IFT88	**-9.97855**	**-2.35104**	-6.16
IFT127	-1.60926	1.932972	0.16
KIF3a	0.232931	-0.51504	-0.14
KIF12	**-13.6**	-1.6	-7.6
Secondary screen candidates	-8.03	-8.06	-8.04

In the genome-wide study (Wheway et al. 2015), KIF12 was found not to be significant in ciliogenesis. In order to gauge how likely it is that KIF12 is truly non-essential in ciliary function, the screen's ability to identify genes known to be essential in ciliogenesis and cilia production as significant hits was checked. IFT proteins known to be essential to primary cilia construction and maintenance in mammals were selected. These were IFT20 (Follit et al. 2006), IFT27 (Qin et al. 2007), IFT46 (Lee et al. 2015), IFT80 (Yang and Wang 2012), IFT88 (Zhu et al. 2009), IFT127 (Gorivodsky et al. 2008) and KIF3a (Boehlke et al. 2010). Z_{cilia} scores for each IFT protein were compared to the median positive control value for the same run in the same batch. In the study, both runs would have to have $z_{cilia} < z_{cilia\ cutoff}$ in order to be taken as a significant hit. Surprisingly, the siRNA-based screen failed to flag all but two (IFT27 and IFT88) of the IFT proteins as significant in reducing the number of ciliated cells in an IMCD3 cell culture when knocked down (Table 1; Wheway et al. 2015). As a result these genes were not taken through for further analysis in the secondary screen.

The mean z_{cilia} score for secondary screen candidates was -8.04 (Table 1; Wheway et al. 2015), almost double that of the IFT proteins (-4.32), excluding KIF12. This suggests that the cut-off value set was incredibly stringent as it filtered out five of seven known genes essential in ciliogenesis and cilia maintenance. The mean KIF12 z_{cilia} score across the two runs (-7.6) was greater than the average z_{cilia} score for the selected IFT proteins, and just shy of the mean z_{cilia} secondary screen candidates score. Having a higher mean z_{cilia} than the collective IFT mean is suggestive of a role in ciliogenesis or cilia maintenance in mammalian cells; this is consistent with the initial hypothesis posed in this study.

The median Pearson's correlation coefficient for the two runs of ciliogenesis data in the siRNA data was 0.71 (Wheway et al. 2015). This indicates that there were some issues with reproducibility. With a candidate gene requiring both runs to exceed the z_{cilia} score to be considered significant hits, issues with reproducibility may lead to many essential genes being overlooked. A second cause of possible essential genes being overlooked is the use of the median positive control z scores for each batch as the threshold for significance. This means that, when knocked down, genes would have to have a more profound impact on the variable measured than the median positive control sample in both runs to be taken as a significant hit. In other words, genes may be marked as not-significant, despite still impacting the production and maintenance of the primary cilia when knocked down, if not causing as large a phenotypic change on the population as a positive control gene known to be essential in the process of ciliogenesis and cilia maintenance.

The difference in z_{cilia} scores for KIF12 in runs 1 and 2, of -13.6 and -1.6, respectively, shows large variability in the siRNA knockdown method used (Table 1). The value for the first run is considerably higher than that of the median positive control score in the same batch (-5.2), as well as higher than the median scores for the positive controls in any other batches across both repeats. These results from the genome-wide screen (Wheway et al. 2015) are consistent with a role for KIF12 in ciliogensis and/or cilia maintenance, but are not conclusive.

To determine how KIF12 compared with the other genes in the siRNA study the z_{cilia} scores from Wheway et al. (2015) across the library were evaluated. The data set was separated into "IFT proteins and ciliary motors" (IFT20, IFT27, IFT46, IFT80, IFT88,

IFT127 and Kif3a), "Secondary screen candidates" (the significant hits in the studies initial screen) and KIF12. Median absolute deviations (MAD) from the median positive control values in each batch were used to calculate the z_{cilia} (the number of ciliated cells in the IMCD3 cell culture). Z_{cilia} runs 1 and 2 were plotted against one another (Figure 32). KIF12 has a higher Z_{cilia} score than most of the secondary screen candidates in run 1 (higher than 56 of 68 genes). Compared to the vast majority of the library, KIF12 is skewed further towards an axis, thus showing that the KIF12 results show some of the greatest differences in Z_{cilia} score value between runs.

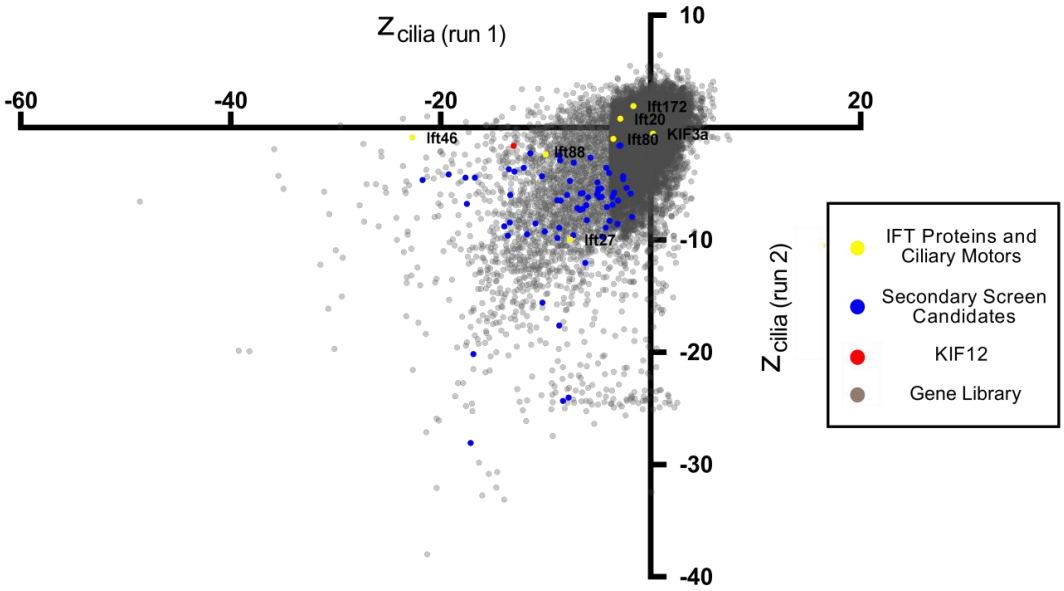


Figure 32. The effect of KIF12 siRNA knockdown on ciliogenesis and cilia maintenance is inconclusive. siRNA knockdown of genes within the mouse gene library was completed in duplicate, with the result from each plotted as a single dot of result from "run 1" against result from "run 2". The axis values refer to the deviations from the mean value. KIF12 is labelled as the protein of interest, whilst IFT proteins IFT20, IFT27, IFT46, IFT80, IFT88, IFT127 and Kif3a are also labelled yellow - these are known to be essential in cilia function and thus act as an indicator for experimental reliability. For other colour representations refer to the key. Data from Wheway et al. (2015).

4.2.2 Evidence for KIF12 essentiality in cell viability is inconclusive

As a continuation into the investigation of KIF12 essentiality in cell function it would be important to determine if Kif12 is essential in

cell viability. KIF12 essentiality in cell survival would show that KIF12 has a non-redundant function and therefore amino acid deletions like that highlighted by Mrug et al. (2005) that impact function, will detrimentally impact the individual.

The same siRNA genome study by Wheway et al. (2015) looked at the impact knockdown that each individual gene in the mouse genome had on IMCD3 cell number 72 hours post siRNA transfection. The z_{cell} scores for KIF12 were more consistent across the two runs, -3.6 and -3.0, respectively (Figure 33), which were both above the median positive control values (-0.5 and -1.0). These knockdown results suggest that KIF12 is essential in the viability of IMCD3 cells when cultured under the conditions outlined in Wheway et al. (2015).

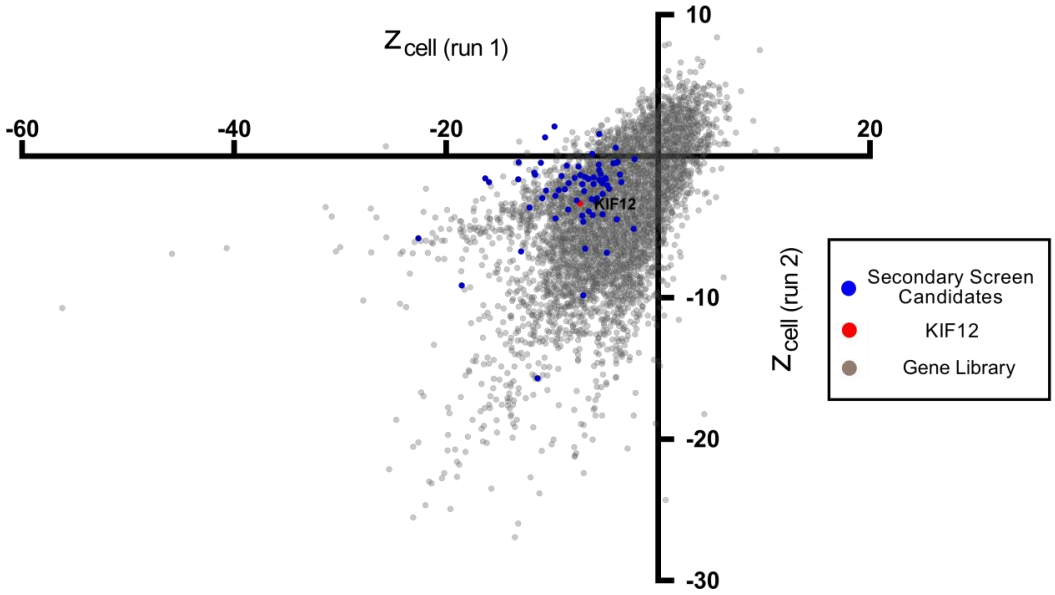


Figure 33. KIF12 knockdown impacts cell survival. Z_{cell} is a measure of how many deviations from the median a given protein is in terms of cell population survival post-gene of interest knockdown. The data set is separated into "secondary screen candidates" (the significant hits in the studies initial screen) shown in blue, and KIF12 labelled and shown in red. Median absolute deviations (MAD) from the median positive control values in each batch were used to calculate the z_{cell} (percentage change in cell number 72 hours post siRNA transfection) scores for each gene. Z_{cell} runs 1 and 2 were plotted against one another. Data from Wheway et al. (2015).

4.2.3 Analysis of IMCD3 cells growth and inhibition

In order to observe KIF12 expression dynamics and localisation within the cells, a model system is required that reflects the tissues and organelles of interest. To meet these criteria the chosen cell line must not only produce primary cilia, but must also be derived from the kidney and a tissue known to express KIF12 (Mrug et al. 2004). With this in mind, IMCD3 cells were selected as an appropriate cellular system. Before experimentation could proceed, analysis of IMCD3 growth and inhibition was required. The IMCD3 growth curve shows that the population reaches stationary phase at ~4 x 10^5 cells/cm^2, suggesting that this is the point where the vast majority of the cell population is contact inhibited (Figure 34). It is at this point that the cell exits the cell cycle and undergoes ciliogenesis.

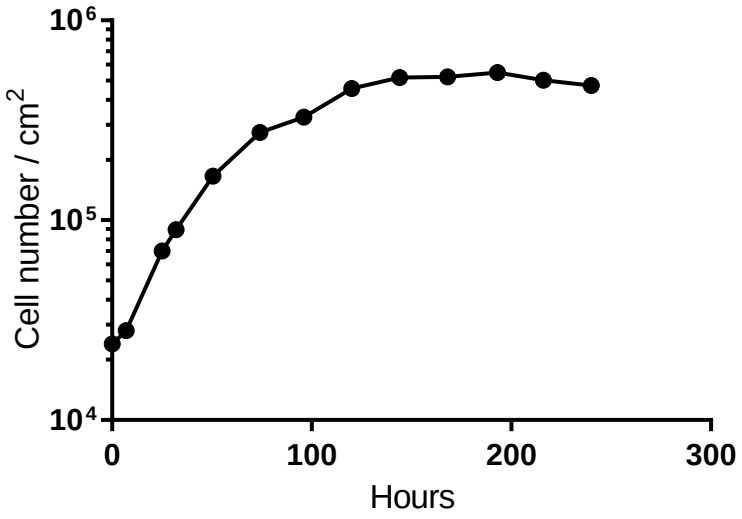


Figure 34. IMCD3 growth rate. Cell number/cm^2 is the number of the cells found within an area of 1 cm^2. Zero hours is the point at which the cells were seeded into the new culture.

4.2.4 Evidence for ciliogenesis in IMCD3 cells

In order to identify evidence for ciliogenesis, IMCD3 cells were grown at various starting densities (1, 2, and 4 x 10^5 cells/cm^2),

with samples of each density taken either at 0 hours or 24 hours post serum starvation. Samples were fixed with methanol and immunostained with anti-acetylated α-tubulin, a known component of the axoneme to enable visualisation of the axoneme, if present, by fluorescence microscopy. Each stained sample showed signal at the apical end of the cells and only a single object per cell (Figure 35). This means IMCD3 cells are capable of producing primary cilium at a range of densities, and also in the presence and absence of serum within the growing media.

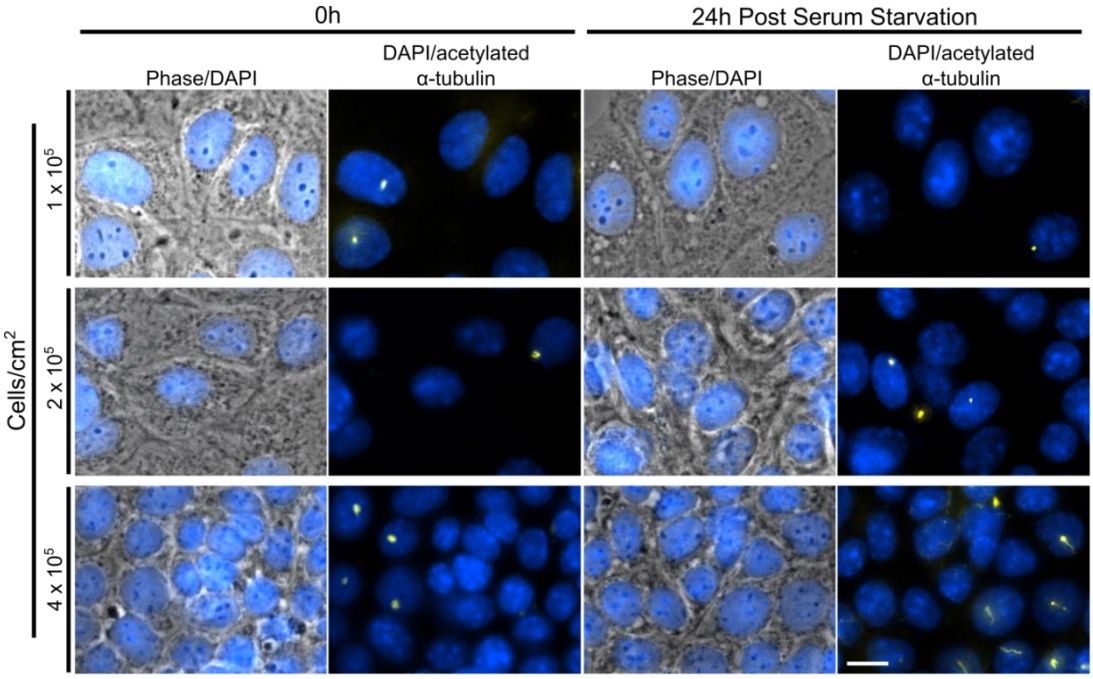


Figure 35. Ciliation of IMCD3 cells. Timings refer to the number of hours the IMCD3 cultures were grown in media without serum. The cells/cm^2 refers to the density of cells in the culture at 0 hours. Nuclear material was stained before imaging using DAPI (shown in blue). Cells were fixed and immunostained with α-acetylated alpha tubulin (shown in yellow). Both phase contrast and DAPI fluorescence micrographs are shown as an overlay. The DAPI/acetylated α-tubulin images are an overlay of images captured by fluorescence microscopy targeting signal for DAPI and TRITC. Scale bar: 10μm.

4.2.5 Lack of robust induction of ciliogenesis by contact inhibition or serum starvation

In order to investigate the expression dynamics of KIF12 during ciliogenesis and cilia maintenance, an inducible system for ciliogenesis is required. Previous studies have used contact

inhibition or serum starvation as a means of encouraging IMCD3 cells to exit the cell cycle and produce primary cilia. Using both contact inhibition and serum starvation, it is possible to induce ciliogenesis in over 80% of the cell population (Pugacheva et al. 2007). In an attempt to replicate this inducible system, IMCD3 cells were cultured at a range of densities, as well as in the presence or absence of serum in the growing medium.

The cells were seeded at a sub-confluent density in media containing serum in an attempt to maintain a low percentage of ciliated cells. Cells were then cultured for 24 hours, in the presence or absence of serum, allowing them to reach a density where the majority of cells would be contact inhibited. The ability to obtain a large increase in the percentage of ciliated cells present in the cultures in a controlled manner would be advantageous as any upregulation of KIF12 expression throughout ciliogenesis would be easier to identify.

In order to determine whether ciliogenesis could be induced in IMCD3 cells, the number of ciliated cells at each time point needed to be calculated. To do this, the cells were fixed and probed for acetylated α-tubulin, and then the number of ciliated cells present within the fixed sample via fluorescence microscopy was counted (Figure 36).

Once the cells were fixed and probed for acetylated α-tubulin, the samples for the percentage of ciliated cell present were counted (Figure 36). Two distinct morphologies were observed, a long feature and a dot. Punctate α-tubulin signal at the apical end of the cells was categorised as a "dot", whilst thread-like α-tubulin signal at the apical end of the cells was categorised as a "long profile"; examples of which are shown in Figures 39-42. In the initial counts, both morphologies were counted as being primary cilia.

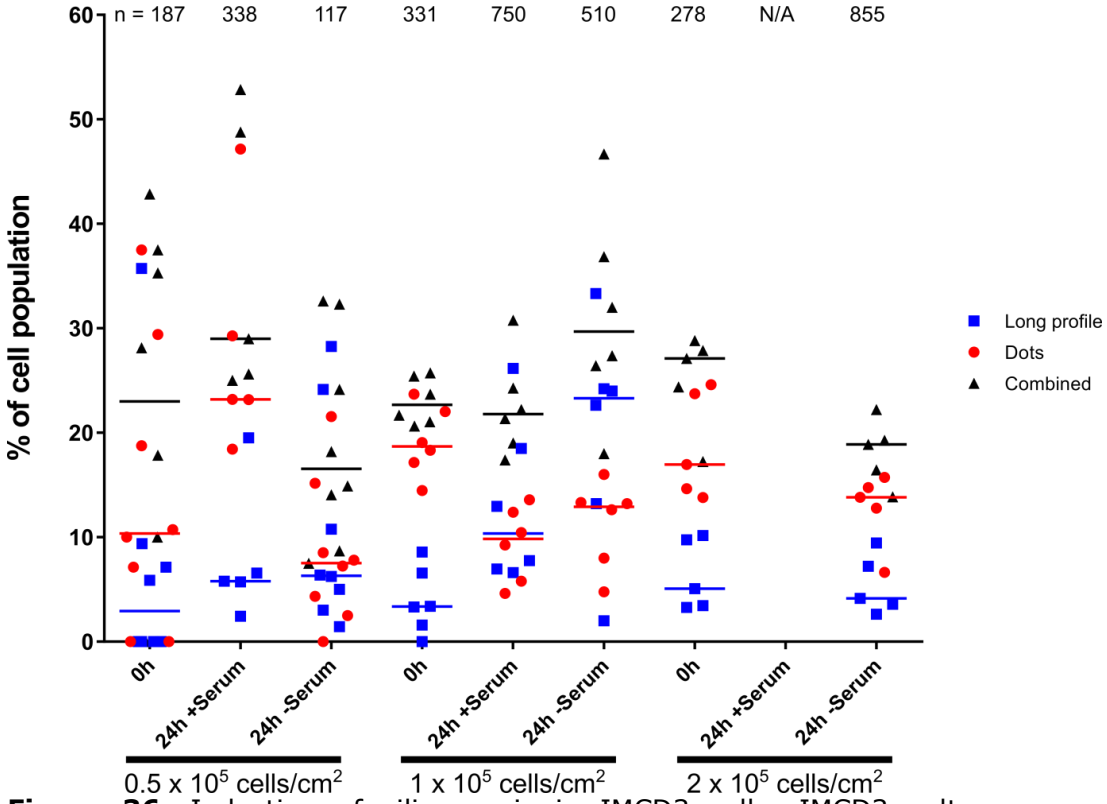


Figure 36. Induction of ciliogenesis in IMCD3 cells. IMCD3 cultures were counted, via microscopy, in terms of the percentage of cells harbouring a primary cilium. "n" denotes the number of cells counted for each samples and is shown above each dataset. The cell densities refer to the density of cells at 0 hours. +/- serum denotes the presence or absence of serum from the cell culture growing medium. Data for 2 x 10^5 cells/cm^2 was not collected. α-tubulin signal was categorised and counted in terms of the signal profile; dots and long profiles. The counts were added together to create a "combined" group as a best case percentage of ciliated cells of those counted. Percentages of cells showing dot or long profile are plotted as a red circle or blue square, respectively, whilst the combined result is plotted as a black triangle. Each data plot is the percentage value of signal profile present in the population of cells found in a single random field of view. The median values for each group within each sample are represented by a straight line in the same colour as the plotted values.

Using this counting system, the results showed that the density and growth conditions (+/- serum) had no substantial impact on the percentage of ciliated cells within a culture (Figure 36). The basal percentage of ciliated cells in a population appears to be around 20%, with the exception of 0.5 x 10^5 cells/cm^2 24h +serum. However, attempts to increase the percentage of ciliated cells using contact inhibition and withdrawal of serum from the

growing media failed to increase it by more than 10%. This difference in percentage of ciliated cells was considered inadequate for investigating the upregulation of KIF12 protein production.

The low percentage of ciliated IMCD3 cells post-serum starvation was unexpected due to the high rates of ciliation (above 80%) achieved in previous research when cells were grown in the absence of serum for 24 hours (Pugacheva et al. 2007). To test if the low levels of ciliogenesis might be a result of seeding density, the proportion of ciliated cells were observed at varying densities. The three densities used for the initial ciliogenesis induction experiment (0.5, 1 and 2 x 10^5 cells/cm^2) were still at least a doubling away from reaching stationary phase and therefore may not have allowed the majority of cells within those cultures to be fully contact inhibited within the 24 hours growth period. In addition, seeding of cells in these cultures took place 16 hours before t=0. As a result, in an attempt to create a reproducible inducible system for ciliogenesis in IMCD3 cells, cells were seeded at a density that would reach stationary phase by t=0 (4 x 10^5 cells/cm^2). A re-experiment with densities 1 and 2 x 10^5 cells/cm^2 with seeding of cell cultures taking place further in advance of t=0 was carried out in an attempt to reduce the impact residual trypsin might be having on ciliogenesis (t= -42 hours compared to t= -16 previously for 1 and 2 x 10^5 cells/cm^2, whilst 4 x 10^5 cells/cm^2 was seeded at t= -96 hours).

The investigation of how varying densities of IMCD3 would impact the proportion of ciliated cells in an attempt to create an inducible system for ciliogenesis was unsuccessful. The increased time between seeding and t=0 for 1 and 2 x 10^5 cells/cm^2 resulted in a much increased percentage of ciliated cells at t=0, over double for both samples, when counting both dots and long profile signal as

evidence for possession of primary cilia. The extended period between seeding and t=0 appears to have had a marked effect on the percentage of ciliated cells at t=0 with over half of the cells present in both seeded at 1 and 2 x 10^5 cells/cm^2 samples being ciliated (Figure 37). However, 24 hours further growth and removal of serum from the growth media caused negligible change in the percentage of ciliated cells across the densities (1 x 10^5 cells/cm^2: 66.6% to 63.4%; 2 x 10^5 cells/cm^2: 51.5% to 53.3%; 4 x 10^5 cells/cm^2: 22.7% to 23.1%) (Figure 37). This means that the system, while increasing the overall percentage of ciliated cells, is not inducible with the removal of serum or by promoting greater contact inhibition through 24 hours additional growth time.

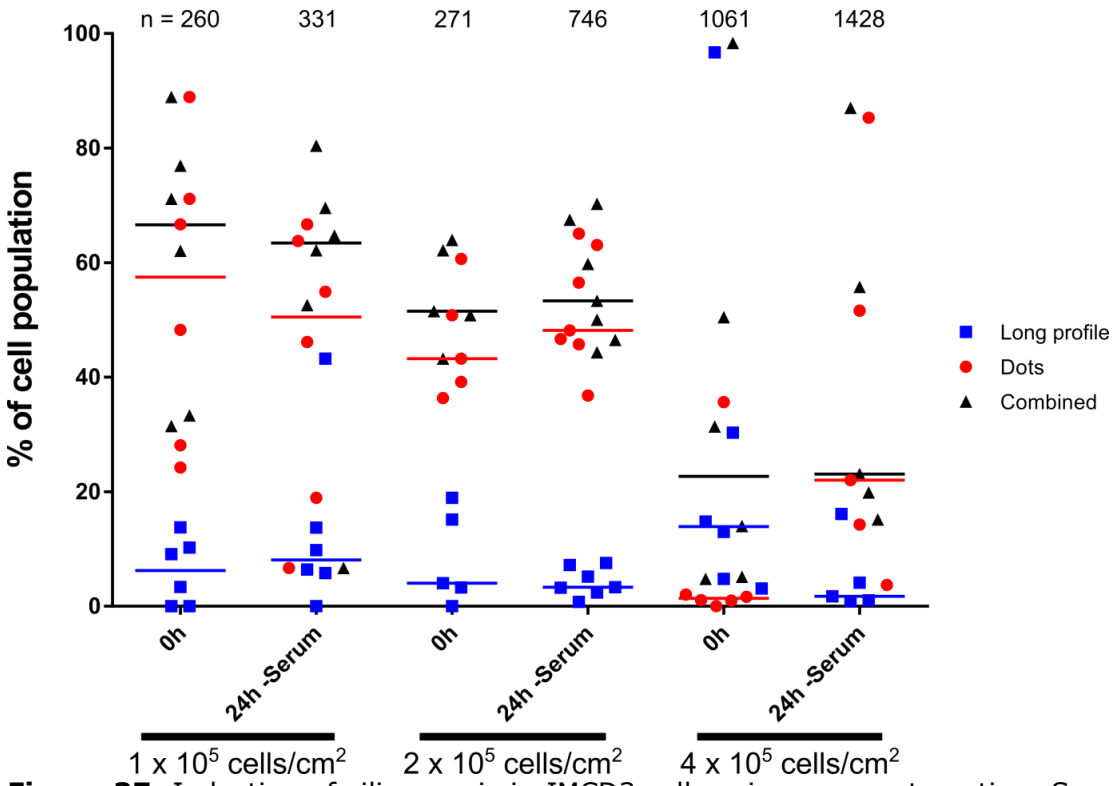


Figure 37. Induction of ciliogenesis in IMCD3 cells using serum starvation. See legend for Figure 36.

Also of note was that the increased density (4 x 10^5 cells/cm^2) did not result in a higher percentage of ciliated cells at either t=0 or 24 hours later, having been starved of serum in the growth media (Figure 37). The percentage of ciliated cells was over half that of

both 1 and 2 x 10^5 cells/cm^2 samples, which is surprising due the increased contact between the cells. From this experiment it was concluded that the density of cells was not playing a significant role in increasing the percentage of ciliated cells within culture.

4.2.6 Length of serum starvation has no effect on ciliation in IMCD3 cells

As it appeared that cell density was not playing a role in increasing the rate of ciliation, the incubation period without serum was extended from 24 to 48 hours, to observe whether this would have a more marked impact on induction of ciliogenesis. The seeding density chosen for this experiment was 1 x 10^5 cells/cm^2, as this was the only density where a noticeable increase in ciliated cells occurred between 0 hours and 24 hours post-serum starvation (Figure 36), albeit a modest one. The percentage of ciliated cells was again calculated by marking cells possessing either a dot or long profile as having a primary cilium.

The results show that the proportion of ciliated cells, i.e. cells presenting α-tubulin dot or long signal profiles at their apical end, actually reduces when left over time, from 37.8% (0h) to 20.2% and 30.2% (24h and 48h, respectively; Figure 38). This means that neither approach (contact inhibition nor serum starvation) reliably stimulated an increase in the percentage of ciliated cells. As mentioned above, previous research using the same cell type have been able to induce upwards of 80% of cell ciliation within populations using either/or serum starvation and contact inhibition. The lack of success in replicating these results suggests that the cell line being used, or the method of processing and calculating the results, is responsible for this difference rather than the method used for growing and inducing ciliogenesis in IMCD3 cells.

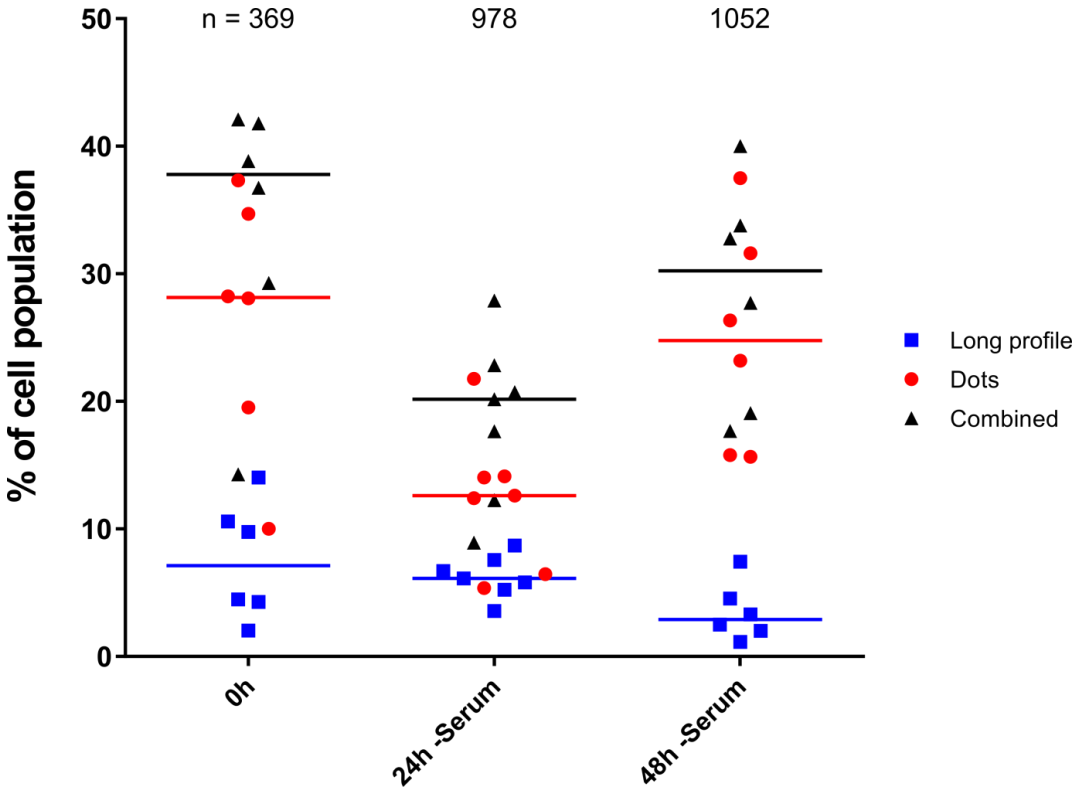


Figure 38. Induction of ciliogenesis in IMCD cells using prolonged serum starvation. Cell cultures, at 0 hours, were at a density of 1 x 10^5 cells/cm^2. Samples labelled 24h and 48h –Serum were grown in the absence of serum for the 24 and 48 hours respectively. See legend for Figure 36.

4.2.7 Docked basal bodies produce confounding signal for analysis of ciliogenesis

The apparent failure to induce ciliogenesis in IMCD3 cells prompted a re-evaluation of the classification of primary cilia when immunostained. This focused on the structure of single punctate signals (dots) found in the fixed cell cultures. Initially thought of as elongated primary cilium extending in the Z-axis, it is possible that the "dot" signal co-localised with the cells may not all be primary cilia, but instead docked basal bodies without the formation of the cilium itself.

In order to clarify whether the dot profiles were either docked basal bodies or primary cilia, the fluorescent microscopy images taken at a range of focal planes were analysed for each sample. If the dots did extend into the Z-axis this would suggest that they

were like the long profiles observed in single slices that were counted as primary cilia. If the dots did not extend into the Z-axis it would be clear that they were not primary cilia, but rather docked basal bodies at the apical end of the cell. The long profiles could be confidently categorised as primary cilia as they matched the characteristic shape of primary cilia highlighted in imaging in other research. Therefore, it would be appropriate to compare the dot profile against the long profile as a means of characterising the dots as cilia or not.

Images captured for samples at all four trialled densities (0.5, 1, 2 and 4 x 10^5 cells/cm^2) were analysed. Dot profiles (punctate α-tubulin signal at the apical end of the cells) of at least three for each time point, were turned from an XY slide to XZ in order to look for extension of signal into the Z-axis (Figures 39-42). This signal was compared to long profiles from the same time point. This re-analysis showed that no dots analysed matched the characteristic signal from the long profile. This means that the dots, classified in previous calculations as primary cilia, are in fact docked basal bodies. These results also indicate the long profile signals, which can confidently be called primary cilia, are pushed over during the immunostaining process, thus making their longitudinal profile visible in the XY axes (Figures 39-42).

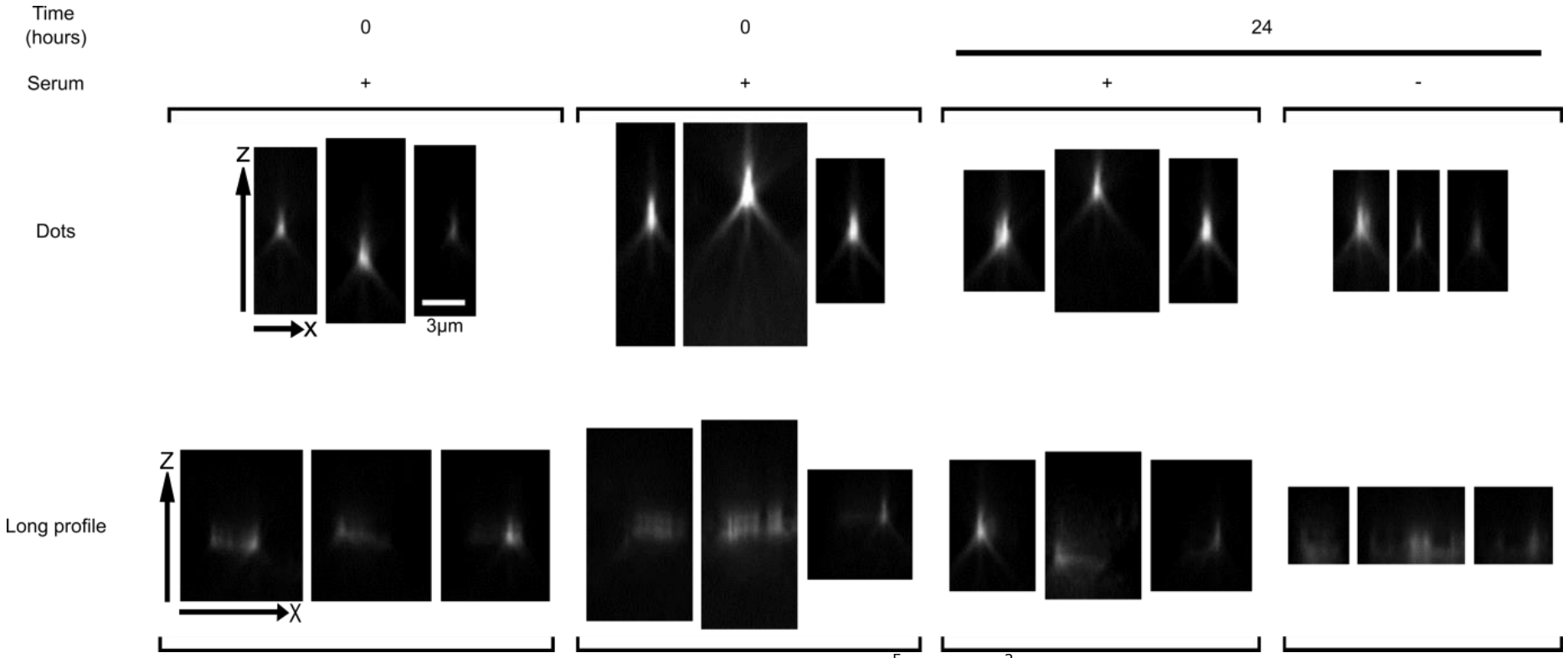


Figure 39. Acetylated α-tubulin signal profiles from IMCD3 cells at 0.5 x 10^5 cells/cm^2. Fluorescence images taken at a range of focal planes were turned from XY to ZX to enable visualisation of α-tubulin signal profiles at the apical end of IMCD3 cells into the Z-axis. Depending on the signal profile observed, cells were either categorised as "dots" or "cilia". Cell cultures, at 0 hours, were at a density of 0.5 x 10^5 cells/cm^2. Cell cultures were seeded 16 hours prior to this in case trypsin treatment caused a delay in ciliogenesis and were grown in the presence of serum. The -/+ in the serum row denotes that the culture was grown in the absence or presence of serum post-0 hours. The arrow labelled "Z" shows points from the posterior to the anterior end of the cell.

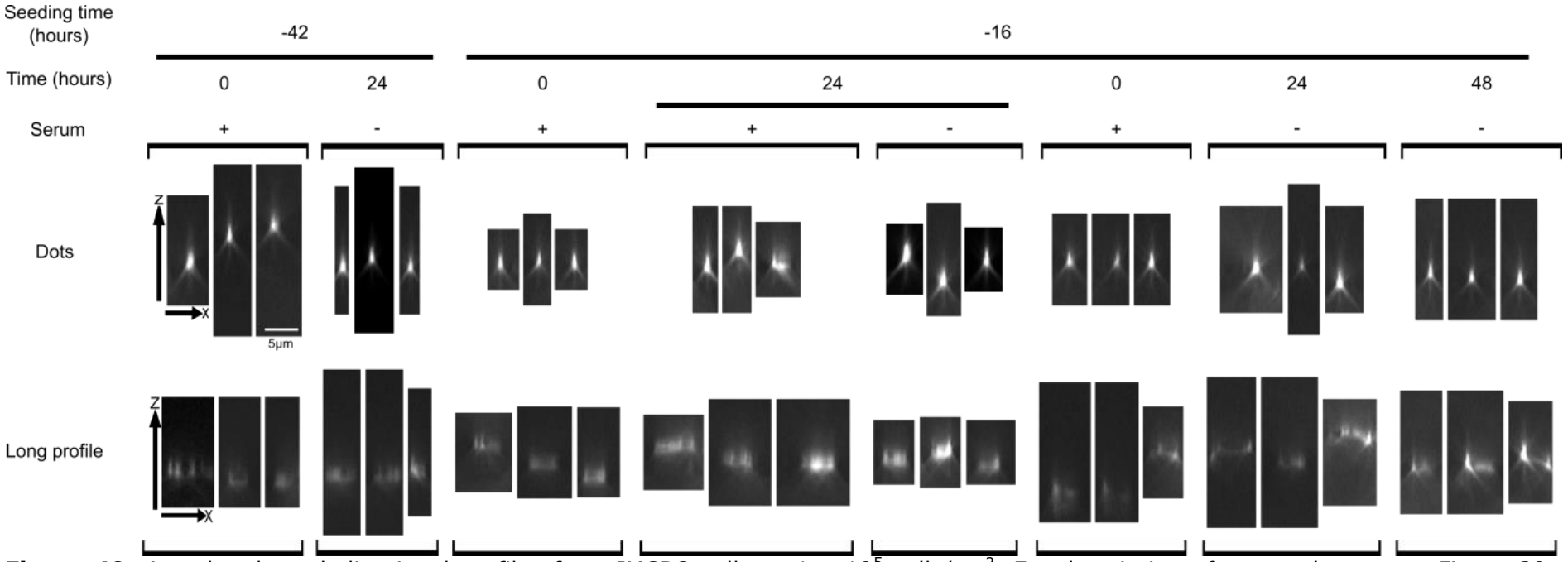


Figure 40. Acetylated α-tubulin signal profiles from IMCD3 cells at 1 x 10^5 cells/cm^2. For description of nomenclature see Figure 39 legend.

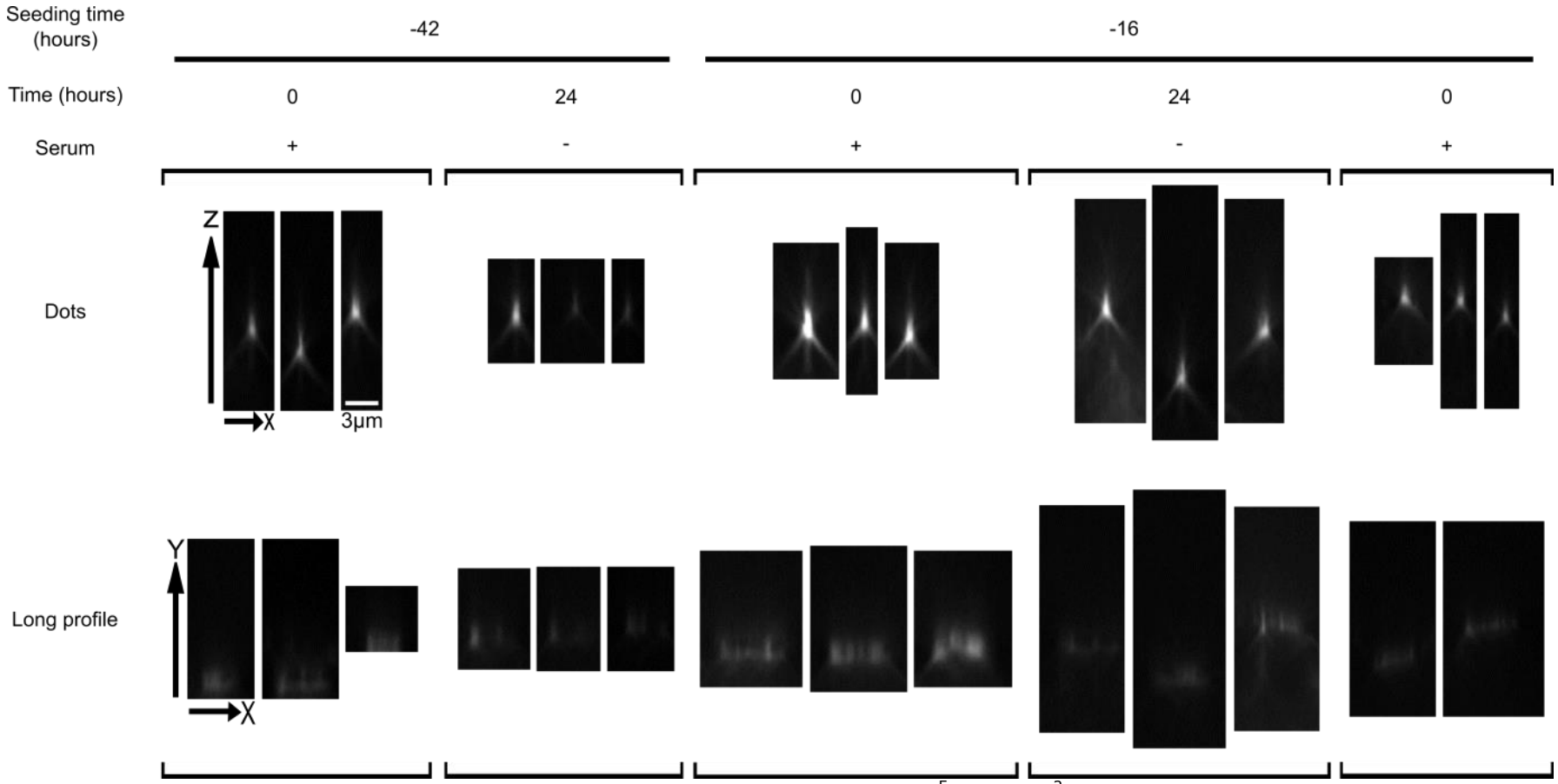


Figure 41. Acetylated alpha tubulin signal profiles from IMCD3 cells at 2 x 10^5 cells/cm^2. For description of nomenclature see Figure 39 legend.

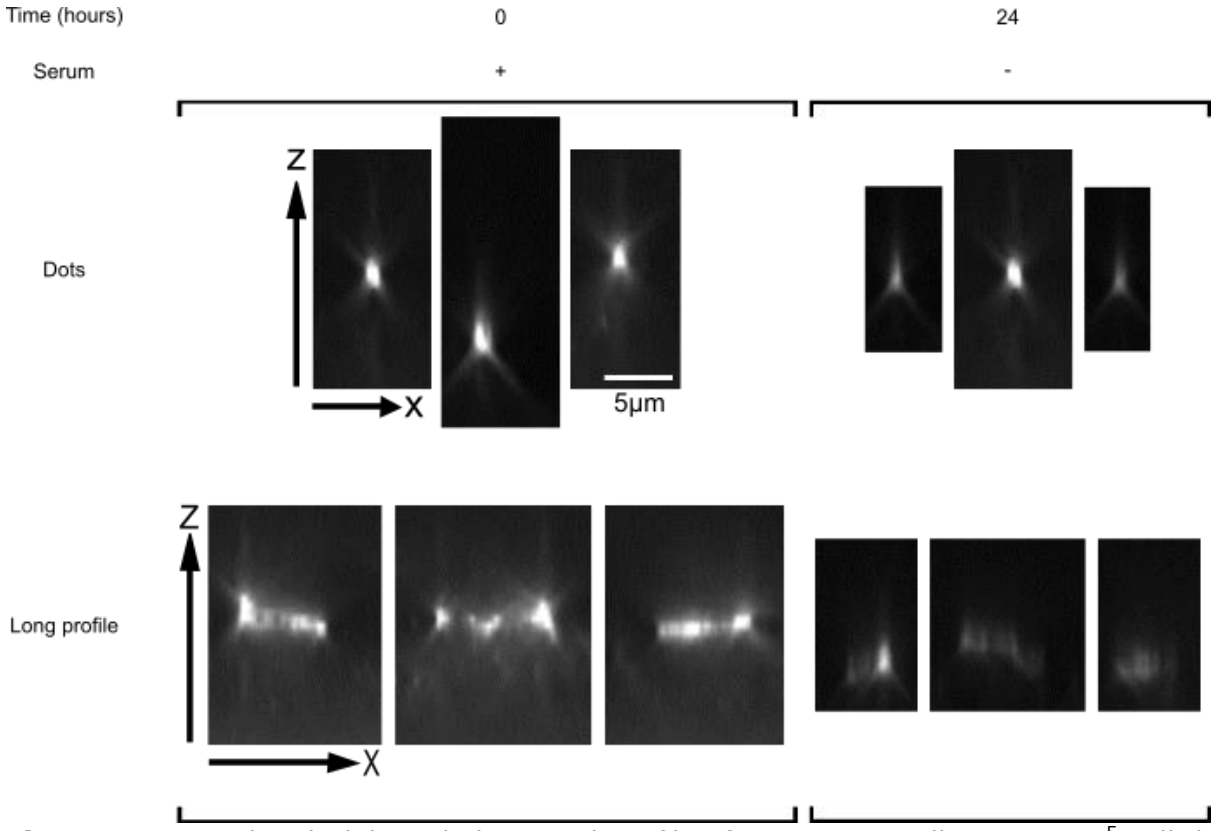


Figure 42. Acetylated alpha tubulin signal profiles from IMCD3 cells at 4 x 10^5 cells/cm^2. For description of nomenclature see Figure 39 legend.

Recalculation of the percentage of ciliated cells in each sample, and removing the dot profiles, yielded similar results to the combined (dot and long profile) percentage values calculated initially. The initial induction experiment, where densities 0.5, 1 and 2 x 10^5 cells/cm^2 were seeded and incubated for 24 hours after t=0 in the presence or absence of serum, resulted in all three time points for both 0.5 and 2 x 10^5 cells/cm^2 harbouring less than 10% of ciliated cells in their populations (Figure 36). 1 x 10^5 cells/cm^2 showed an increase from 3.4% (0h) to 10.4% and 23.3% (24h in the presence or absence of serum, respectively; Figure 36). In itself this result is encouraging, but subsequent experiments for the same density result in all time points less than 10% of ciliated cells within their populations.

Additional attempts at constructing an inducible system for ciliogenesis showed almost all samples at all time points to possess 10% or less ciliated cells (Figures 37 and 38). The sole exception was the 0h time point for 4 x 10^5 cells/cm^2 which harboured 13.9% ciliated cells within its population, but this percentage then dropped to 1.7 after incubation for 24 hours in the absence of serum (Figure 37).

The ciliation results show that the system used here to induce ciliogenesis in IMCD3 cells is not robust. The methods applied here mirror those successfully implemented in other research looking at primary cilia in IMCD3 cells. This suggests that in this study, or previous research groups that have used the cells prior to them being donated for this research, have cultured the cells sub-optimally to such an extent that they no longer behave in the manner expected.

4.3 Characterisation of the *T. brucei* sp. kinesin 13 repertoire

The research interests of this study lie in the characterisation of kinesin function within the primary cilium. The kinesin 16 family was highlighted as having a potential role within this organelle when Wickstead et al. (2006) characterised kinesin family 16 and found them to be associated with organisms that possess cilia. Mrug et al. (2004) found evidence of a role of mouse KIF12 in the severity of PKD. This led to a partial focus of this research on KIF12. Other kinesins are known to function within the primary cilium, including members of the Kinesin 13B subfamily such as KIF2A (Miyamoto et al. 2015), which are known to harbour MT depolymerisers. However, the kinesin 13 family is diverse and not much is known about the roles played by the other two subfamilies 13A and 13C.

T. brucei possesses an expanded Kinesin-13 repertoire of seven proteins. The reference sequence database identifies the seven *T. brucei* Kinesin-13 family proteins presented by Wickstead et al. 2006) only as "kinesin" or putative "Mitotic centromere-associated kinesin (MCAK). These proteins referred to here as Kin13-1, -2, -3, -4a, -4b, -5 and -6 remain consistent with the nomenclature previously used in the literature. Only one of these, Kin13-1, has been found to play a role as a mitotic kinesin (Wickstead et al. 2010b), suggesting that the others harbour extra-nuclear roles. The following research in this section looks to characterise the MT-kinesin interaction, and MT dynamics in the presence of these kinesins, *in vitro*.

4.3.1 *T. brucei* kinesin-13 gene sequences appear to be correctly defined

In particular, having experienced issues with the incomplete human Kif12 reference standard sequence, it was prudent to check the *T. brucei* Kinesin-13 family proteins before attempting to

produce pure recombinant protein. The seven *T. brucei* Kinesin-13 proteins were aligned using the same sequences as used in Wickstead et al. (2010b). The alignment showed that all four conserved nucleotide binding motifs found in kinesin motor domains were present in each of these seven Kinesin-13 sequences (Figure 43).

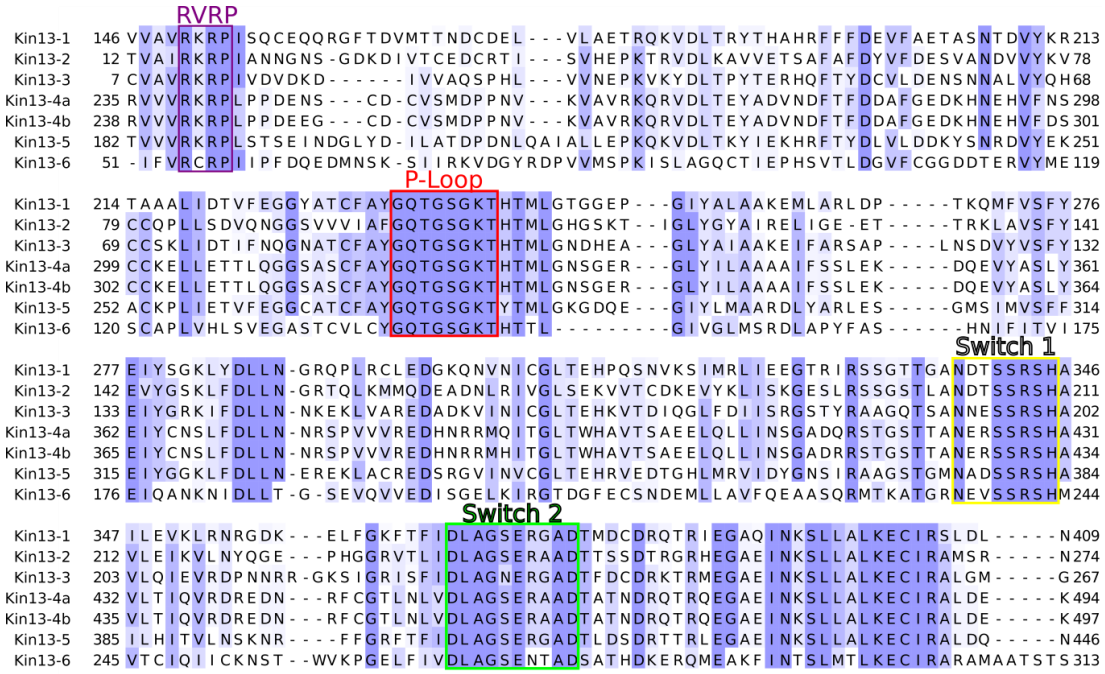


Figure 43. Protein alignment of *T. brucei* Kinesin-13s motor domains. The seven *T. brucei* Kinesin-13s aligned are named Kin13-1 (EAN76453), -2 (EAN79430), -3 (EAN79493), -4a (AAX69505), -4b (AAX70024), -5 (EAN79298), and -6 (XP_827285); GenBank accession numbers for each respective Kinesin-13 protein sequence is in brackets. Accession numbers are taken from the NCBI RefSeq database. The sequences for the four nucleotide binding motifs in kinesin motor domains RXRP, P-loop, Switch 1 and Switch 2 are boxed in purple, red, yellow and green, respectively.

As *T. brucei* does not possess introns there was no ISR data, nor is there a "major splive variant" to identify. Sequence annotations erroneously identifying the start codon downstream from the *bona fide* gene start codon may be an issue. However, the 5' untranslated regions (UTRs) in *T. brucei* are well defined, aiding correct annotation of the gene start codon. Further support for the correct characterisation of the genes start codon is provided by results in Wickstead et al. (2010b) whereby Western blotting of the

seven kinesin-13 proteins (C-terminally tagged) showed that the proteins ran to their expected molecular weights.

The amino acid alignment of the *T. brucei* Kinesin-13s motor domains (Figure 43), the *T. brucei* Kinesin-13s Western blot (Wickstead et al. 2010b), and the absence of introns in *T. brucei* provide enough evidence to suggest the seven identified *T. brucei* Kinesin-13 sequences are the functional genes.

4.3.2 Tb-Kin13s are successfully expressed in Sf9 cells.

In order to characterise the *T. brucei* kinesin-13s the recombinant kinesin-13s would need to be expressed and purified. As Kin13-4a and Kin13-4b appear to be a result of a gene duplication event, evidenced by 72% sequence identity and being present in the large-scale duplication region shared between chromosomes four and eight (Jackson, 2007), it was decided to omit Kin13-4a from the characterisation study.

To produce purified protein for characterisation, the six remaining *T. brucei* kinesin-13 genes were taken through the baculovirus expression system, as described previously. Each kinesin was tagged at the N-terminus with either 6 x histidine or 6 x histidine and GFP. I checked each GFP tagged kinesin Sf9 expression culture for the presence of GFP to ensure that at least the first part of the recombinant protein was being expressed and folded correctly. This was the case for all GFP tagged samples. To ensure the full length protein expression, and not a truncation, whole cell lysates were analysed by SDS-PAGE (Figures 44, 45 and 46). This showed that for all GFP and non-GFP *T. brucei* kinesin-13 variant samples there were detectible bands at the calculated molecular weight for each Kinesin-13 protein that were not present in the negative control. These results strongly suggest that the kinesin-13 proteins were

expressed, but further experimentation would be required to ascertain whether the folding is correct and the motors functional.

4.3.3 *T. brucei* Kin13-1, -3 and -6 are soluble

In order to test the expressed recombinant proteins for ATP turnover and interaction with MTs, conditions in which the *T. brucei* Kinesin-13s were soluble, in as well as correctly folded, would need to be found. Cultures were lysed and separated into what was soluble and insoluble. Under these conditions, the majority of protein matching the predicted molecular weight for Kin13-1, -3 and -6 was present in the soluble fraction (Figures 44, 45 and 46).

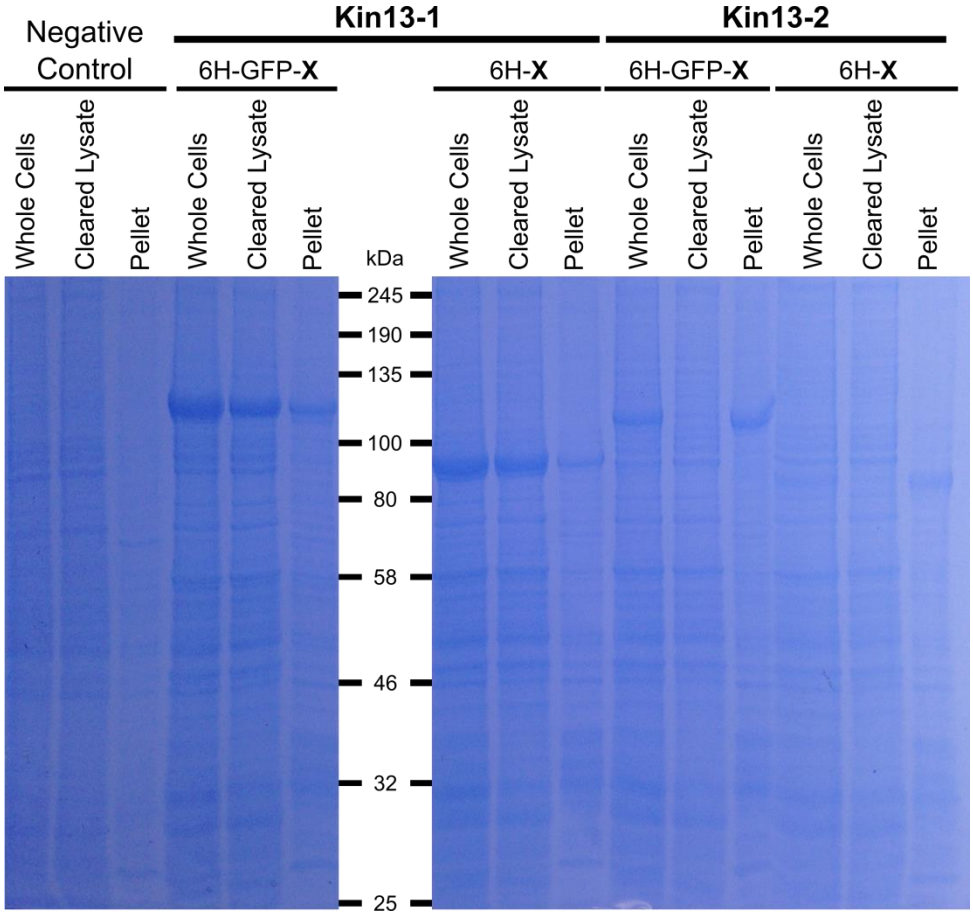


Figure 44. SDS-PAGE of Kin13-1 and 2 Sf9 expression cultures. Whole cells samples contain the protein content of Sf9 cells (taken from the expression cultures) post-lysis. Cleared lysate and Pellet samples were derived from the whole cells sample but separated based on solubility under the conditions the cells were exposed to. The negative control samples were taken from a cell culture taken through the transfection methodology in the absence of vector

DNA. The "X" present in sample names denotes the position of the Kinesin in the recombinant protein.

The vast majority of Kin13-2, -4 and -5 expression cell culture lysates was found to be present in the insoluble fraction (Figures 44, 45 and 46). Both Kin13-2 and -4 were, relative to the other kinesin expression cultures, poorly expressed (Figures 44, 45 and 46). The protein purification results showed that, under the experimental conditions used, only Kin13-1, -3 and -6 samples have a high percentage of their proteome as soluble protein of a matching molecular weight to that predicted. The large protein quantities seen at the predicted molecular weights of each Kin13 protein, whilst being absent from the negative control, strongly suggest that these are in fact the Kin13 proteins, and thus will be referred to as such from here.

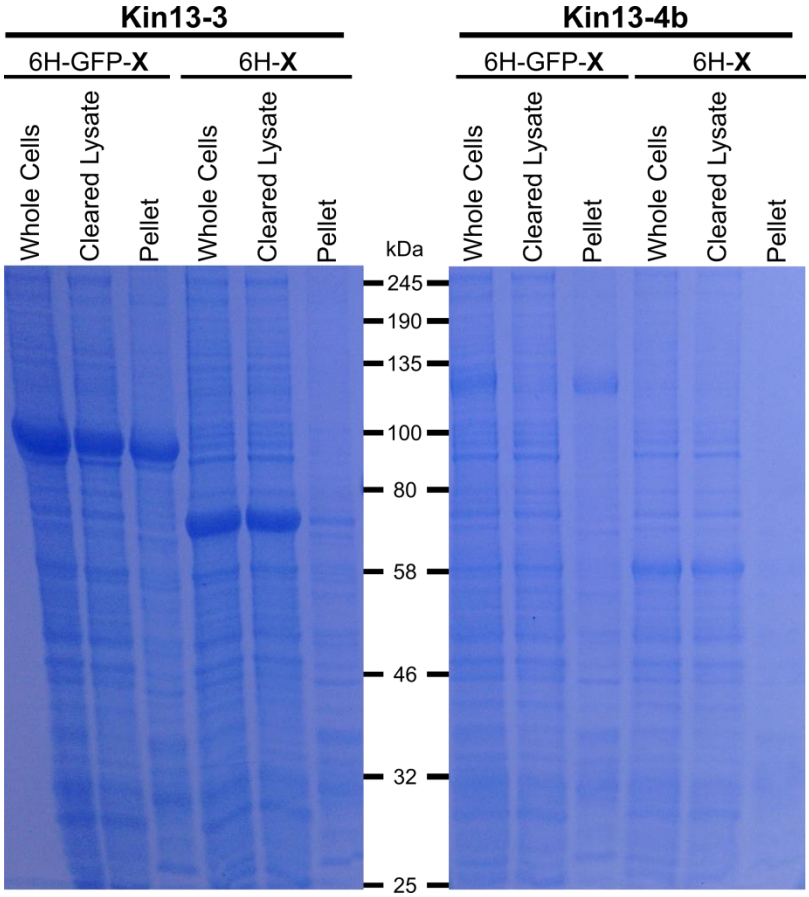


Figure 45. SDS-PAGE of Kin13-3 & 4b Sf9 expression cultures. See legend in Figure 44.

Due to time limitations, the proteins that were insoluble under the conditions used (Kin13-2, -4 and -5) were abandoned for the study. Instead, only Kin13-1, -3 and -4 were taken forward for protein purification.

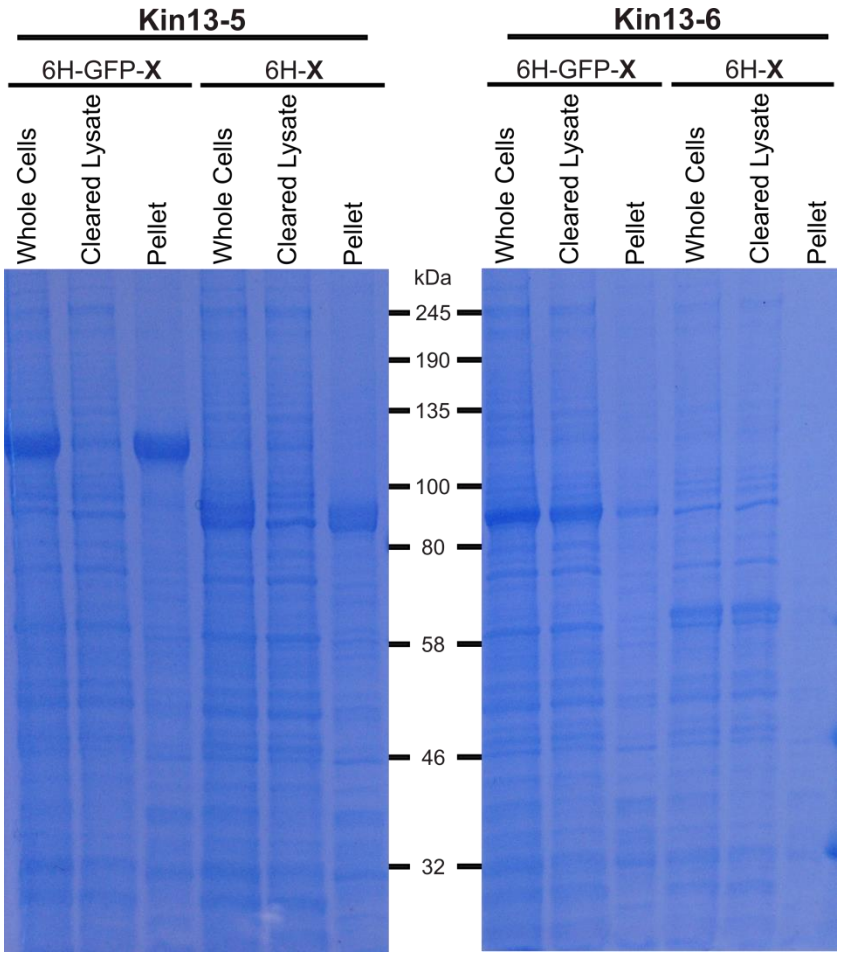


Figure 46. SDS-PAGE of Kin13-5 & 6 Sf9 expression cultures. See legend in Figure 44.

4.3.4 Kin13-1, -3 and -6 can be purified using 1-step Nickel-affinity.

In order to characterise the ATP turnover and interaction with MTs, an attempt was made to purify Kin13-1, -3 and -6 using Nickel-affinity purification. Nickel-affinity purification was carried out on non-GFP tagged Kin13-1, -3 and -6 only as the *in vitro* depolymerisation assay to be used for characterisation of kinesin-

MT interaction does not require a fluorescent tag on the motor (Figure 47 - 49).

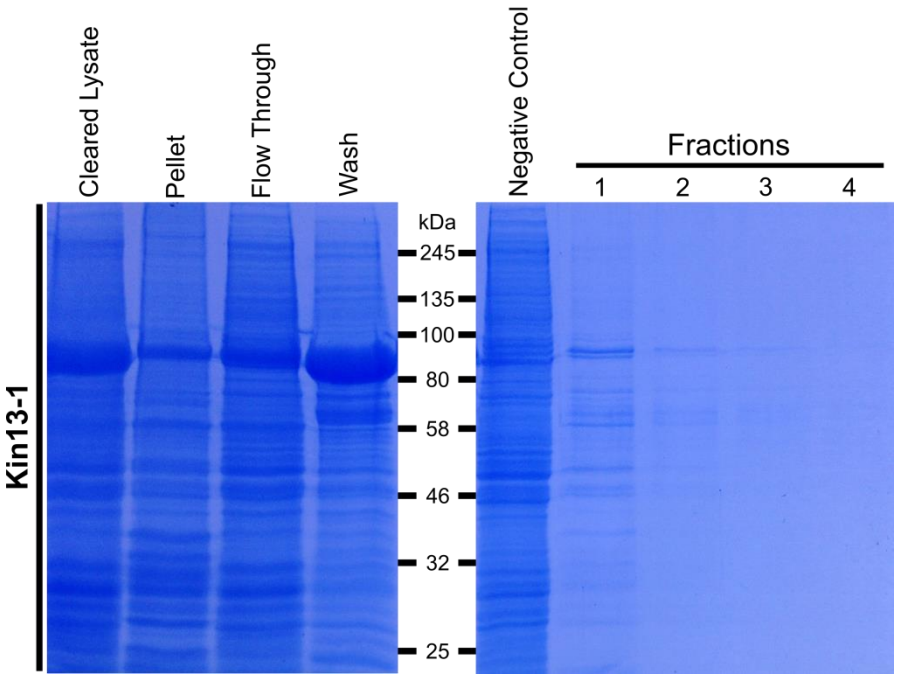


Figure 47. Nickel-affinity chromatography of Kin13-1 expressing Sf9 cells. Kin13-1 Sf9 expression culture cells were separated out into the cleared lysate (soluble) and pellet (insoluble). The cleared lysate was applied to the Nickel-affinity column with the unbound proteins collected in the flow through. The proteins in each sample, including the wash solution and fractions (washed in an increasing concentration of imidazole) were separated by SDS-PAGE. Negative control is explained in Figure 46.

Nickel-affinity purification of 6H-Kin13-1 resulted in roughly 50% of the protein content in fractions 1 and 2 being comprised of Kin13-1 (Figure 47). Subsequent fractions appear to show similar ratios of Kin13-1 to non-target protein, but due to the low protein yield in these, fractions 1 and 2 were pooled together to prevent too much dilution of protein concentration. Both the wash and the flow through contain a strong band at the predicted molecular weight for Kin13-1 (Figure 47) indicating that the concentration of imidazole used was too high for both steps, resulting in the loss of roughly 90% of the Kin13-1 present in the initial soluble sample. The results showed that the 1-step purification process using Nickel-affinity did not yield protein of the desired purity, most likely

due to the imidazole concentrations used (70mM wash and 200mM elution).

The purification Kin13-3 using Nickel-affinity was more successful than for Kin13-1. The fractions collected show that Kin13-3 makes up over an estimated 90% of the protein present (Figure 48). As for Kin13-1, the flow through and wash step samples harbour a large quantity of Kin13-3 (Figure 48), suggesting that the concentration of imidazole used during these steps was high enough to cause unbinding of a large percentage of the Kin13-3 bound to the Nickel-affinity column. The SDS-PAGE of the Kin13-3 sample shows that the protein fractions collected are pure, with a high enough yield to take forward for *in vitro* experimentation.

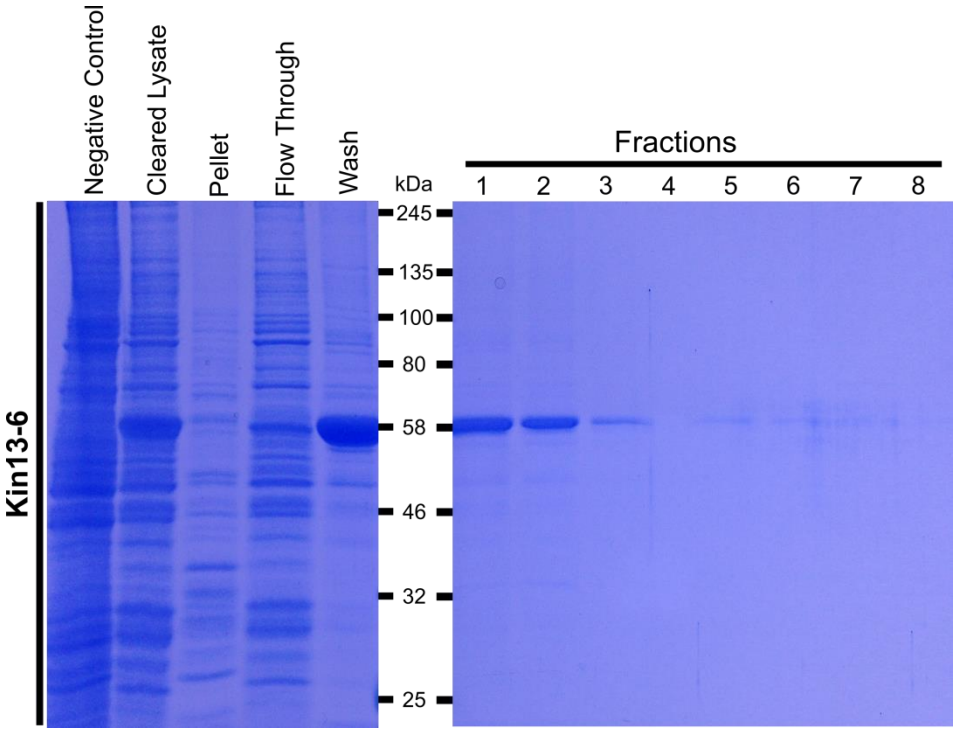


Figure 48. Nickel-affinity chromatography of Kin13-3 expressing Sf9 cells. The process matches that outlined in figure as. Details of the negative control found in Figure 46.

Fractions 1, 2 and 3 of the 1-step Kin13-6 protein purification were made up of roughly 95% Kin13-6 (Figure 49). Like the purification results for Kin13-1 and 3, the wash samples contained a high

quantity of the protein of interest. This lost Kin13-6 in the wash step equates to more than that present in the fractions that were collected afterwards (Figure 49). This shows that the 1-step Nickel-affinity purification process, under the conditions used, was a successful technique in isolating Kin13-6 from the expression culture cell lysates.

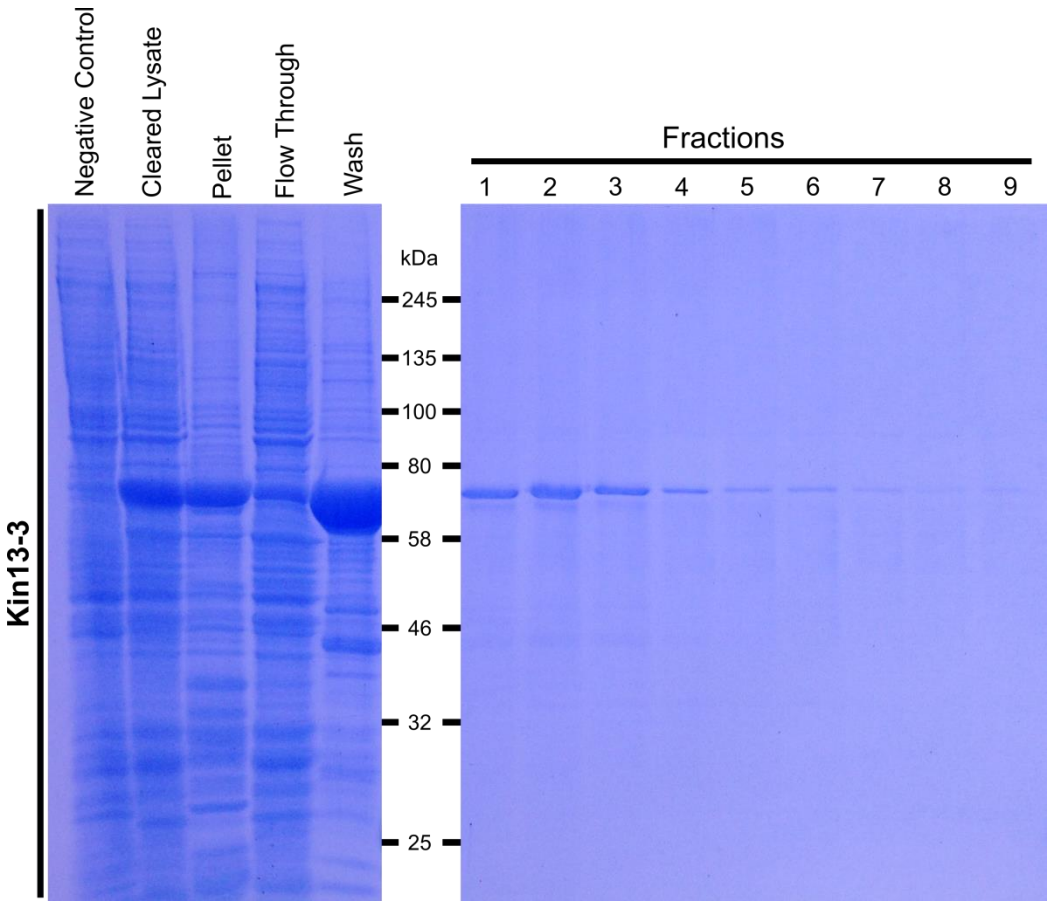


Figure 49. Nickel-affinity chromatography of Kin13-6 expressing Sf9 cells. The process matches that outlined in Figure 47. Details of the negative control found in Figure 46.

If time had permitted, an attempt would have been made to optimise the conditions used for this 1-step process, in particular the concentrations of imidazole used at each step of the process in an attempt to limit the loss of Kin13 during flow-through and wash steps. Further to this, implementation of a 2-step process introducing cation exchange purification may have been required to

obtain a higher purity. However, the resulting fractions from the Nickel-affinity purification of Kin13-1, -3 and -6 were taken forward (including the contaminants present) for *in vitro* analyses.

4.3.5 Kin13-3 causes slow depolymerisation of MTs

The depolymerisation assay showed a small, but significant increase in the rate of MT depolymerisation in the presence of Kin13-3 (Table 2; Figure 50). This means that under these *in vitro* conditions, Kin13-3 is able to aid depolymerisation of MTs. This subtle increase in rate of depolymerisation above the no protein control is also exhibited in Figure 51 where the kymograph shows a significant decrease in MT length over time.

Table 2. Depolymerisation rate of MTs in the presence of *Trypanosoma brucei* kinesin-13s. Kin13-1 cleaved and uncleaved data differentiates between the experiments in which cleavage events were observed and experiments where MTs did not cleave, all in the presence of Kin13-1. The no protein sample acts as the negative control whereby the MTs are exposed to the same buffer, but in the absence of a kinesin. MCAK, a known depolymeriser, is included as a positive control. The median rate of depolymerisation shows the median length a MT will shorten by per minute. The MAD scores (Median adjusted deviation) and the range show the variability between repeats.

Samples	Median rate of depolymerisation (μm min^{-1})	MAD	Range
Kin13-1 (Uncleaved)	0.085	0.022	0.063 - 0.107
Kin13-1 (Cleaved)	0.218	0.051	0.166 - 0.268
Kin13-3	0.169	0.052	0.117 - 0.221
Kin13-6	0.081	0.058	0.023 - 0.138
MCAK	2.842	0.388	2.454 - 3.230
No Protein	0.050	0.023	0.027 - 0.073

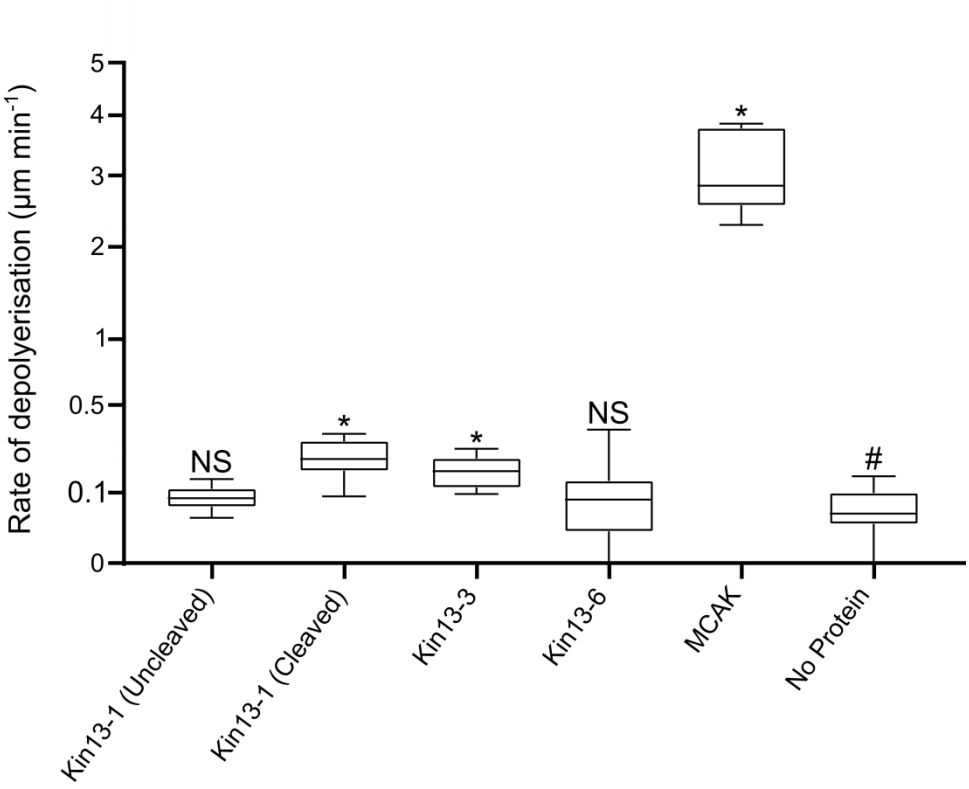


Figure 50. Depolymerisation rate of MTs in the presence of *T. brucei* kinesin-13s. Rate of depolymerisation is measured as the amount of MT shortening per minute (µm min^{-1}). The significance of each rate of depolymerisation was measured in a pair-wise comparison with the no protein (negative) control. NS = no significant difference in the rate of depolymerisation, * = a rate of depolymerisation significantly above the no protein control. Description of Kin13-1 cleaved and uncleaved provided in Table 2.

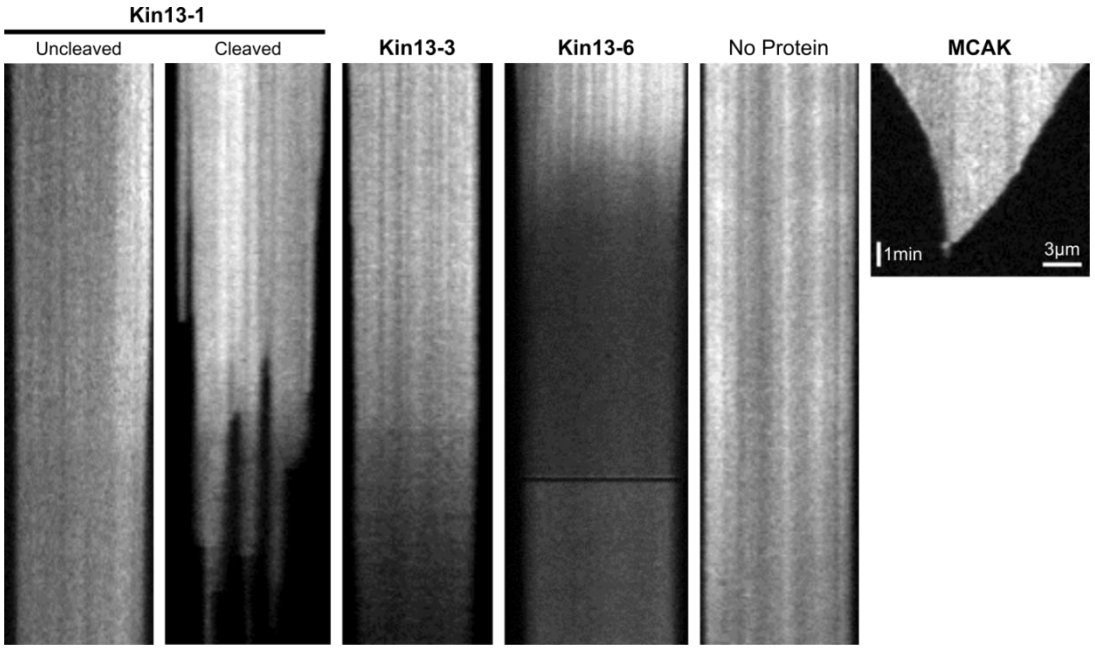


Figure 51. Kinesin 13-dependent MT depolymerisation. MTs of similar lengths were analysed for depolymerisation over a 20 minute period – MCAK image is

truncated as the MT has fully depolymerised before 20 minutes – having been immobilised above the glass surface by anti-tubulin antibodies. Time is shown along the Y axis with the top of the image being t = 0 – the addition of kinesin to the assay. Images were recorded at 5-second intervals. The "no protein" channel (negative control) shows a MT adhered to the coverslip in the same manner as for the other samples, submerged in the same buffer, but in the absence of kinesins.

4.3.6 The depolymerisation assay fails to show Kin13-6 as a MT depolymeriser

In order to uncover the interaction between motor and MT, including what effect the Kin13s may have on MT structure and dynamics, an *in vitro* assay that enabled visualisation of MTs in the presence and absence of the Kin13s was used. This assay, named within the research group as the depolymerisation assay, uses rhodamine-labelled tubulin to allow imaging by fluorescence microscopy. The kinesin protein is unlabelled to reduce the risks of altering its function. The change in the MT length is recorded by snapshots taken at 5-second intervals, this allows for calculation of rates of MT depolymerisation.

All three *T. brucei* kinesin-13s, along with MCAK and "No Protein" (acting as positive and negative controls, respectively), were independently added to GMPCPP (a slowly hydrolysable GTP analogue) stabilised MTs. Once the motor was added, the change in MT length was observed and rates of depolymerisation (μm min^{-1}) calculated (Figure 50 and Table 2). MCAK was used as the positive control as it is a known MT depolymeriser and has been used successfully in this assay within our research group.

The results of the depolymerisation assay show that the rate of MT depolymerisation in the presence of Kin13-6 was not significantly higher than the no protein control (Table 2; Figure 50). This means that, under the purification and assay conditions used, Kin13-6 is not a MT depolymeriser *in vitro*.

4.3.7 Kin13-1 displays MT severing behaviour

In order to observe whether any of the soluble Kin13 proteins affected MTs other than to catalyse MT depolymerisation, individual MTs from the depolymerisation assay were analysed (Figure 51). This analysis showed that some MTs, in the presence of Kin13-1, underwent multiple cleavage events (Figures 51, 52 and 54). The rate of cleavage events per 1µm MT in the presence of Kin13-1 was significantly higher than all other experimental and control samples. This suggests that Kin13-1 may function like katanin, severing MTs at the lattice.

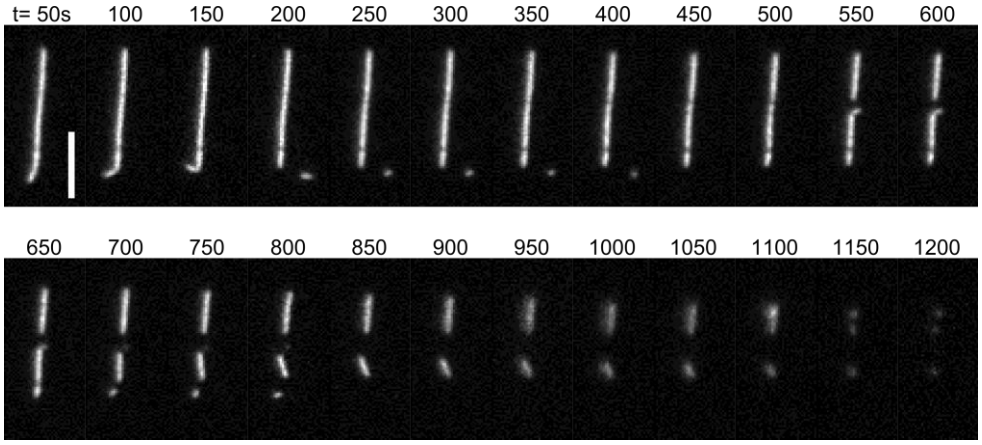


Figure 52. MT dynamics in the presence of Kin13-1. Images show the change in MT integrity and length over a 20 minute period. Images are spaced in 50 second intervals. Scale bar: 10µm

However, these results involving Kin13-1 have to be taken with caution due to the relative impurity of the fractions collected (Figure 47). Even low quantities of a given contaminant may vastly change the outcome of the *in vitro* depolymerisation assay.

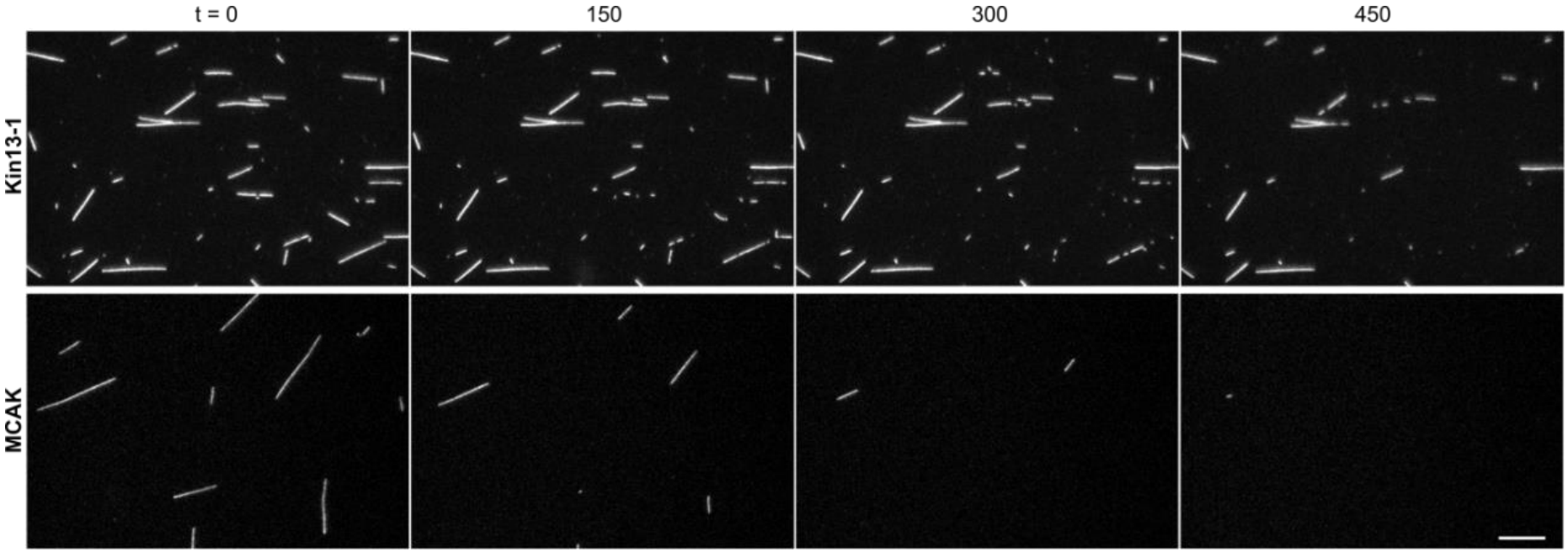


Figure 53. Comparison of MT dynamics in the presence of Kin13-1 and MCAK. Images of the respective *in vitro* depolymerisation assays carried out, captured using rhodomine signal (MTs of rhodomine dyed). Images are at 150 second intervals. T = 0 represents the time at which the kinesin was introduced to the assay. Scale bar: 10μm.

The MT severing events occurring in the presence of Kin13-1 occurred in only half the fields of view analysed. This amounted to three (out of six) fields of view spread across the two repeats. This is thought to be caused by an issue with the flow of solutions (and the proteins suspended within them) through channels where MTs are stuck. Any heterogeneity in flow would cause heterogeneity in the concentration of Kin13-1 throughout the slide. Nevertheless, the incidence of multiple cleavage events in numerous MTs within each of the three fields that this was observed, across two repeats, suggests that the phenotype is caused by the proteins present in the fractions, contaminants or not.

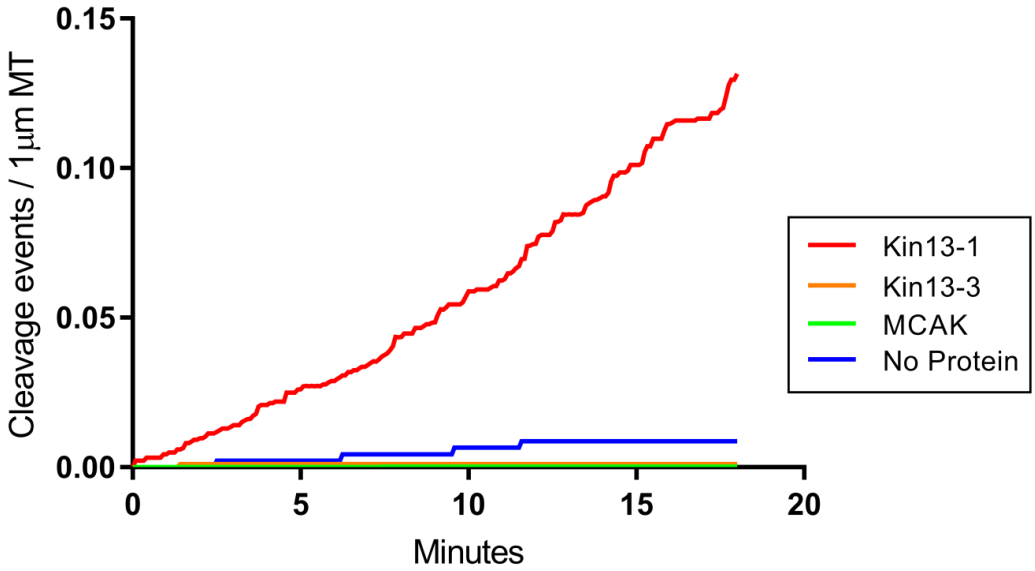


Figure 54. MT cleavage events in the presence of Kineisn 13s. A cleavage event is being defined as a break anywhere in the MT lattice. Cleavage events are measured by the incidence of cleavages within a 1µm stretch of MT, measured over time. The cleavage events are recorded cumulatively over the 20 minute period. MTs analysed in the presence of Kin13-1 were chosen from experiments where cleavage of MTs had been observed, but all MTs within that experiment were analysed, not just those that have cleaved. MCAK and no protein samples were used as controls.

5 Discussion

The aim of this research was to identify novel roles for kinesin families, with a specific interest in those functioning in the primary cilium, and the mechanisms used to fulfil these functions. The kinesin-16 family was investigated as members of this family are only found in organisms that build cilia/flagella, strongly suggesting a ciliary role (Figure 10). Human KIF12 was used as a Kinesin-16 representative from which to decipher the cellular roles this family might play, due to its localisation within the cilium (Mrug et al. 2015), and its identification as a modifier gene for PKD (Mrug et al. 2005). The Kinesin-13 family was also investigated as this family is only absent in organisms that do not build a cilium/flagellum (Figure 10). Many Kinesin-13 family members have been shown to have ciliary function such as KIF24 and KIF2A (both *Homo sapiens*) and LmjKIN13-2 (*Leishmania major*). However, the role of motors in the Kinesin-13C subfamily have yet to be defined.

Kinesin-13s from *Trypanosoma brucei* were used to investigate the potential roles of Kinesin-13 motors in the cilia/flagella, as the flagellum is present at all points in the *T. brucei* life-cycle. Further, *T. brucei* possesses an expanded collection of Kinesin-13s.

5.1 Expression and purification of recombinant protein

An *in vitro* model assay was used to identify MT depolymerisation activity of the kinesins under investigation. Studying kinesin-MT systems in the absence of other cellular components enables the characterisation of the direct effect of a particular kinesin on MT dynamics. The principle *in vitro* assay used in this work involved visualisation of fluorescent microtubules in the presence of purified kinesin. Expression and purification of recombinant kinesins was

required for analysis of kinesin-MT interaction within this depolymerisation assay. The Sf9 insect expression system was the initial, or only, expression system used with all kinesins investigated in this research. Despite none of the kinesins investigated here being insect-derived, previous success expressing and purifying a wide range of kinesins in Sf9 cells in our research group and in the wider scientific community made it a logical choice to begin with (Helenius et al. 2006; Patel et al. 2016; Varga et al. 2009). Only in the event of expression and purification difficulties using the insect system would an alternative expression system be sought.

Cation-exchange chromatography and Nickel-affinity chromatography were selected as the two means of purifying expressed kinesins. Cation-exchange was selected due to the successful purification of other kinesins by this method (Patel et al. 2016), and Nickel-affinity chromatography was chosen due to the presence of a 6 x Histidine tag on all expression proteins.

5.1.1 Human KIF12

5.1.1.1 Expression and purification of RefSeq rsKif12 and rsKif12MD

To investigate the behaviour of the Kinesin-16 family, a human Kinesin-16, Kif12, was cloned. *rsKif12* was believed to the major splice variant in human kidney cells, a cell type known for high Kif12 expression (Figure 31). The use of *rsKif12* seemed sensible as it was sequenced from mRNA so it exists as a human transcript and the reference standard sequences in RefSeq match the MSV far more frequently than the predicted models. A motor domain-only sample was also created for expression trials as the long coiled coil regions found in many kinesin tail domains can cause poor expression and insolubility issues. The rsKif12MD sequence was defined by comparing the motor domain to the mouse Kinesin-

1, KIF5B, as the sequence is well defined. The protein samples were tagged at the N-terminus as C-terminal tagging might interfere with cargo binding in the rsKif12 protein. It was felt that this was valid as there was nothing in the literature to suggest that tagging at either terminus was more successful.

Expression trials indicated that both rsKif12 and rsKif12MD had poor solubility in both insect and mammalian expression systems. The inability to obtain soluble rsKif12 and rsKif12MD from insect expression cultures, under the conditions used, was initially surprising as many kinesins have been expressed and purified in the same manner. The change to a mammalian expression system failed to ameliorate these problems, despite expressing a human protein in human and mouse cell lines.

5.1.1.2 rskif12 does not represent the full human *KIF12* sequence

The rsKif12 sequence was analysed in the search for anything that might result in the observed poor solubility. The rsKif12 sequence was found to lack two of four nucleotide-binding motifs found in the highly conserved kinesin motor domain. The lack of these two characteristic kinesin motor domain sequence motifs shows that a substantial portion of the motor domain is missing from the rsKif12 sequence. It is unlikely that this partial motor domain sequence could fold correctly, thus providing an explanation for the solubility issues observed for both full-length and motor only versions of this kinesin in both insect and mammalian expression systems. If the partial motor domain sequence is responsible for solubility issues it would explain why even the motor domain-only sample failed to solubilise.

To determine the human *KIF12* sequence, RNA sequencing data was analysed from human kidney tissue.The full KIF12 sequence was created by selecting the most abundant ISRs from the data.

The final *KIF12* sequence was then checked for the four conserved nucleotide-binding domains found in all kinesin motor domains studied to date.

The major human KIF12 isoform sequence, a direct translation from the *KIF12* sequence that had been constructed, was aligned against the mouse rsKif12 sequence. Close sequence identity between the two sequences would provide further evidence that the KIF12 sequence I had defined was the major human KIF12 isoform. The main difference between the two sequences was a five amino acid sequence (PPGGG) found in human KIF12, but not in mouse rsKif12. PPGGG was previously highlighted as an INDEL in an inbred mouse line (Mrug et al. 2005). The rsKif12 sequence was constructed from RNA sequencing data also from an inbred mouse line. To check whether the wild type mouse KIF12 sequence possessed the PPGGG, inbred and outbred mouse line Kif12 sequences were aligned. The outbred mouse line Kif12 sequences possessed the PPGGG sequence indicating that the major wild type mouse KIF12 isoform does contain the PPGGG sequence. The presence of PPGGG in the wild type mouse sequence supports the inclusion of PPGGG in the human KIF12 sequence.

To ensure that the presence of PPGGG in human KIF12 was not due to a splicing error in the DNA coding sequence, the splice sites for KIF12 were checked. The start of the DNA sequence encoding for the PPGGG amino acid sequence was the tenth nucleotide from the splice site of the exon on which it is found. The final analysis used to confirm the presence of PPGGG in human KIF12 was a protein alignment of Kif12 homologue sequences from across the animal kingdom against human KIF12. This alignment provided enough evolutionary diversity to detect the gain or loss of PPGGG sequence in mice. The results of the analysis from the sequence

alignments and splice sites provide strong evidence that the PPGGG sequence is present in the human KIF12 major isoform.

The stringent bioinformatics approach taken to determine which human KIF12 sequence to use in this study is further supported by Katoh and Katoh (2005) who defined the same sequence *in silico* using a different analytical approach.

5.1.1.3 Expression and purification of human KIF12 and kif12ΔPPGGG

To characterise the function of KIF12, both KIF12 and kif12ΔPPGGG were expressed in insect cells. KIF12ΔPPGGG was expressed, as well as wild type KIF12 as polycystic kidney disease mouse models with KIF12ΔPPGGG have less severe forms of polycystic kidney disease (Mrug et al. 2005). Successfully expressed and soluble protein was purified using a two-step method of cation exchange chromatography followed by Nickel-affinity chromatography. Both KIF12 and kif12ΔPPGGG expression constructs contained a 6xHistidine tag.

Expression trials were performed on a variety of Kif12 constructs. Both wild-type Kif12 and the ΔPPGGG mutant were expressed as full-length and motor domain-only constructs. Additionally each Kif12 construct was expressed with the tags at either the N- or C-terminus. Both KIF12 and kifΔPPGGG were insoluble when expressed in Sf9 cells under the laboratory conditions used despite part of the each sequence being codon optimised for *S. frugiperda*.

5.1.1.4 Expression and purification of human Kif12MD

The insolubility of KIF12 and kifΔPPGGG led to an attempt to produce soluble recombinant Kif12MD. The Kif12MD sequence was expressed with either C- or N-terminal tagging. Unexpectedly, despite the use of the same experimental conditions, the terminus on which Kif12MD was tagged made a difference to its solubility.

Kif12MD is soluble under the laboratory conditions used when tagged at the C-terminal end.

Defining human KIF12 allows for more accurate characterisation of its interaction with MTs *in vitro* compared with rsKif12. This is due to the expected ability of KIF12 to bind ATP, whereas rsKif12 lacks the conventional motifs in its motor domain to do so. However, the inability to acquire soluble KIF12 protein, despite possessing a complete motor domain with the expected nucleotide-binding domains, is surprising. Producing soluble Kif12MD shows that it is not the motor domain for KIF12 that is causing insolubility issues under the laboratory conditions used.

5.1.1.5 Limitations of computational approaches to determine KIF12

Attempts to express and purify KIF12 and KIF12ΔPPGGG have been limited by the use of a sequence constructed *in silico* but not yet fully sequenced from a human tissue. If there are mistakes present, they might lead to misfolding and aggregation of the recombinant protein.

Determination of human KIF12 was limited by the sequencing data. RNA sequencing read lengths are typically short, making piecing sequencing together potentially more difficult. The final KIF12 sequence was an amalgamation of two predicted isoforms. As a result, it is not known whether the *KIF12* sequence truly exists as a post-splicing mRNA transcript in human cells.

The expression and solubility trials carried out show that a motor domain-only version of Kif12 with a C-terminal GFP tag is soluble when expressed in Sf9 cells. This is a step forward in enabling to characterisation of this kinesin *in vitro*. However, future investigations into the function of KIF12 will be hampered by the use of Kif12MD, as any roles of the tail domain will be missed. This

could include binding to cargo or interaction with other motors (or motor associated proteins) or self-interaction if it forms a multimeric protein.

In order to multimerise KIF12, it may be possible to find a truncated version of Kif12 with a partial tail that is soluble but retains the ability to dimerise, as suggested by the predicted coiled-coil region. This approach has been applied successfully to kinesin-1, for example to the K560 construct (Vale et al. 1996). Alternatively, the addition of a leucine zipper to the soluble C-terminally tagged Kif12-MD may encourage the binding of motors together to create a motility-competent dimer. This has been successful in experiments with the budding yeast motor Kip3 (Su et al. 2011).

Another method that may help create multimers from the initial soluble Kif12MD protein would be to use split GFP tags, as has been successfully implemented in the multimerisation of TDP-43 (an RNA-binding protein; Foglieni et al. 2017). Two pools of Kif12MD, tagged with a different half of the split GFP protein, could be expressed and then mixed. The presence of correctly multimerised motors could be confirmed by the presence of the now complete GFP marker.

5.1.2 *T. brucei* Kinesin-13 repertoire

In order to characterise the seven distinct *T. brucei* kinesin-13 proteins *in vitro*, it was necessary to first ensure that the gene sequences were correctly defined.

The protein sequences for the Kinesin-13s were checked to ensure that the four conserved motor domain nucleotide-binding motifs were present; all seven possessed these motifs. Correct annotation of the start codons for each *T. brucei* Kinesin-13 protein was

verified by ensuring that it was immediately downstream from the well-defined 5' untranslated regions. *T. brucei* does not possess introns, so there is no major splice variant to identify. Finally, previous research by Wickstead et al. (2010b) and Chen et al. (2010) showed distinct localisations for each of the Kinesin-13 proteins compared to control samples in *T. brucei*. These points put together are strong evidence that the functional kinesin-13 genes in *T. brucei* are correctly defined.

In order to characterise the seven distinct *T. brucei* kinesin-13 proteins *in vitro*, it was necessary to express them recombinantly in Sf9 cells (for the reasons previously given) and purify them using Nickel-affinity chromatography. As Kin13-4a and -4b are so closely related, Kin13-4a was not taken through the expression procedure. Expression of *T. brucei* Kinesin-13s led to solubility for only Kin13-1, -3 and -6 under the lysis conditions used. These three proteins were then purified in preparation for characterisation *in vitro*.

T. brucei possesses kinesin-13s from two of the three defined kinesin-13 subfamilies (A and C; Wickstead et al. 2010). Expression and purification of Kin13-1 and -3 (13A) and Kin13-6 (13C) ensures that these two subfamilies are represented during *in vitro* characterisation. Kin13-2, shown to localise to the flagellum in the *T. brucei* procyclic stage (Wickstead et al. 2010b), was not soluble under laboratory conditions, meaning a potential role in flagellar length regulation could not be investigated.

5.2 Kinesin-mediated microtubule regulation

The depolymerisation assay was carried out for the purified soluble recombinant *T. brucei* Kin13-1, -3 and -6. Kin13-1 displayed possible MT cleaving activity *in vitro*. Cleavage occurred on the MT

lattice. This severing promoted significant depolymerisation in the resulting smaller MTs. There does not appear to be any length-dependent bias in terms of which MTs are cleaved. Instead, cleavage appears to be indiscriminate, with MT cleavage incidence proportional to the overall length.

Kin13-3 significantly increases the rate of MT depolymerisation in vitro. Whilst Kin13-6 was found not to alter MT dynamics when compared with the no-protein control *in vitro* suggesting that its role lies outside of MT regulation.

5.3 Essentiality of KIF12 in cilia function and cell viability

Wheway et al. (2015) carried out a siRNA-based functional genomics screen for the identification of regulators of ciliogenesis and ciliopathy genes in IMCD3 cells. This study failed to highlight KIF12 as essential in cilia production and/or maintenance, or cell viability. It was decided to analyse the data to gain specific insight into how KIF12 had performed. To do this the z_{cilia} scores (standard deviations of the median impact on ciliogenesis and/or cilia maintenance) for KIF12 from the experiment were compared against other known essential proteins in cilia structure that were not flagged as "hits" (Wheway et al. 2015). In Wheway et al. (2015), a "hit" was any gene that, when knocked down, had a z_{cilia} value higher than the median positive control score. Consequently, even if a gene is essential, it would only flag up as a gene essential to cilia function if the impact is greater than the median positive control. As a result, comparing KIF12 against genes known to be essential in cilia function that were not hits seemed to be the most valid way of gaining an insight into whether KIF12 is essential in this process or not.

The results suggested that KIF12 is essential in the functioning of primary cilia in IMCD3 cells. This was due to having a more profound impact on cilia building and/or maintenance than five of the seven known essential cilia proteins it was compared against. This result is consistent with other research on Kif12. Kif12 is known to localise to the cilium (Mrug et al. 2015), but other research has implicated it as a modifier gene for PKD (Mrug et al. 2005), a disease caused by malfunctioning primary cilia.

5.4 Inducing ciliogenesis in IMCD3 cells

In order to investigate the expression dynamics, location and functional partners of KIF12 during the cilia cycle, an inducible system was required for ciliogenesis. IMCD3 cells were chosen as the cell line in which to design the inducible system. IMCD3 cells were chosen due to having siRNA knockdown (Wheway et al. 2015), expression and cilia localisation experiments for KIF12 carried out in this cell line (Mrug et al. 2015).

Induction of ciliogenesis was attempted using serum starvation and/or contact inhibition. This was a valid method of achieving cilia induction as ciliation has been achieved by both methods in the literature previously (Pugacheva et al. 2007). Identification of ciliated cells is achieved by using α-acetylated β-tubulin, a post-translational modification enriched in the primary cilia, under fluorescence microscopy (Reviewed by Hua and Ferland, 2017).

A significant and consistent method of inducing ciliogenesis in the IMCD3 cells used in the laboratory was not devised here. Various cell densities were trialled, as well as incubation periods in the absence of serum, with all failing to induce significantly different levels of ciliogenesis compared with the standard incubation conditions used. This is inconsistent with the literature where

contact inhibition and serum starvation both cause IMCD3 cells to exit the cell cycle and build a primary cilium (Breslow et al. 2013).

Identification of primary cilia through fluorescence microscopy proved problematic. The use of acetylated β-tubulin as a primary cell marker failed to provide distinguishable signal profiles for the axoneme and docked basal bodies. The signal from the basal body in IMCD3 cells was as strong, if not stronger, than that for the axoneme. This created issues in initial ciliated counts from IMCD cell populations.

Methanol-fixed immunostained cell cultures presented with two types of signal profile: "dot" and "long". The most sensible way to differentiate the two was to stack the images taken at multiple focal depths to form a three-dimensional image and turn the display from XY axes to XZ. This enables visualisation of "dots" into the Z axis to measure whether the lengths were more typical of a basal body or a cilium. Identification of cilia and docked basal bodies from XZ imaged did not meet expectations as almost all "dot" signals were indeed docked basal bodies and not primary cilia extending into the Z axis. This further underlined the inability to induce significant proportions of the IMCD3 cell cultures to undergo ciliogenesis.

The findings in this research that the IMCD3 cells used could not be induced repeatedly to undergo ciliogenesis suggest that IMCD3 cells can forgo sensory stimuli that would, under usual circumstances, induce ciliogenesis. The IMCD3 cells used in this research were kindly donated to our research lab. However, information on the passage number or how the cells were handled were not provided. As a result, it is possible that the IMCD3 cells, before donation, were handled in such a way that selected for cells

that did not exit the cell cycle under contact inhibition and therefore would not undergo ciliogenesis.

The findings from cilia marking with α-acetylated β-tubulin showed that in IMCD3 cells other markers could be used to increase the ease at which primary cilia and docked basal bodies can be differentiated. The fixation and immunostaining method used to fix IMCD3 cells was also limiting as it relied upon the placing of cell cultures grown on coverslips to be placed face down onto different substances and materials. This may be problematic as the removal of the cover slip may apply a shearing force strong enough to remove primary cilia from their cells. This may explain the near complete absence of primary cilia extending into the Z axis; although it is also possible that the mounting of coverslips to slides causes all present primary cilia to be pushed over to the side.

5.5 *T. brucei* kinesin-13 motors differ in their interaction with microtubules

5.5.1 Katanin-like activity of Kin13-1 gives insight into possible chromosome segregation mechanism in *T. brucei*

Kinesin-13 and eight family members such as MCAK and Kif18A have been identified as essential in the correct segregation of chromosomes during mitosis (Maney et al. 1998; Mayr et al. 2007). *T. brucei* does not possess any Kinesin-8s, and only Kin13-1 is present in the nucleus during its closed mitosis. Kin13-1 is essential for correct segregation of both large and mini-chromosomes in *T. brucei*, with Kin13-1 knockdown resulting in "spindle-like structures persisting in non-mitotic cells" (Wickstead, et al. 2010b). This evidence strongly suggests that Kin13-1 is involved in spindle-length regulation, but how it achieves this is stillunknown.

Kin13-1 displayed MT cleaving activity with cleavage events taking place along the MT lattice *in vitro*. Kin13-1 activity at the MT lattice is consistent with its localisation along the mitosis spindle in *T. brucei*. The cleaving activity of Kin13-1 on MTs is a novel kinesin-MT interaction. MT cleaving activity has only previously been observed for non-motor proteins such as Katanin, Spastin and Fidgetin (McNally and Vale, 1993; Errico et al. 2003; Zhang et al. 2007). The site of MT regulation by Kin13-1, the MT lattice, is also novel among kinesins. All other known MT polymerisers and depolymerisers function at the MT tips. As *T. brucei* lacks any members from the Kinesin-13B family, such as MCAK, it is possible that the organism has evolved to regulate spindle length through cleavage of the MT lattice, rather than depolymerisation of the spindle MT ends. This unique method of regulating MT-length suggests that Kin13-1 regulates the mitotic spindle, and thus chromosome segregation, in a novel manner.

In addition to Kin13-1, *T. brucei* possess another MT-severing protein in katanin. *T. brucei* katanin does not localise to the nucleus at any point during the cell cycle, instead localising to the flagellum (Casanova et al. 2009; Benz et al. 2012). Knockdown of katanin results in issues with cytokinesis, but not with replication of nuclear material (Benz et al. 2012). This nuclear exclusion of katanin shows Kin13-1 as, to date, the only MT-severing protein, and only MT-length regulating kinesin, involved in *T. brucei* chromosome segregation. The absence of katanin from the nucleus provides further evidence that the essentiality of Kin13-1 in correct chromosome segregation during mitosis is due to its MT-cleaving activity.

5.5.2 *T. brucei* possesses extra-nuclear depolymerisers

Kin13-3 significantly depolymerises MT *in vitro*. This result is not wholly surprising as Kin13-3 is part of the 13A kinesin subfamily, which contains other MT regulators such as KIF24, AtKinesin13-A and –B, and LmjKin13-2. Kin13-3 was found to depolymerise MTs, but at a much slower rate than MCAK.

Kin13-3 is excluded from the nucleus in procyclic *T. brucei* cells, meaning it is non-mitotic in function, at least in this stage of the lifecycle. Instead, Kin13-3 is found in the cell body (Wickstead et al. 2010b). If Kin13-3 behaves *in vivo* as it does *in vitro* then this result is the first evidence of an extra-nuclear MT depolymeriser in *T. brucei*; although it is highly probable that there are others that regulate the length of the flagellar axoneme.

5.5.3 Kin13-6 does not regulate microtubule length

This preliminary data would suggest that Kin13-6, and possibly, as a representative of the subfamily, Kinesin-13Cs do not depolymerise MTs. As previously no other Kinesin-13C motor interactions with MTs have been studied, there is no expected outcome. However, the vast majority of Kinesin-13s studied (as mentioned above) do regulate MT dynamics. If Kin13-6 is truly a non-MT regulator, than this opens up the possibility of a functional role for Kinesin-13Cs, differing from the rest of their kinesin family.

5.5.4 Limitations of the *T. brucei* kinesin-13 depolymerisation assays

MTs used in the depolymerisation assay are taken from porcine brain tissue. As a result, the interactions kinesins have with these MT *in vitro* may differ from those in their native organism. The most likely differences between MT types are the post-translational modifications rather than structural as α and β-tubulin subunits are tightly conserved across the eukaryotic domain.

Kin13 motor domain activity in the recombinant protein has yet to be checked. In the cases of Kin13-1 and Kin13-3 where their presence did change MT dynamics compared with no protein control, it is highly likely that the motors are functional. However, for Kin13-6 it is a much stronger argument that Kin13-6 does not function as a MT deploymeriser if there is proof that the motor does turnover ATP. As a result, until this experimentation takes place, it is difficult to provide strong evidence for a different cellular role for Kin13-6, and 13Cs in general, compared with the rest of the Kinesin-13 family.

The inability to obtain completely "pure" protein samples raises the possibility that contaminants present within the protein samples may alter the kinesin or the MT behaviour under experimental conditions. The Kin13-1 protein sample harboured only ~50% Kin13-1, which leaves lots of non-specific protein present when carrying out the depolymerisation assay. This may have distorted what the true outcome of the assay would have been had a pure Kin13-1 sample been used.

The MT-cleaving phenotype observed for Kin13-1 *in vitro* was not consistent across the flow channels used. MT-cleaving activity was observed in three of the six channels used across two repeats. The cleaving activity was observed in both repeats, and so is less likely to be an artefact of a specific experiment. The most likely reason for this inconsistency is the flow rates in each channel. This would lead to non-uniform spread of the protein across the channel, thereby starving some locations within the channel of motor proteins.

5.6 Recommendations for future work

5.6.1 Characterisation of KIF12

In order to verify the human KIF12 sequence defined here, it would be beneficial to produce cDNA from *KIF12* transcripts taken from kidney, liver or pancreatic tissue, and sequence it. This would help identify any discrepancies between the suggested KIF12 sequence and the KIF12 MSV encoded in the cDNA.

Different expression systems to produce soluble KIF12 and KIF12ΔPPGGG that could be used in *in vitro* assays should be tested. Many other expression systems have proven to be fruitful in producing functional kinesins. If this cannot be achieved, than producing a Kif12ΔPPGGG motor-domain only variant by the same means as Kif12MD-GFP should be achievable.

Further research should include checking KIF12MD motor activity by looking at its ATP turnover. KIF12MD-MT interactions should be observed using the depolymerisation assay (described in the Materials and Methods section). If expression and purification of KIF12 and KIF12ΔPPGGG can be achieved, then these proteins could be characterised using biochemical and biophysical techniques to determine if they differ in regards to their ability to turnover ATP or in their interaction with MTs. Studies of this type should highlight the impact ΔPPGGG has on motor function. KIF12 is predicted to be a translocator; this needs to be verified using *in vitro* MT interaction assays such as a gliding assay, to determine if KIF12 does support MT motility.

5.6.2 Functional analysis of *T. brucei* kinesin-13s

Follow up research from these depolymerisation assays should be to provide evidence of Kin13 motor activity through ATP turnover. Proof of motor activity would lead to stronger confidence in

extrapolating MT-motor interaction *in vitro* to *in vivo*. For Kin13-1, purification of the expression culture using lower concentrations of imidazole in the wash should help to increase the percentage of protein made up by Kin13-1. A second purification step (cation exchange chromatography) is likely to increase the purity of the protein sample. Once this has been achieved, then the depolymerisation can be repeated with more confidence in the outcomes observed.

In order to fully understand the Kin13-1 mechanism of function, structural analysis will be required. Future experiments should look to achieve this through X-ray crystallography, allowing mapping of the Kin13-1 tertiary structure. If this can be achieved then the structure can be used to aid identification of the loops and helices involved in MT binding by Cryo-EM, as was the case for MCAK (Ogawa et al. 2003; Asenjo et al. 2003) and whether the motor binding is at the intra- or inter-tubulin dimer interface. The essentiality of the tertiary structures identified as present in the motor-MT binding interface can be verified by specific point mutations in those structures, as was carried out in MCAK (Patel et al. 2016).

The use of TIRF microscopy would allow observation of how single motor molecules interact with MTs. For both Kin13-1 and -3 it would provide a means of confirming the observed phenotypes by the presence of the motor at the site of either a cleavage or depolymerising event. TIRF microscopy could also be used to look at whether cleavage of MTs is length dependent, or dependent on Kin13-1 concentration. The use of TIRF microscopy to identify concentration-dependent severing of MTs has already been successfully achieved for human Katanin (Bailey et al. 2015).

The apparent similarities in MT length regulation between Kin13-1 and katanin means that it would be worth investigating whether Kin13-1 also cleaves at MT lattice defects (Diaz-Valencia et al. 2011). Structural defects can be replicated by growing MTs in the presence of GMPCPP, resulting in MTs with 14 protofilaments (20), then, having removed excess GMPCPP and tubulin, growing taxol-stabilised MTs, which are assembled of 13 protofilaments (21) with tubulin labelled with a different marker (Diaz-Valencia et al. 2011). If the site of MT cleavage in the presence of Kin13-1 is at the 13-14 protofilament junction, then, as for katanin, cleavage at the lattice takes place at sites of structural defect.

Localisation and knockdown experiments of *T. brucei* Kinesin-13 family members have already been carried out by Wickstead et al. (2010b), but it is not known whether the motors are multimeric, or whether they possess other binding partners. As a result, investigation into Kin13-protein binding should be investigated through pull-down assays.

6 Conclusions

In this research the goal was to identify novel roles for kinesin families, with a particular interest in those involved in primary cilia function. The kinesin-16 family are only associated with organisms that build cilia/flagellum, whilst kinesin-13s are only absent in organisms that do not build these organelles. As a result, this research focussed on members of those two families.

The work presented here has highlighted novel methods of achieving similar goals, but not yet novel roles for specific protein families. Members of the *T. brucei* Kinesin-13 set, Kin13-1 and Kin13-3, were identified as MT depolymerisers. Kin13-1 has been discovered to regulate MT length by cleavage at the lattice. This is a novel mechanism in the kinesin superfamily. The cleavage activity observed in Kin13-1 also raises the possibility of novel regulation of the mitotic spindle, and chromosome segregation. There is evidence to support the role of Kin13-3 as an extra-nuclear MT length regulator. The roles of kinesin13C motors are still to be elucidated, with a possible cellular function outside of MT regulation.

Analysis of a functional genomics screen provided evidence for an essential role of KIF12 in ciliogenesis and cilia maintenance, further linking Kinesin-16s with a ciliary function. Unfortunately, research into KIF12-MT interactions and the expression dynamics of *KIF12* during the cell cycle were not completed. However, the newly defined human KIF12 sequence will hopefully provide the opportunity for accurate characterisation in the future.

7 References

Ahmed, Noveera T. Chunlei Gao, Ben F. Lucker, Douglas G. Cole, and David R. Mitchell. 2008. "ODA16 Aids Axonemal Outer Row Dynein Assembly through an Interaction with the Intraflagellar Transport Machinery." *Journal of Cell Biology.* 183, 313–22. doi:10.1083/jcb.200802025.

Amos, Linda A, and Robert A Cross. 1997. "Structure and Dynamics of Molecular Motors." *Current Opinion in Structural Biology.* 7, 239–46. doi:10.1016/S0959-440X(97)80032-2.

Arnal, Isabelle and Richard H. Wade. 1995. "How does taxol stabilize microtubules?" 5 (8): 900-908. doi: 10.1016/S0960-9822(95)00180-1.

Asenjo, Ana B, Chandrima Chatterjee, Dongyan Tan, Vania DePaoli, William J Rice, Ruben Diaz-Avalos, Mariena Silvestry, and Hernando Sosa. 2013. "Structural Model for Tubulin Recognition and Deformation by Kinesin-13 Microtubule Depolymerases." *Cell Reports*. 3, 759–68. doi:10.1016/j.celrep.2013.01.030.

Atherton, Joseph, Irene Farabella, I-Mei Yu, Steven S Rosenfeld, Anne Houdusse, Maya Topf and Carolyn A Moores. 2014. "Conserved mechanisms of microtubule-stimulated ADP release, ATP binding, and force generation in transport kinesins." *eLife.* doi: 10.7554/eLife.03680.

Avidor-Reiss, Tomer, and Michel R Leroux. 2015. "Shared and Distinct Mechanisms of Compartmentalized and Cytosolic Ciliogenesis." *Current Biology.* 25. Elsevier Ltd: R1143–50. doi:10.1016/j.cub.2015.11.001.

Badano, Jose L, Norimasa Mitsuma, Phil L Beales, and Nicholas Katsanis. 2006. "The Ciliopathies: An Emerging Class of Human Genetic Disorders." *Annual Review of Genomics and Human Genetics.* 7, 125–48. doi:10.1146/annurev.genom.7.080505.115610.

Bailey, Megan E, Dan L Sackett, and Jennifer L Ross. 2015. "Katanin Severing and Binding Microtubules Are Inhibited by Tubulin." *Biophysical Journal.* 109, 2546-2561. doi:10.1016/j.bpj.2015.11.011.

Benz, Corinna, Caroline Clucas, Jeremy C. Mottram, Tansy C. Hammarton. 2012. "Cytokinesin in bloodstream stage *Trypanosoma brucei* requires a family of katanins and spastin." *PLOS ONE*. 7 (3). doi.org/10.1371/journal.pone.0030367.

Bernstein, Mitchell, Peter L. Beech, Samuel G. Katz, and Joel L. Rosenbaum. 1994. "A New Kinesin-like Protein (Klp1) Localized to a Single Microtubule of the Chlamydomonas Flagellum." *Journal of Cell Biology.* 125, 1313–26. doi:10.1083/jcb.125.6.1313.

Bhogaraju, Sagar, Benjamin D Engel, and Esben Lorentzen. 2013. "Intraflagellar Transport Complex Structure and Cargo Interactions." *Cilia.* 2, 10. doi:10.1186/2046-2530-2-10.

Blacque, Oliver E, Michael J Reardon, Chunmei Li, Jonathan Mccarthy, Moe R Mahjoub, Stephen J Ansley, Jose L Badano, et al. 2004. "Loss of" 1: 1630–42. doi:10.1101/gad.1194004.copeptide.

Blaineau, Christine, Magali Tessier, Pascal Dubessay, Lena Tasse, Lucien Crobu, Michel Pagès, and Patrick Bastien. 2007. "A Novel Microtubule-Depolymerizing Kinesin Involved in Length Control of a Eukaryotic Flagellum." *Current Biology.* 17, 778–82. doi:10.1016/j.cub.2007.03.048.

Breslow, David K, Elena F Koslover, Federica Seydel, Andrew J Spakowitz, and Maxence V Nachury. 2013. "An in Vitro Assay for Entry into Cilia Reveals Unique Properties of the Soluble Diffusion Barrier." *The Journal of Cell Biology.* 203, 129–47. doi:10.1083/jcb.201212024.

Brown, Jason M. Deborah A. Cochran, Branch Craige, Tomohiro Kubo, and George B. Witman. 2015. "Assembly of IFT Trains at the Ciliary Base Depends on IFT74." *Current Biology .* 25. Elsevier Ltd: 1583–93. doi:10.1016/j.cub.2015.04.060.

Buisson, Johanna, Nicolas Chenouard, Thibault Lagache, Thierry Blisnick, Jean-Christophe Olivo-Marin, and Philippe Bastin. 2013. "Intraflagellar Transport Proteins Cycle between the Flagellum and Its Base." *Journal of Cell Science* 126 (Pt 1): 327–38. doi:10.1242/jcs.117069.

Casanova, Magali. Lucien Crobu, Christine Blaineau, Nathalie Bourgeois, Patrick Bastien, and Michel Pages. 2009. "Microtubule-severing proteins are involved in flagellar length

control and mitosis Trypanosomatids." *Molecular Microbiology.* 71 (6): 1353 - 1370. doi:10.1111/j.1365-2958.2009.06594.

Case, Ryan B. Daniel W. Pierce, Nora Hom-Booher, Cynthia L. Hart, and Ronald D. Vale. 1997. "The Directional Preference of Kinesin Motors Is Specified by an Element outside of the Motor Catalytic Domain." *Cell* 90 (5): 959–66. doi:10.1016/S0092-8674(00)80360-8.

Cassimeris, L U, R A Walker, N K Pryer, and E D Salmon. 1987. "Dynamic Instability of Microtubules." *BioEssays : News and Reviews in Molecular, Cellular and Developmental Biology* 7 (4): 149–54. doi:10.1002/bies.950070403.

Chan, Kuan Yoow, and Klaus Ersfeld. 2010. "The Role of the Kinesin-13 Family Protein TbKif13-2 in Flagellar Length Control of Trypanosoma Brucei." *Molecular and Biochemical Parasitology* 174 (2). Elsevier B.V.: 137–40. doi:10.1016/j.molbiopara.2010.08.001.

Chan, Kuan Yoow, Keith R. Matthews, and Klaus Ersfeldk. 2010. "Functional Characterisation and Drug Target Validation of a Mitotic Kinesin-13 in Trypanosoma Brucei." *PLoS Pathogens* 6 (8): 45–46. doi:10.1371/journal.ppat.1001050.

Cole, Douglas G, and William J Snell. 2009. "SnapShot: Intraflagellar Transport." *Cell* 137 (4): 784–784.e1. doi:10.1016/j.cell.2009.04.053.

Cole, Douglas G. Dennis R. Diener, Amy L. Himelblau, Peter L. Beech, Jason C. Fuster, and Joel L. Rosenbaum. 1998. "Chlamydomonas Kinesin-II-Dependent Intraflagellar Transport (IFT): IFT Particles Contain Proteins Required for Ciliary Assembly in Caenorhabditis Elegans Sensory Neurons." *Journal of Cell Biology* 141 (4): 993–1008. doi:10.1083/jcb.141.4.993.

Conde, Cecilia, and Alfredo Cáceres. 2009. "Microtubule Assembly, Organization and Dynamics in Axons and Dendrites." *Nature Reviews. Neuroscience* 10 (5): 319–32. doi:10.1038/nrn2631.

Connolly, Amy a. Kenji Sugioka, Chien Hui Chuang, Joshua B. Lowry, and Bruce Bowerman. 2015. "KLP-7 Acts through the Ndc80 Complex to Limit Pole Number in C. Elegans Oocyte Meiotic Spindle Assembly." *Journal of Cell Biology* 210 (6): 917–32. doi:10.1083/jcb.201412010.

Coy, D L, W O Hancock, M Wagenbach, and J Howard. 1999. "Kinesin's Tail Domain Is an Inhibitory Regulator of the Motor Domain." *Nature Cell Biology* 1 (5): 288–92. doi:10.1038/13001.

Craft, Julie M. J. Aaron Harris, Sebastian Hyman, Peter Kner, and Karl F. Lechtreck. 2015. "Tubulin Transport by IFT Is Upregulated during Ciliary Growth by a Cilium-Autonomous Mechanism." *Journal of Cell Biology* 208 (2): 223–37. doi:10.1083/jcb.201409036.

Dawson, Scott C. Meredith S. Sagolla, Joel J. Mancuso, David J. Woessner, Susan a. House, Lillian Fritz-Laylin, and W. Zacheus Cande. 2007. "Kinesin-13 Regulates Flagellar, Interphase, and Mitotic Microtubule Dynamics in Giardia Intestinalis." *Eukaryotic Cell* 6 (12): 2354–64. doi:10.1128/EC.00128-07.

Deane, James A. and Sharon D. Ricardo. 2012. *Emerging Roles for Renal Primary Cilia in Epithelial Repair*. *International Review of Cell and Molecular Biology*. 1st ed. Vol. 293. Elsevier Inc. doi:10.1016/B978-0-12-394304-0.00011-7.

Demonchy, Raphaël, Thierry Blisnick, Caroline Deprez, Géraldine Toutirais, Céline Loussert, William Marande, Philippe Grellier, Philippe Bastin, and Linda Kohl. 2009. "Kinesin 9 Family Members Perform Separate Functions in the Trypanosome Flagellum." *Journal of Cell Biology* 187 (5): 615–22. doi:10.1083/jcb.200903139.

Diaz-Valencia, Juan Daniel, Margaret M. Morelli, Megan Bailey, Dong Zhang, David J. Sharp and Jennifer L. Ross. 2011. "*Drosophila* katanin-60 depolymerizes and severs at microtubule defects." *Biophysical Journal.* 100: 2440-2449. doi:10.1016/j.bpj.2011.03.062.

Dishinger, John F, Hooi Lynn Kee, Paul M Jenkins, Shuling Fan, Toby W Hurd, Jennetta W Hammond, Yen Nhu-Thi Truong, Ben Margolis, Jeffrey R Martens, and Kristen J Verhey. 2010. "Ciliary Entry of the Kinesin-2 Motor KIF17 Is Regulated by Importin-beta2 and RanGTP." *Nature Cell Biology* 12 (7). Nature Publishing Group: 703–10. doi:10.1038/ncb2073.

Endow, S A, S J Kang, L L Satterwhite, M D Rose, V P Skeen, and E D Salmon. 1994. "Yeast Kar3 Is a Minus-End Microtubule Motor Protein That Destabilizes Microtubules Preferentially at the

Minus Ends." *The EMBO Journal* 13 (11): 2708–13. http://www.ncbi.nlm.nih.gov/pubmed/7912193.

Engel, Benjamin D. William B. Ludington, and Wallace F. Marshall. 2009. "Intraflagellar Transport Particle Size Scales Inversely with Flagellar Length: Revisiting the Balance-Point Length Control Model." *Journal of Cell Biology* 187 (1): 81–89. doi:10.1083/jcb.200812084.

Errico, A. A. Ballabio, A. and E. I. Rugarli. 2002. "Spastin, the protein mutated in autosomal dominant hereditary spastic paraplegia, is involved in microtubule dynamics." *Human Molecular Genetics.* 11 (2): 153-163.

Fan, S. E. L. Whiteman, T. W. Hurd, J. C. McIntyre, J. F. Dishinger, C. J. Liu, J. R. Martens, K. J. Verhey, U. Sajjan, and B. Margolis. 2011. "Induction of Ran GTP Drives Ciliogenesis." *Molecular Biology of the Cell* 22: 4539–48. doi:10.1091/mbc.E11-03-0267.

Folkers, Ulrike, Victor Kirik, U. Schöbinger, S. Falk, S. Krishnakumar, Mary a. Pollock, David G. Oppenheimer, et al. 2002. "The Cell Morphogenesis Gene *ANGUSTIFOLIA* Encodes a CtBP/BARS-like Protein and Is Involved in the Control of the Microtubule Cytoskeleton." *The EMBO Journal* 21 (6): 1280–88. doi:10.1093/emboj/21.6.1280.

Friedman, D S, and R D Vale. 1999. "Single-Molecule Analysis of Kinesin Motility Reveals Regulation by the Cargo-Binding Tail Domain." *Nature Cell Biology* 1 (5): 293–97. doi:10.1038/13008.

Friel, Claire T, and Jonathon Howard. 2011. "The Kinesin-13 MCAK Has an Unconventional ATPase Cycle Adapted for Microtubule Depolymerization." *The EMBO Journal* 30 (19): 3928–39. doi:10.1038/emboj.2011.290.

Fujikura, Ushio, Lore Elsaesser, Holger Breuninger, Clara Sánchez-Rodríguez, Alexander Ivakov, Thomas Laux, Kim Findlay, Staffan Persson, and Michael Lenhard. 2014. "Atkinesin-13A Modulates Cell-Wall Synthesis and Cell Expansion in Arabidopsis Thaliana via the THESEUS1 Pathway." *PLoS Genetics* 10 (9). doi:10.1371/journal.pgen.1004627.

Ganem, Neil J. and Duane A. Compton. 2004. "The KinI Kinesin Kif2a Is Required for Bipolar Spindle Assembly through a

Functional Relationship with MCAK." *Journal of Cell Biology* 166 (4): 473–78. doi:10.1083/jcb.200404012.

Garcia-Gonzalo, Francesc R. and Jeremy F. Reiter. 2012. "Scoring a Backstage Pass: Mechanisms of Ciliogenesis and Ciliary Access." *Journal of Cell Biology* 197 (6): 697–709. doi:10.1083/jcb.201111146.

Gibbons, I R, and A V Grimstone. 1960. "On Flagellar Structure in Certain Flagellates." *J Biophys Biochem Cytol* 7 (4): 697–716. doi:10.1083/jcb.7.4.697.

Gong, Yimei, Zhendong Ma, Vishal Patel, Evelyne Fischer, Thomas Hiesberger, Marco Pontoglio, and Peter Igarashi. 2009. "HNF-1beta Regulates Transcription of the PKD Modifier Gene Kif12." *Journal of the American Society of Nephrology : JASN* 20 (1): 41–47. doi:10.1681/ASN.2008020238.

Guay-Woodford, L M, C J Wright, G Walz, and G a Churchill. 2000. "Quantitative Trait Loci Modulate Renal Cystic Disease Severity in the Mouse Bpk Model." *Journal of the American Society of Nephrology : JASN* 11 (7): 1253–60.

Han, Xue, Kelly Adames, Ellen M.E. Sykes, and Martin Srayko. 2015. "The KLP-7 Residue S546 Is a Putative Aurora Kinase Site Required for Microtubule Regulation at the Centrosome in C. Elegans." *PLoS ONE* 10 (7): 1–23. doi:10.1371/journal.pone.0132593.

He, Mu, Radhika Subramanian, Fiona Bangs, Tatiana Omelchenko, Karel F Liem, Tarun M Kapoor, and Kathryn V Anderson. 2014. "The Kinesin-4 Protein Kif7 Regulates Mammalian Hedgehog Signalling by Organizing the Cilium Tip Compartment." *Nature Cell Biology* 16 (7): 663–72. doi:10.1038/ncb2988.

Helenius, Jonne, Gary Brouhard, Yannis Kalaidzidis, Stefan Diez, and Jonathon Howard. 2006. "The Depolymerizing Kinesin MCAK Uses Lattice Diffusion to Rapidly Target Microtubule Ends." *Nature* 441 (7089): 115–19. doi:10.1038/nature04736.

Hibbel, Anneke, Aliona Bogdanova, Mohammed Mahamdeh, Anita Jannasch, Marko Storch, Erik Schäffer, Dimitris Liakopoulos, and Jonathon Howard. 2015. "Kinesin Kip2 Enhances Microtubule Growth in Vitro through Length-Dependent Feedback on Polymerization and Catastrophe." *eLife* 4 (NOVEMBER2015): 1–11. doi:10.7554/eLife.10542.

Hirokawa, Nobutaka, Yasuko Noda, Yosuke Tanaka, and Shinsuke Niwa. 2009. "Kinesin Superfamily Motor Proteins and Intracellular Transport." *Nature Reviews. Molecular Cell Biology* 10 (10). Nature Publishing Group: 682–96. doi:10.1038/nrm2774.

Hou, Xiaoying, Michal Mrug, Bradley K. Yoder, Elliot J. Lefkowitz, Gabriel Kremmidiotis, Peter D'Eustachio, David R. Beier, and Lisa M. Guay-Woodford. 2002. "Cystin, a Novel Cilia-Associated Protein, Is Disrupted in the Cpk Mouse Model of Polycystic Kidney Disease." *Journal of Clinical Investigation* 109 (4): 533–40. doi:10.1172/JCI200214099.

Hu, Chi Kuo, Margaret Coughlin, Christine M. Field, and Timothy J. Mitchison. 2011. "KIF4 Regulates Midzone Length during Cytokinesis." *Current Biology* 21 (10). Elsevier Ltd: 815–24. doi:10.1016/j.cub.2011.04.019.

Hua, K. & Ferland, R.J. 2017. Fixation methods can differentially affect ciliary protein immunolabeling. *Cilia*, 6, p.5.

Hunter, Andrew W. Michael Caplow, David L. Coy, William O. Hancock, Stefan Diez, Linda Wordeman, and Jonathon Howard. 2003. "The Kinesin-Related Protein MCAK Is a Microtubule Depolymerase That Forms an ATP-Hydrolyzing Complex at Microtubule Ends." *Molecular Cell* 11 (2): 445–57. doi:10.1016/S1097-2765(03)00049-2.

Hyman, Anthony A. Denis Chretien, Isabelle Arnal and Richard H. Wade. 1995. "Structure changes accompanying GTP hydrolysis in microtubules: Information from a slowly hydrolyzable analogue Guanylyl-(α,β)-Methylene-Diphosphate. *Journal of Cell Biology*. 128 (1): 177-125. doi: 10.1083/jcb.128.1.117.

Igarashi, P. 2002. "Genetics and Pathogenesis of Polycystic Kidney Disease." *Journal of the American Society of Nephrology* 13 (9): 2384–98. doi:10.1097/01.ASN.0000028643.17901.42.

Imanishi, Miki, Nicholas F. Endres, Arne Gennerich, and Ronald D. Vale. 2006. "Autoinhibition Regulates the Motility of the C. Elegans Intraflagellar Transport Motor OSM-3." *Journal of Cell Biology* 174 (7): 931–37. doi:10.1083/jcb.200605179.

Ishikawa, Hiroaki, and Wallace F Marshall. 2011. "Ciliogenesis: Building the Cell's Antenna." *Nature Reviews. Molecular Cell*

Biology 12 (4). Nature Publishing Group: 222–34. doi:10.1038/nrm3085.

Janke, Carsten, Jennifer Ortíz, Tomoyuki U Tanaka, Johannes Lechner, and Elmar Schiebel. 2002. "Four New Subunits of the Dam1-Duo1 Complex Reveal Novel Functions in Sister Kinetochore Biorientation." *The EMBO Journal* 21 (1-2): 181–93. doi:10.1093/emboj/21.1.181.

Kamal, Adeela, Gorazd B Stokin, Zhaohaui Yang, Chun-Hong Xia, and Lawrence S.B Goldstein. 2000. "Axonal Transport of Amyloid Precursor Protein Is Mediated by Direct Binding to the Kinesin Light Chain Subunit of Kinesin-I." *Neuron* 28 (2): 449–59. doi:10.1016/S0896-6273(00)00124-0.

Katoh, K. et al. 2002. MAFFT: a novel method for rapid multiple sequence alignment based on fast Fourier transform. *Nucleic Acids Research*. 30, 3059–3066.

Kee, Hooi Lynn, John F. Dishinger, T. Lynne Blasius, Chia-Jen Liu, Ben Margolis, and Kristen J. Verhey. 2012. "A Size-Exclusion Permeability Barrier and Nucleoporins Characterize a Ciliary Pore Complex That Regulates Transport into Cilia." *Nature Cell Biology* 14 (4). Nature Publishing Group: 431–37. doi:10.1038/ncb2450.

Kim, Haein, Cindy Fonesca and Jason Stumpff. 2014. A unique kinesin-8 surface loop provides specificity for chromosome alignment. *Molecular Biology of the Cell.* 25 (21): 3319-3329. doi: 10.1091/mbc.E14-06-1132.

Kim, Sehyun, Kwanwoo Lee, Jung-Hwan Choi, Niels Ringstad, and Brian David Dynlacht. 2015. "Nek2 Activation of Kif24 Ensures Cilium Disassembly during the Cell Cycle." *Nature Communications* 6. Nature Publishing Group: 8087. doi:10.1038/ncomms9087.

Kim, Sehyun, and Leonidas Tsiokas. 2011. "Cilia and Cell Cycle Re-Entry: More than a Coincidence." *Cell Cycle* 10 (16): 2683–90. doi:10.4161/cc.10.16.17009.

Kline-Smith, Susan L, Alexey Khodjakov, Polla Hergert, and Claire E Walczak. 2004. "Depletion of Centromeric MCAK Leads to Chromosome Congression and Segregation Defects due to Improper Kinetochore Attachments." *Molecular Biology of the Cell* 15 (3): 1146–59. doi:10.1091/mbc.E03-08-0581.

Kobayashi, Tetsuo, and Brian D. Dynlacht. 2011. "Regulating the Transition from Centriole to Basal Body." *Journal of Cell Biology* 193 (3): 435–44. doi:10.1083/jcb.201101005.

Kobayashi, Tetsuo, William Y. Tsang, Ji Li, William Lane, and Brian David Dynlacht. 2011. "Centriolar Kinesin Kif24 Interacts with CP110 to Remodel Microtubules and Regulate Ciliogenesis." *Cell* 145 (6): 914–25. doi:10.1016/j.cell.2011.04.028.

Kozminski, Keith G, Karl A Johnson, Paul Forscher, and Joel L Rosenbaum. 1993. "A Motility in the Eukaryotic Flagellum Unrelated to Flagellar Beating" 90 (June): 5519–23.

Kozminski, Keith G. Peter L. Beech, and Joel L. Rosenbaum. 1995. "The Chlamydomonas Kinesin-like Protein FLA10 Is Involved in Motility Associated with the Flagellar Membrane." *Journal of Cell Biology* 131 (6 I): 1517–27. doi:10.1083/jcb.131.6.1517.

Kull, F Jon, Elena P Sablin, Rebecca Lau, Robert J Fletterick, and Ronald D Vale. 1996. "NIH Public Access" 380 (6574): 550–55. doi:10.1038/380550a0.Crystal.

Lambacher, Nils J. Ange-Line Bruel, Teunis J. P. van Dam, Katarzyna Szymańska, Gisela G. Slaats, Stefanie Kuhns, Gavin J. McManus, et al. 2015. "TMEM107 Recruits Ciliopathy Proteins to Subdomains of the Ciliary Transition Zone and Causes Joubert Syndrome." *Nature Cell Biology* 18 (1): 122–31. doi:10.1038/ncb3273.

Lawrence, C J, N R Morris, R B Meagher, and R K Dawe. 2001. "Dyneins Have Run Their Course in Plant Lineage." *Traffic (Copenhagen, Denmark)* 2 (5): 362–63. doi:tra020508 [pii].

Lawrence, Carolyn J, R Kelly Dawe, Karen R Christie, Don W Cleveland, Scott C Dawson, Sharyn a Endow, Lawrence S B Goldstein, et al. 2004. "A Standardized Kinesin Nomenclature." *The Journal of Cell Biology* 167 (1): 19–22. doi:10.1083/jcb.200408113.

Lechtreck, Karl F. 2015. "IFT-Cargo Interactions and Protein Transport in Cilia." *Trends in Biochemical Sciences* xx. Elsevier Ltd: 1–14. doi:10.1016/j.tibs.2015.09.003.

Lechtreck, Karl Ferdinand, Eric C. Johnson, Tsuyoshi Sakai, Deborah Cochran, Bryan a. Ballif, John Rush, Gregory J. Pazour, Mitsuo Ikebe, and George B. Witman. 2009. "The

Chlamydomonas Reinhardtii BBSome Is an IFT Cargo Required for Export of Specific Signaling Proteins from Flagella." *Journal of Cell Biology* 187 (7): 1117–32. doi:10.1083/jcb.200909183.

Li, Z. J. E. Nieuwenhuis, W. Nien, X. Zhang, J. Zhang, V. Puviindran, B. J. Wainwright, P. C. W. Kim, and C.-c. Hui. 2012. "Kif7 Regulates Gli2 through Sufu-Dependent and -Independent Functions during Skin Development and Tumorigenesis." *Development* 139 (22): 4152–61. doi:10.1242/dev.081190.

Linck, Richard W. Hector Chemes, and David F. Albertini. 2016. "The Axoneme: The Propulsive Engine of Spermatozoa and Cilia and Associated Ciliopathies Leading to Infertility." *Journal of Assisted Reproduction and Genetics* 33 (2): 141–56. doi:10.1007/s10815-016-0652-1.

Linck, Richard W. and Raymond E. Stephens. 2007. "Functional Protofilament Numbering of Ciliary, Flagellar, and Centriolar Microtubules." *Cell Motility and the Cytoskeleton* 64 (7): 489–95. doi:10.1002/cm.20202.

Lippincott-Schwartz, Jeniffer, Nelson B Cole, Alex Marotta, Patricia a Conrad, and George S Bloom. 1995. "Kinesin Is a Motor for Microtuble-Mediated Golgi-to-ER Membrane Traffic." *J. Cell Biol.* 128 (3): 293–306. doi:10.1083/jcb.128.3.293.

Lohret, Timothy A, F J McNally, and Lynne M Quarmby. 1998. "A Role for Katanin-Mediated Axonemal Severing during Chlamydomonas Deflagellation." *Molecular Biology of the Cell* 9 (5): 1195–1207. doi:10.1091/mbc.9.5.1195.

McNally, Francis J. and Ronald D. Vale. 1993. "Identification of katanin, an ATPase that severs and disassembles stable microtubules." *Cell*. 75 (3): 419-429. doi:10.1016/0092-8674(93)90377.

Malicki, Jarema, and Tomer Avidor-Reiss. 2014. "From the Cytoplasm into the Cilium: Bon Voyage." *Organogenesis* 10 (1): 138–57. doi:10.4161/org.29055.

Maney, Todd, Andrew W. Hunter, Mike Wagenbach, and Linda Wordeman. 1998. "Mitotic Centromere-Associated Kinesin Is Important for Anaphase Chromosome Segregation." *Journal of Cell Biology* 142 (3): 787–801. doi:10.1083/jcb.142.3.787.

Marshall, Wallace F. and Joel L. Rosenbaum. 2001. "Intraflagellar Transport Balances Continuous Turnover of Outer Doublet Microtubules: Implications for Flagellar Length Control." *Journal of Cell Biology* 155 (4): 405–14. doi:10.1083/jcb.200106141.

Matsuzaki, Motomichi, Osami Misumi, Tadasu Shin-I, Shinichiro Maruyama, Manabu Takahara, Shin-Ya Miyagishima, Toshiyuki Mori, et al. 2004. "Genome Sequence of the Ultrasmall Unicellular Red Alga Cyanidioschyzon Merolae 10D." *Nature* 428 (6983): 653–57. doi:10.1038/nature02398.

Mayr, M.I. et al. 2007. The human kinesin Kif18A is a motile microtubule depolymerase essential for chromosome congression. *Current Biology : CB*, 17(6), pp.488–98.

Mazumdar, Manjari, Suma Sundareshan, and Tom Misteli. 2004. "Human Chromokinesin KIF4A Functions in Chromosome Condensation and Segregation." *Journal of Cell Biology* 166 (5): 613–20. doi:10.1083/jcb.200401142.

Miyamoto, Tatsuo, Kosuke Hosoba, Hiroshi Ochiai, Ekaterina Royba, Hideki Izumi, Tetsushi Sakuma, Takashi Yamamoto, Brian David Dynlacht, and Shinya Matsuura. 2015. "The Microtubule-Depolymerizing Activity of a Mitotic Kinesin Protein KIF2A Drives Primary Cilia Disassembly Coupled with Cell Proliferation." *Cell Reports* 10 (5). The Authors: 664–73. doi:10.1016/j.celrep.2015.01.003.

Moore, Ayana T, Kathleen E Rankin, George von Dassow, Leticia Peris, Michael Wagenbach, Yulia Ovechkina, Annie Andrieux, Didier Job, and Linda Wordeman. 2005. "MCAK Associates with the Tips of Polymerizing Microtubules." *The Journal of Cell Biology* 169 (3): 391–97. doi:10.1083/jcb.200411089.

Morsci, Natalia S. and Maureen M. Barr. 2011. "Kinesin-3 KLP-6 Regulates Intraflagellar Transport in Male-Specific Cilia of Caenorhabditis Elegans." *Current Biology* 21 (14). Elsevier Ltd: 1239–44. doi:10.1016/j.cub.2011.06.027.

Mrug, Michal, Renhua Li, Xiangqin Cui, Trenton R Schoeb, Gary a Churchill, and Lisa M Guay-Woodford. 2005. "Kinesin Family Member 12 Is a Candidate Polycystic Kidney Disease Modifier in the Cpk Mouse." *Journal of the American Society of Nephrology : JASN* 16 (4): 905–16. doi:10.1681/ASN.2004121083.

Mrug, Michal, Juling Zhou, Chaozhe Yang, Bruce J. Aronow, Xiangqin Cui, Trenton R. Schoeb, Gene P. Siegal, Bradley K. Yoder, and Lisa M. Guay-Woodford. 2015. "Genetic and Informatic Analyses Implicate Kif12 as a Candidate Gene within the Mpkd2 Locus That Modulates Renal Cystic Disease Severity in the Cys1cpk Mouse." *PLoS ONE* 10 (8): 1–15. doi:10.1371/journal.pone.0135678.

Nachury, Maxence V, E Scott Seeley, and Hua Jin. 2010. "Trafficking to the Ciliary Membrane: How to Get across the Periciliary Diffusion Barrier?" *Annual Review of Cell and Developmental Biology* 26: 59–87. doi:10.1146/annurev.cellbio.042308.113337.

Nicastro, D. X. Fu, T. Heuser, a. Tso, M. E. Porter, and R. W. Linck. 2011. "Cryo-Electron Tomography Reveals Conserved Features of Doublet Microtubules in Flagella." *Proceedings of the National Academy of Sciences* 108 (42): E845–53. doi:10.1073/pnas.1106178108.

Niwa, Shinsuke, Kazuo Nakajima, Harukata Miki, Yusuke Minato, Doudou Wang, and Nobutaka Hirokawa. 2012. "KIF19A Is a Microtubule-Depolymerizing Kinesin for Ciliary Length Control." *Developmental Cell* 23 (6). Elsevier Inc.: 1167–75. doi:10.1016/j.devcel.2012.10.016.

Nour-Eldin, H.H. et al. 2006. Advancing uracil-excision based cloning towards an ideal technique for cloning PCR fragments. *Nucleic Acids Research*, 34.

Oda, Y. and H. Fukuda. 2013. "Rho of Plant GTPase Signaling Regulates the Behavior of Arabidopsis Kinesin-13A to Establish Secondary Cell Wall Patterns." *The Plant Cell* 25 (11): 4439–50. doi:10.1105/tpc.113.117853.

Oda, Yoshihisa, and Hiroo Fukuda. 2013. "The Dynamic Interplay of Plasma Membrane Domains and Cortical Microtubules in Secondary Cell Wall Patterning." *Front. Plant Sci.* 4 (December): 511. doi:10.3389/fpls.2013.00511.

Ogawa, Tadayuki, Ryo Nitta, Yasushi Okada and Nobutaka Hirokawa. 2003. "A common mechanism for microtubule destabilisers - M type kinesins stabilise curling of the protofilament using the class-specific neck and loops." *Cell.* 116 (4): 591-602. doi: 10.1016/s0092-8674(04)00129-1.

Okada, Yasushi, Hiroto Yamazaki, Yoko Sekine-Aizawa, and Nobutaka Hirokawa. 1995. "The Neuron-Specific Kinesin Superfamily Protein KIF1A Is a Uniqye Monomeric Motor for Anterograde Axonal Transport of Synaptic Vesicle Precursors." *Cell* 81 (5): 769–80. doi:10.1016/0092-8674(95)90538-3.

Patel, J.T. Belsham, H. R. Rathbone, A. J. Wickstead, B. Gell, C. and Friel, C. T . 2016. The family-specific α4-helix of the kinesin-13, MCAK, is critical to microtubule end recognition. *Open Biology*, 6, 160223.

Pazour, Gregory J. Nathan Agrin, John Leszyk, and George B. Witman. 2005. "Proteomic Analysis of a Eukaryotic Cilium." *Journal of Cell Biology* 170 (1): 103–13. doi:10.1083/jcb.200504008.

Pedersen, Lotte B. Stefan Geimer, and Joel L. Rosenbaum. 2006. "Dissecting the Molecular Mechanisms of Intraflagellar Transport in Chlamydomonas." *Current Biology* 16 (5): 450–59. doi:10.1016/j.cub.2006.02.020.

Pedersen, Lotte B. Iben R. Veland, Jacob M. Schrøder, and Søren T. Christensen. 2008. "Assembly of Primary Cilia." *Developmental Dynamics* 237 (8): 1993–2006. doi:10.1002/dvdy.21521.

Piao, Tian, Minna Luo, Liang Wang, Yan Guo, De Li, Peng Li, William J Snell, and Junmin Pan. 2009. "A Microtubule Depolymerizing Kinesin Functions during Both Flagellar Disassembly and Flagellar Assembly in Chlamydomonas." *Proceedings of the National Academy of Sciences of the United States of America* 106 (12): 4713–18. doi:10.1073/pnas.0808671106.

Pigino, Gaia, Stefan Geimer, Salvatore Lanzavecchia, Eugenio Paccagnini, Francesca Cantele, Dennis R. Diener, Joel L. Rosenbaum, and Pietro Lupetti. 2009. "Electron-Tomographic Analysis of Intraflagellar Transport Particle Trains in Situ." *Journal of Cell Biology* 187 (1): 135–48. doi:10.1083/jcb.200905103.

Pihan, German, and Stephen J. Doxsey. 2003. "Mutations and Aneuploidy: Co-Conspirators in Cancer?" *Cancer Cell* 4 (2): 89–94. doi:10.1016/S1535-6108(03)00195-8.

Piperno, Gianni, Edward Siuda, Scott Henderson, Margarethe Segil, Heikki Vaananen, and Massimo Sassaroli. 1998. "Distinct Mutants of Retrograde Intraflagellar Transport (IFT) Share Similar Morphological and Molecular Defects." *Journal of Cell Biology* 143 (6): 1591–1601. doi:10.1083/jcb.143.6.1591.

Plotnikova, Olga V. Elena N Pugacheva, and Erica a Golemis. 2009. "Primary Cilia and theCell Cycle." *Methods Cell Biology* 94 (08): 137–60. doi:10.1016/S0091-679X(08)94007-3.Primary.

Prevo, Bram, Pierre Mangeol, Felix Oswald, Jonathan M Scholey, and Erwin J G Peterman. 2015. "Functional Differentiation of Cooperating Kinesin-2 Motors Orchestrates Cargo Import and Transport in *C. Elegans* Cilia." *Nature Cell Biology* 17 (12): 1536–45. doi:10.1038/ncb3263.

Pugacheva, E.N. Jablonski, S. A. Hartman, T. R. Henske, E. P. and Golemis, E. A. 2007. HEF1-Dependent Aurora A Activation Induces Disassembly of the Primary Cilium. *Cell*. 129, 1351–1363.

Qin, Hongmin, Zhaohui Wang, Dennis Diener, and Joel Rosenbaum. 2007. "Intraflagellar Transport Protein 27 Is a Small G Protein Involved in Cell-Cycle Control." *Current Biology* 17 (3): 193–202. doi:10.1016/j.cub.2006.12.040.

Reiter, Jeremy F, Oliver E Blacque, and Michel R Leroux. 2012. "The Base of the Cilium: Roles for Transition Fibres and the Transition Zone in Ciliary Formation, Maintenance and Compartmentalization." *EMBO Reports* 13 (7). Nature Publishing Group: 608–18. doi:10.1038/embor.2012.73.

Richards, Thomas a, and Thomas Cavalier-Smith. 2005. "Myosin Domain Evolution and the Primary Divergence of Eukaryotes." *Nature* 436 (7054): 1113–18. doi:10.1038/nature03949.

Robert, Aude, Germain Margall-Ducos, Jacques-Emmanuel Guidotti, Olivier Brégerie, Claude Celati, Christian Bréchot, and Chantal Desdouets. 2007. "The Intraflagellar Transport Component IFT88/polaris Is a Centrosomal Protein Regulating G1-S Transition in Non-Ciliated Cells." *Journal of Cell Science* 120 (Pt 4): 628–37. doi:10.1242/jcs.03422.

Rosenbaum, Joel L, and George B Witman. 2002. "Intraflagellar Transport." *Nature Reviews. Molecular Cell Biology* 3 (11): 813–25. doi:10.1038/nrm952.

Rotureau, Brice, Miguel a. Morales, Philippe Bastin, and Gerald F. Späth. 2009. "The Flagellum-Mitogen-Activated Protein Kinase Connection in Trypanosomatids: A Key Sensory Role in Parasite Signalling and Development?" *Cellular Microbiology* 11 (5): 710–18. doi:10.1111/j.1462-5822.2009.01295.x.

Sang, Liyun, Julie J. Miller, Kevin C. Corbit, Rachel H. Giles, Matthew J. Brauer, Edgar a. Otto, Lisa M. Baye, et al. 2011. "Mapping the NPHP-JBTS-MKS Protein Network Reveals Ciliopathy Disease Genes and Pathways." *Cell* 145 (4). Elsevier Inc.: 513–28. doi:10.1016/j.cell.2011.04.019.

Sardar, Harjinder S. Vincent G. Luczak, Maria M. Lopez, Bradford C. Lister, and Susan P. Gilbert. 2010. "Mitotic Kinesin CENP-E Promotes Microtubule plus-End Elongation." *Current Biology* 20 (18). Elsevier Ltd: 1648–53. doi:10.1016/j.cub.2010.08.001.

Scarabelli, Guido, Virupakshi Soppina, Xin-Qiu Yao, Joseph Atherton, Carolyn A. Moores, Kristen J. Verhey and Barry J.. Grant. "Mapping the processivity determinants of the kinesin-3 motor domain. *Biophysical Journal.* 109: 1537-1540. doi: 10.1016/j.bpj.2015.08.027.

Schneider, C. A. Rasband, W.S. & Eliceiri, K.W. 2012. NIH Image to ImageJ: 25 years of image analysis. *Nature Methods.* 9, 671–675.

Sinden, R. E. a. Talman, S. R. Marques, M. N. Wass, and M. J E Sternberg. 2010. "The Flagellum in Malarial Parasites." *Current Opinion in Microbiology* 13 (4). Elsevier Ltd: 491–500. doi:10.1016/j.mib.2010.05.016.

Song, Zhu, Xiaoli Zhang, Shuo Jia, Pamela C. Yelick, and Chengtian Zhao. 2016. "Zebrafish as a Model for Human Ciliopathies." *Journal of Genetics and Genomics* 43 (3). Elsevier Limited and Science Press: 107–20. doi:10.1016/j.jgg.2016.02.001.

Sorokin, Sergei. 1962. "Centrioles Rudimentary and Smooth and the Formation of Cilia Muscle by Fibroblasts." *Cell Biology* 15 (10): 363–77. doi:10.1083/jcb.15.2.363.

Sproul, Lisa R. Daniel J. Anderson, Andrew T. Mackey, William S. Saunders, and Susan P. Gilbert. 2005. "Cik1 Targets the Minus-End Kinesin Depolymerase Kar3 to Microtubule plus Ends." *Current Biology* 15 (15): 1420–27. doi:10.1016/j.cub.2005.06.066.

Stepanek, Ludek, and Gaia Pigino. 2016. "Microtubule Doublets Are Double-Track Railways for Intraflagellar Transport Trains." *Science* 352 (6286): 721–24. doi:10.1126/science.aaf4594.

Stumpff, Jason, George von Dassow, Michael Wagenbach, Charles Asbury, and Linda Wordeman. 2008. "The Kinesin-8 Motor Kif18A Suppresses Kinetochore Movements to Control Mitotic Chromosome Alignment." *Developmental Cell* 14 (2): 252–62. doi:10.1016/j.devcel.2007.11.014.

Sturgill, Emma G. and Ryoma Ohi. 2013. "Microtubule-Regulating Kinesins." *Current Biology* 23 (21). Elsevier: R946–48. doi:10.1016/j.cub.2013.08.012.

Su, Xiaolei, Weihong Qui, Mohan Gupta Jr, Jose B. Pereira-Leal, Samara L. Reck-Peterson and David Pellman. 2011. "Mechinisms Underlying the Dual-Mode Regulation of Microtubule Dynamics by Kip3/Kinesin-8." *Molecular Cell* 43: 751-763. doi:10.1016/j.molcel.2011.06.027.

Sung, Ching-Hwa, and Michel R Leroux. 2013. "The Roles of Evolutionarily Conserved Functional Modules in Cilia-Related Trafficking." *Nature Cell Biology* 15 (12). Nature Publishing Group: 1387–97. doi:10.1038/ncb2888.

Takao, Daisuke, and Kristen J. Verhey. 2016. "Gated Entry into the Ciliary Compartment." *Cellular and Molecular Life Sciences* 73 (1). Springer Basel: 119–27. doi:10.1007/s00018-015-2058-0.

Tanenbaum, Marvin E. Libor Macůrek, Aniek Janssen, Erica F. Geers, Mónica Alvarez-Fernández, and René H. Medema. 2009. "Kif15 Cooperates with Eg5 to Promote Bipolar Spindle Assembly." *Current Biology* 19 (20): 1703–11. doi:10.1016/j.cub.2009.08.027.

Taschner, Michael, Sagar Bhogaraju, and Esben Lorentzen. 2012. "Architecture and Function of IFT Complex Proteins in Ciliogenesis." *Differentiation* 83 (2). Elsevier: S12–22. doi:10.1016/j.diff.2011.11.001.

Tytell, Jessica D, and Peter K Sorger. 2006. "Analysis of Kinesin Motor Function at Budding Yeast Kinetochores." *The Journal of Cell Biology* 172 (6): 861–74. doi:10.1083/jcb.200509101.

Vaisberg, E, M Koonce, and J McIntosh. 1993. "Cytoplasmic Dynein Plays a Role in Mammalian Mitotic Spindle Formation." *The*

Journal of Cell Biology 123 (4): 849–58. http://www.ncbi.nlm.nih.gov/entrez/query.fcgi?cmd=Retrieve&db=PubMed&dopt=Citation&list_uids=8227145\npapers2://publication/uuid/1C5736C9-D943-46B9-AB89-7369D01063C3.

Vale, Ronald D, Takashi Funatsu, Daniel W Pierce, Laura Romberg, Yoshie Harada and Toshio Yanagida. 1996. "Direct observation of single kinesin molecules moving along microtubules." *Nature.* 380, 451-453. doi:10.1038/380451a0.

Vannuccini, Elisa, Eugenio Paccagnini, Francesca Cantele, Mariangela Gentile, Daniele Dini, Federica Fino, Dennis Diener, Caterina Mencarelli, and Pietro Lupetti. 2016. "Two Classes of Short Intraflagellar Transport Train with Different 3D Structures Are Present in Chlamydomonas Flagella." *Journal of Cell Science* 129 (10): 2064–74. doi:10.1242/jcs.183244.

Varga, Vladimir, Jonne Helenius, Kozo Tanaka, Anthony a Hyman, Tomoyuki U Tanaka, and Jonathon Howard. 2006. "Yeast Kinesin-8 Depolymerizes Microtubules in a Length-Dependent Manner." *Nature Cell Biology* 8 (9): 957–62. doi:10.1038/ncb1462.

Varga, Vladimir, Cecile Leduc, Volker Bormuth, Stefan Diez, and Jonathon Howard. 2009. "Kinesin-8 Motors Act Cooperatively to Mediate Length-Dependent Microtubule Depolymerization." *Cell* 138 (6). Elsevier Ltd: 1174–83. doi:10.1016/j.cell.2009.07.032.

Verhey, Kristen J, and Jennetta W Hammond. 2009. "Traffic Control: Regulation of Kinesin Motors." *Nature Reviews. Molecular Cell Biology* 10 (11). Nature Publishing Group: 765–77. doi:10.1038/nrm2782.

Verhey, Kristen J. John Dishinger, and Hooi Lynn Kee. 2011. "Kinesin Motors and Primary Cilia." *Biochemical Society Transactions* 39 (5): 1120–25. doi:10.1042/BST0391120.

Walczak, Claire E. Eugene C. Gan, Arshad Desai, Timothy J. Mitchison, and Susan L. Kline-Smith. 2002. "The Microtubule-Destabilizing Kinesin XKCM1 Is Required for Chromosome Positioning during Spindle Assembly." *Current Biology* 12 (21): 1885–89. doi:10.1016/S0960-9822(02)01227-7.

Wei, Qing, Kun Ling, and Jinghua Hu. 2015. "The Essential Roles of Transition Fibers in the Context of Cilia." *Current Opinion in*

Cell Biology 35. Elsevier Ltd: 98–105. doi:10.1016/j.ceb.2015.04.015.

Wickstead, Bill and Keith Gull. 2006. A " Holistic " Kinesin Phylogeny Reveals New Kinesin Families and Predicts Protein Functions. *Molecular Biology of the Cell*. 17, 1734–1743.

Wickstead, Bill and Keith Gull. 2007. Dyneins across eukaryotes: A comparative genomic analysis. *Traffic*. 8, 1708–1721.

Wickstead, Bill, Keith Gull and Thomas A. Richards. 2010. Patterns of kinesin evolution reveal a complex ancestral eukaryote with a multifunctional cytoskeleton. *BMC Evolutionary Biology*. 10, 110.

Wickstead, B. Carrington, J.T. Gluenz, E. & Gull, K. 2010b. The expanded kinesin-13 repertoire of trypanosomes contains only one mitotic kinesin indicating multiple extra-nuclear roles. *PLoS ONE*, 5.

Wickstead, Bill and Keith Gull. 2011. The evolution of the cytoskeleton. *The Journal of Cell Biology*. 194, 513–25.

Williams, Corey L. Chunmei Li, Katarzyna Kida, Peter N. Inglis, Swetha Mohan, Lucie Semenec, Nathan J. Bialas, et al. 2011. "MKS and NPHP Modules Cooperate to Establish Basal Body/transition Zone Membrane Associations and Ciliary Gate Function during Ciliogenesis." *Journal of Cell Biology* 192 (6): 1023–41. doi:10.1083/jcb.201012116.

Wingfield, Jenna L. Ilaria Mengoni, Heather Bomberger, Yu Yang Jiang, Jonathon D. Walsh, Jason M. Brown, Tyler Picariello, et al. 2017. "IFT Trains in Different Stages of Assembly Queue at the Ciliary Base for Consecutive Release into the Cilium." *eLife* 6: 1–27. doi:10.7554/eLife.26609.

Wordeman, L, and T J Mitchison. 1995. "Identification and Partial Characterization of Mitotic Centromere- Associated Kinesin, a Kinesin-Related Protein That Associates with Centromeres during Mitosis [see Comments]." *J Cell Biol* 128 (1-2): 95–104. doi:10.1083/jcb.128.1.95.

Wordeman, Linda, Michael Wagenbach, and George von Dassow. 2007. "MCAK Facilitates Chromosome Movement by Promoting Kinetochore Microtubule Turnover." *The Journal of Cell Biology* 179 (5): 869–79. doi:10.1083/jcb.200707120.

Wren, Kathryne N. Julie M. Craft, Douglas Tritschler, Alexandria Schauer, Deep K. Patel, Elizabeth F. Smith, Mary E. Porter, Peter Kner, and Karl F. Lechtreck. 2013. "A Differential Cargo-Loading Model of Ciliary Length Regulation by IFT." *Current Biology* 23 (24). Elsevier Ltd: 2463–71. doi:10.1016/j.cub.2013.10.044.

Yang, Wenxing, Yosuke Tanaka, Miki Bundo, and Nobutaka Hirokawa. 2014. "Antioxidant Signaling Involving the Microtubule Motor KIF12 Is an Intracellular Target of Nutrition Excess in Beta Cells." *Developmental Cell* 31 (2). Elsevier Inc.: 202–14. doi:10.1016/j.devcel.2014.08.028.

Yoder, Bradley K, Xiaoying Hou, and Lisa M Guay-Woodford. 2002. "The Polycystic Kidney Disease Proteins, Polycystin-1, Polycystin-2, Polaris, and Cystin, Are Co-Localized in Renal Cilia." *Journal of the American Society of Nephrology : JASN* 13 (10): 2508–16. doi:10.1097/01.ASN.0000029587.47950.25.

Yokoyama, Ruth, Eileen O'toole, Sudipto Ghosh, and David R Mitchell. 2004. "Regulation of Flagellar Dynein Activity by a Central Pair Kinesin." *Proceedings of the National Academy of Sciences of the United States of America* 101 (50): 17398–403. doi:10.1073/pnas.0406817101.

Zerres, K. G. Mücher, L. Bachner, and G. Deschennes. 1994. "Mapping of the Gene for Autosomal Recessive Polycystic Kidney Disease (ARPKD) to Chromosome 6p21-Cen." *Nature* 8 (4): 340–44. doi:10.1038/ng1294-340.

Zhang, Dong, Gregory C. Rogers, Daniel W. Buster, David J. Sharp. 2007. "Three microtubule severing enzymes contribute to the "Pacman-flux" machinery that moves chromosomes." *Journal of Cell Biology*. 177 (2): 231-239. doi: 10.1083/jcb.200612011

Zhao, C. Y. Omori, K. Brodowska, P. Kovach, and J. Malicki. 2012. "Kinesin-2 Family in Vertebrate Ciliogenesis." *Proceedings of the National Academy of Sciences* 109 (7): 2388–93. doi:10.1073/pnas.1116035109.